Future Measurements of Proton Electromagnetic Form Factors at Large Momentum Transfers

Andrew Puckett
University of Connecticut
ECT* Diquark Correlations Workshop
September 26, 2019

UCONN Jefferson Lab

Outline

- Nucleon Electromagnetic Form factors EMFFs—definitions and connection to observables
- Previous measurements of proton EMFFs
  - Rosenbluth separations
  - Polarization observables
- Summary of high-Q^2 nucleon EMFF measurements at 11 GeV CEBAF
- The upcoming SBS measurement of GEP: E12-07-109. A "deep dive"
  - Overview, technical challenges and solutions
  - Projected results
  - Status
- Prospects for reaching higher Q^2—spacelike proton FFs at an EIC

Acknowledgements

- ECT* and workshop organizers for the opportunity to present this research
- SBS and Hall A collaborations
- Support from US Department Of Energy, Office of Science, Office of Nuclear Physics, Award ID DE-SC0014230 (Early Career research program)
- The University of Connecticut and Jefferson Lab for additional research support

Elastic *eN* scattering and form factors: formalism

$$\mathcal{M} = \frac{4\pi\alpha}{q^2}\bar{u}(k')\gamma^\mu u(k) g_{\mu\nu}\bar{u}(p')\left[F_1(q^2)\gamma^\nu + F_2(q^2)\frac{i\sigma^{\nu\alpha}q_\alpha}{2M}\right]u(p)$$

Invariant amplitude for elastic eN scattering in the one-photon-exchange approximation

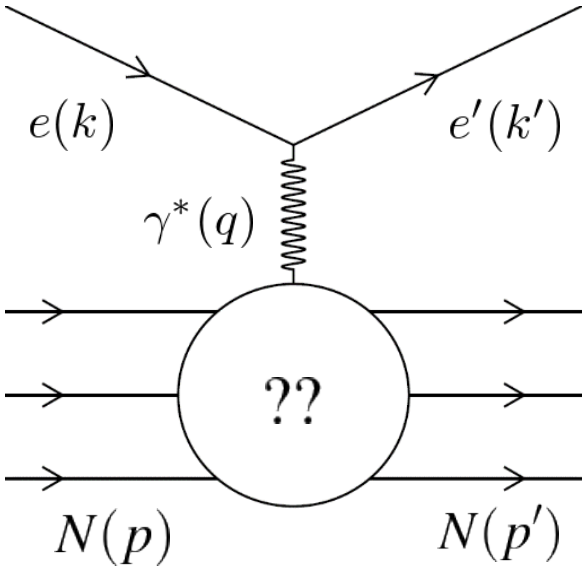

- The most general possible form of the virtual photon-nucleon vertex consistent with Lorentz invariance, parity conservation and gauge invariance is described by two form factors F_1 (Dirac) and F_2 (Pauli):
  - F_1 describes the helicity-conserving amplitude (charge and Dirac magnetic moment)
  - F_2 describes the helicity-flip amplitude (anomalous magnetic moment contribution)

$$G_E \equiv F_1 - \tau F_2$$
$$G_M \equiv F_1 + F_2$$
$$\tau \equiv \frac{Q^2}{4M^2}$$

Sachs Form Factors G_E (electric) and G_M (magnetic), are experimentally convenient linearly independent combinations of F_1, F_2

$$\frac{d\sigma}{d\Omega_e} = \frac{\alpha^2(\hbar c)^2\cos^2\frac{\theta_e}{2}}{4E_e^2\sin^4\frac{\theta_e}{2}}\frac{E_e'}{E_e}\left[\frac{\epsilon G_E^2 + \tau G_M^2}{\epsilon(1+\tau)}\right]$$
$$\frac{1}{\epsilon} \equiv 1 + 2(1+\tau)\tan^2\frac{\theta_e}{2}$$

Differential cross section in the nucleon rest frame:
Rosenbluth formula

$$\sigma_R \equiv \frac{\epsilon(1+\tau)\left(\frac{d\sigma}{d\Omega_e}\right)}{\left(\frac{d\sigma}{d\Omega_e}\right)_{Mott}} = \epsilon G_E^2 + \tau G_M^2$$

Rosenbluth Separation Method: Measure cross section at fixed Q^2 as a function of ε to obtain G_E^2 (slope) and G_M^2 (intercept).

Simplistic physical picture of form factors—Scattering of ultra-relativistic electrons from a static charge distribution

$$\frac{d\sigma}{d\Omega} = \left(\frac{d\sigma}{d\Omega}\right)_{Mott} |F(\mathbf{q})|^2$$

$$\left(\frac{d\sigma}{d\Omega}\right)_{Mott} \equiv \frac{\alpha^2(\hbar c)^2}{4E_e^2 \sin^4\frac{\theta}{2}} \frac{E'_e}{E_e} \cos^2\frac{\theta}{2}$$

$$F(\mathbf{q}) = \int \rho(\mathbf{x}) e^{i\mathbf{q}\cdot\mathbf{x}} d^3x$$

- In the one-photon-exchange approximation in QED (equivalent to the first Born approximation in nonrelativistic quantum scattering theory), the cross section factorizes as the product of the "Mott" cross section, and the square of the *form factor* $F(\boldsymbol{q})$, equal to the Fourier transform of the charge density with respect to the three-momentum transfer $\boldsymbol{q} = \boldsymbol{k} - \boldsymbol{k}'$
- The Mott cross section represents the theoretical cross section for scattering of ultrarelativistic, spin-1/2 electrons from a point-like, spin-less target of charge e.
- In the non-relativistic limit, $Q^2 \ll M^2$, we have the correspondence: $|F(\vec{q})| = G_E(Q^2)$

Form Factors for a point nucleon

$$
\begin{aligned}
G_E^p(Q^2=0) &= 1 \\
G_M^p(Q^2=0) &= \mu_p = +2.793 \\
G_E^n(Q^2=0) &= 0 \\
G_M^n(Q^2=0) &= \mu_n = -1.913 \\
F_1^p(0) &= 1 \\
F_2^p(0) &= \kappa_p = \mu_p - 1 = +1.793 \\
F_1^n(0) &= 0 \\
F_2^n(0) &= \kappa_n = -1.913
\end{aligned}
$$

- In the low-Q^2 (long-wavelength) limit, the electric and magnetic form factors reduce to the proton and neutron charges and magnetic moments.
- If the nucleon were pointlike, the form factors would have these constant values at any Q^2

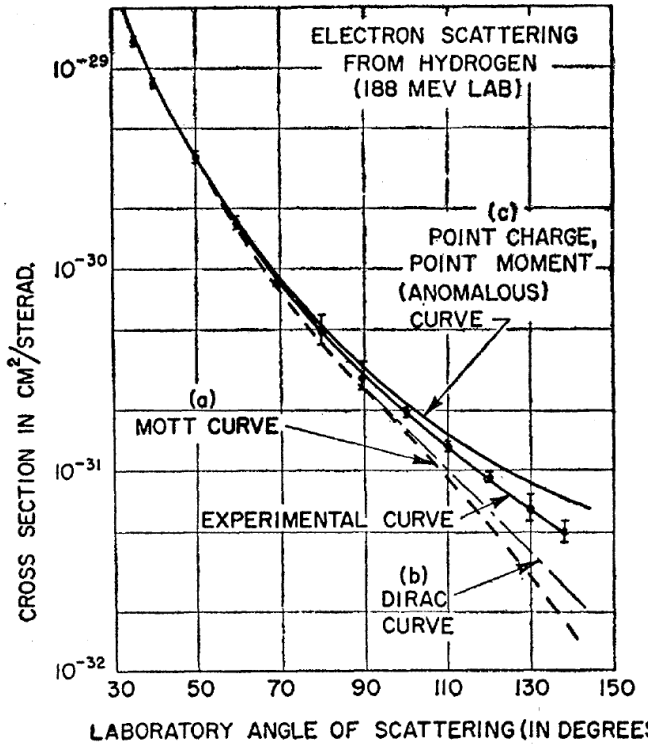

FIG. 24. Electron scattering from the proton at an incident energy of 188 Mev. The experimental points lie below the point-charge point-moment curve of Rosenbluth, indicating finite size effects.

R. Hofstadter, Rev. Mod. Phys., 28, 214 (1956)

R. Hofstadter
Nobel Prize 1961

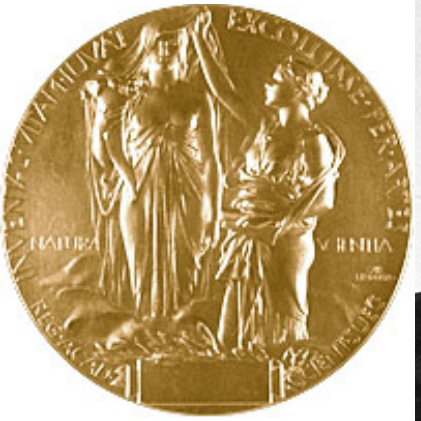

"for his pioneering studies of electron scattering in atomic nuclei and for his thereby achieved discoveries concerning the structure of the nucleons"

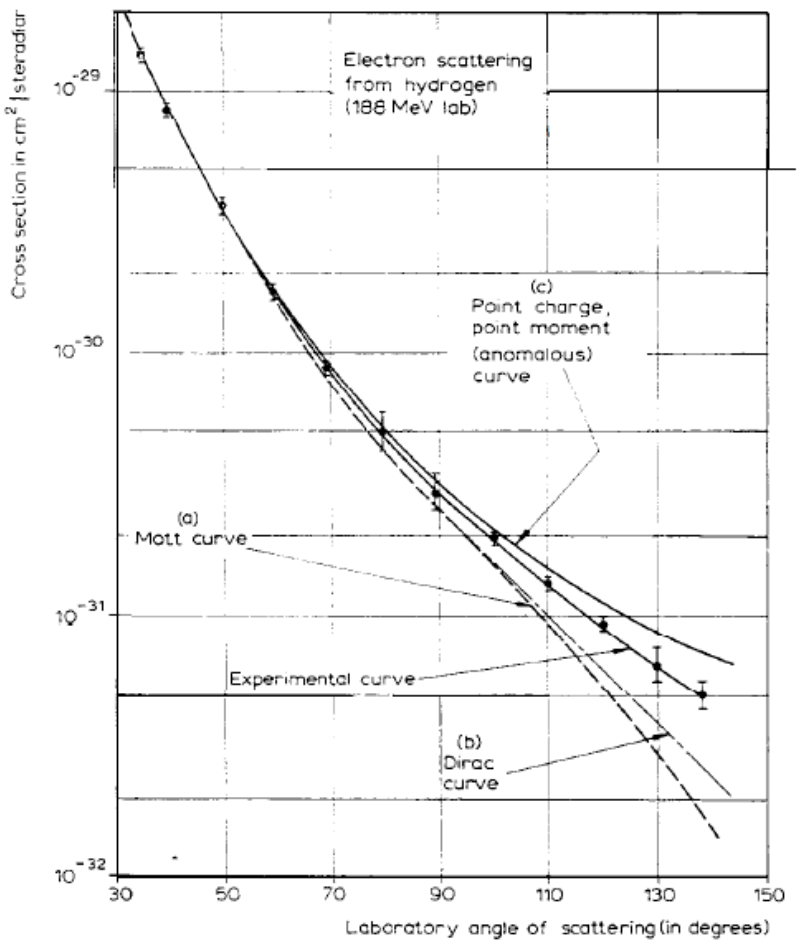

Fig. 9. Electron scattering from the proton at an incident energy of 188 MeV. *Curve (a)* shows the theoretical Mott curve for a spinless point proton. *Curve (b)* shows the theoretical curve for a point proton with a Dirac magnetic moment alone. *Curve (c)* shows the theoretical behavior of a point proton having the anomalous Pauli contribution in addition to the Dirac value of the magnetic moment. The deviation of the experimental curve from the Curve (c) represents the effect of form factors for the proton and indicates structure within the proton. The best fit in this figure indicates an rms radius close to $0.7 \cdot 10^{-13}$ cm.

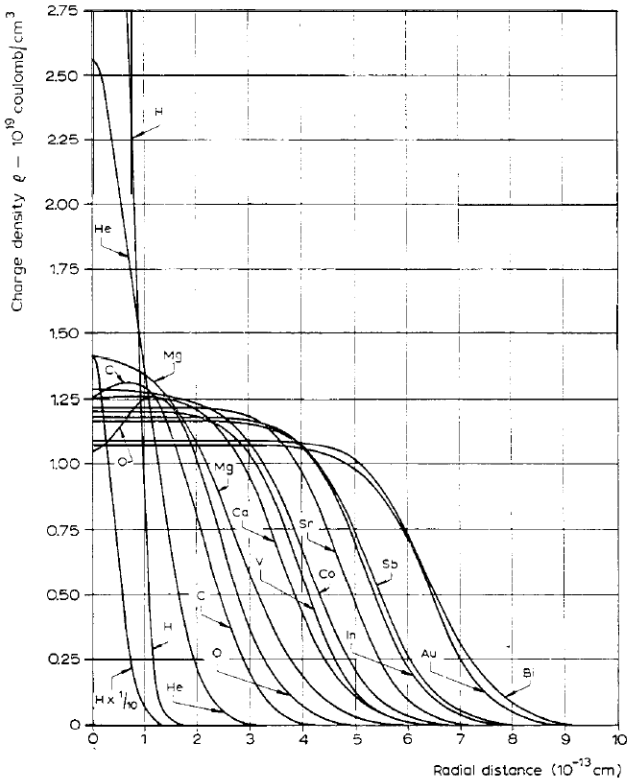

Nuclear Charge Densities

- Above: (R. Hofstadter Nobel lecture): Nuclear charge densities as measured in electron scattering, within Fermi model of the shape
- Top right: example nuclei, $r \sim A^{1/3}$ (volume proportional to number of nucleons)
- Bottom right: "Packing fraction" = ratio of volume of A nucleons to nuclear volume

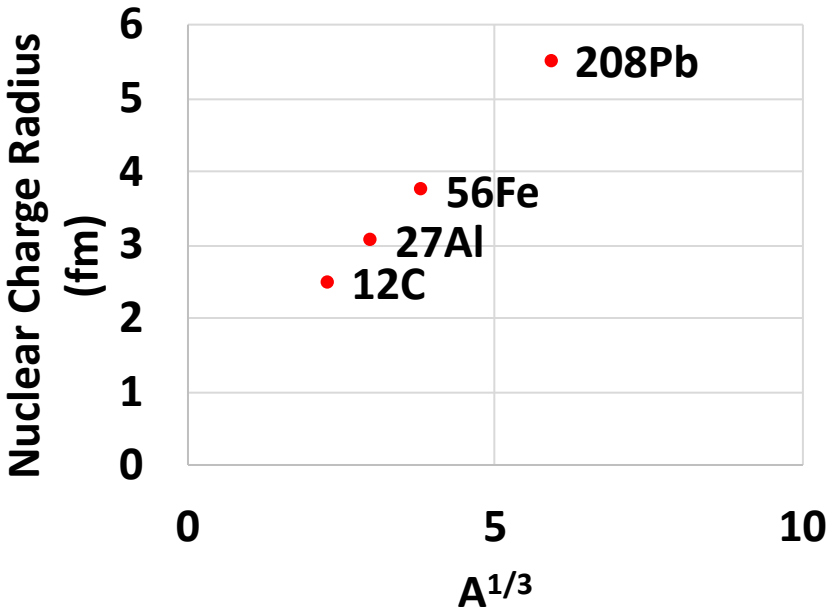

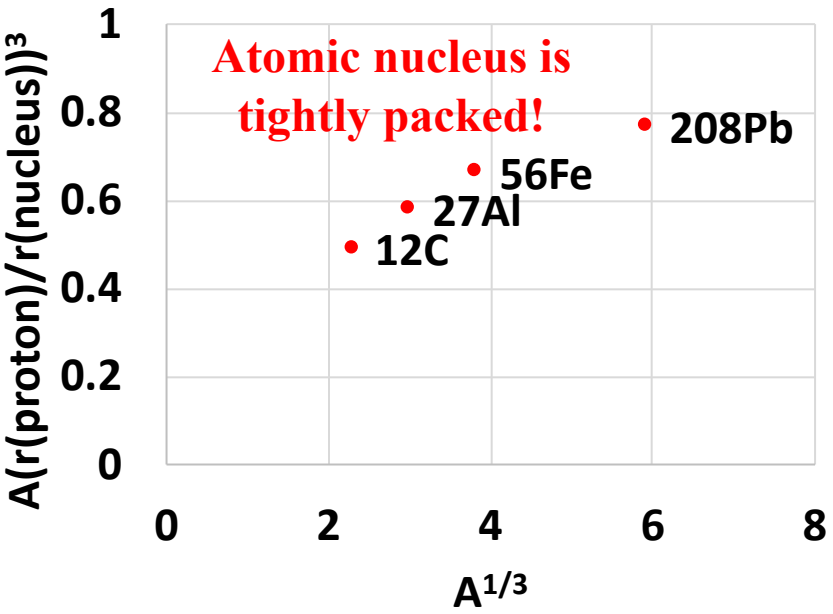

Nucleon "imaging" (traditional): Rest-frame charge and magnetization densities in 3D space

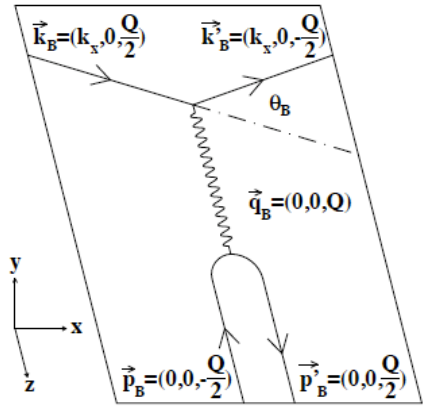

Figure 1-2: Elastic scattering in the Breit frame

$$\lambda_E = \lambda_M = 2$$

$$\tilde{\rho}_{ch}(k) = G_E(Q^2)(1+\tau)^{\lambda_E},$$

$$\mu\tilde{\rho}_m(k) = G_M(Q^2)(1+\tau)^{\lambda_M},$$

$$\rho(r) = \frac{2}{\pi}\int_0^\infty dk\, k^2 j_0(kr)\tilde{\rho}(k).$$

$$\tau = \frac{Q^2}{4M^2}$$

$$k^2 = \frac{Q^2}{1+\tau}$$

$$\rho_{ch}^{NR}(r) = \frac{2}{\pi}\int_0^\infty dQ\, Q^2 j_0(Qr) G_E(Q^2),$$

$$\mu\rho_m^{NR}(r) = \frac{2}{\pi}\int_0^\infty dQ\, Q^2 j_0(Qr) G_M(Q^2),$$

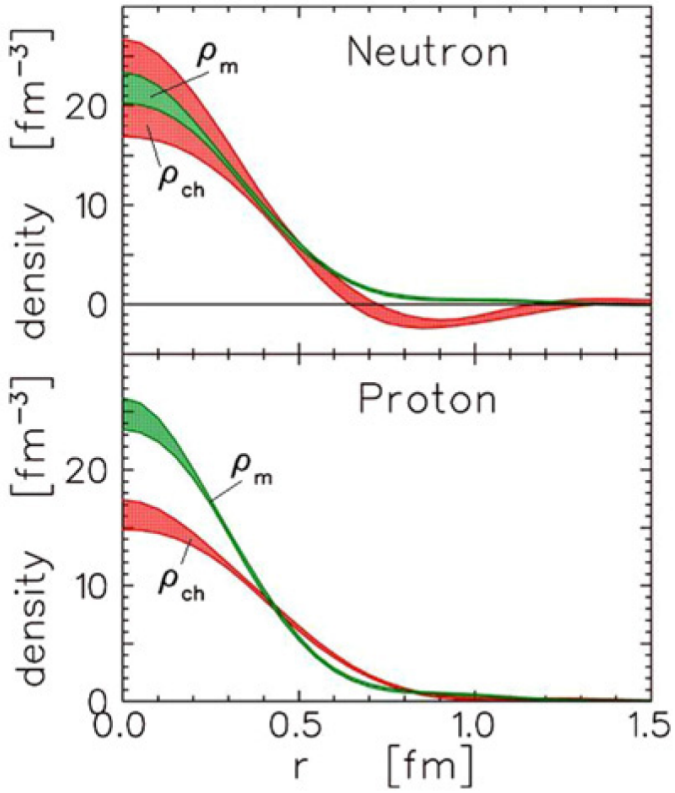

J. J. Kelly: PRC 66, 065203 (2002)

Proton FFs and "imaging": transverse densities, I

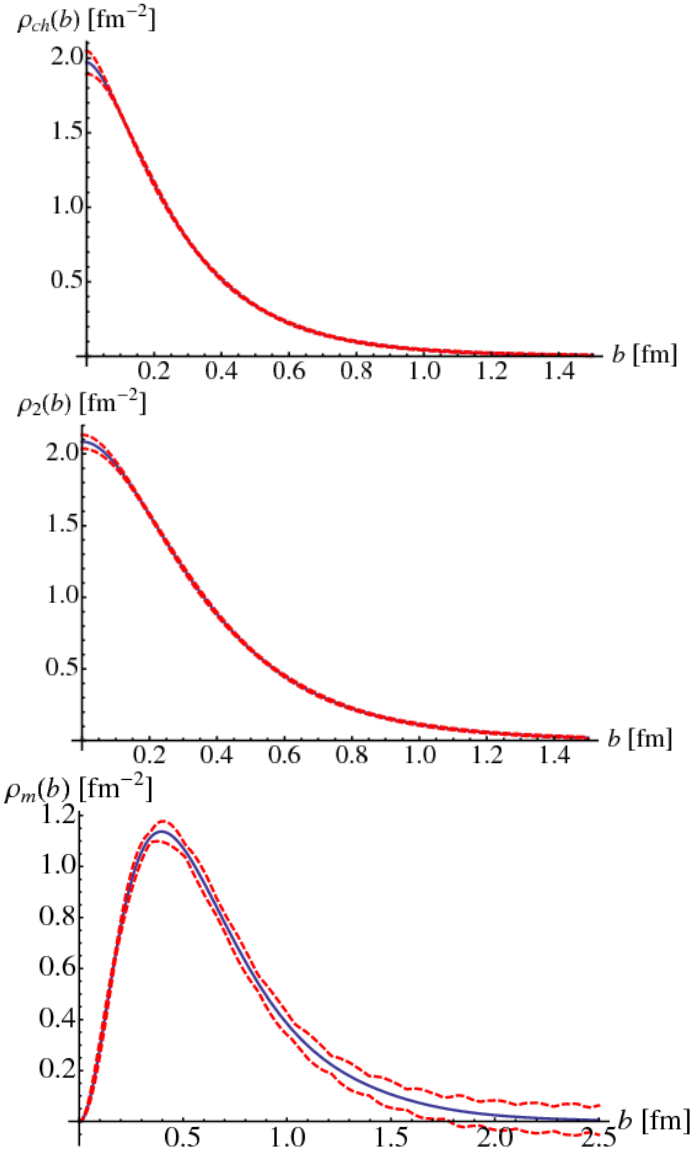

- Miller et al, **Phys. Rev. C, 83, 015203 (2011)**: ***model-independent,*** impact parameter-space charge and magnetization densities in the infinite momentum frame, derived from GPD-FF sum rules.
- Proton results shown for
  - Charge
  - 2D Fourier transform of F_2 (Pauli FF)
  - Anomalous magnetization density

$$\rho_{ch}(b) = \frac{1}{2\pi}\int QdQJ_0(Qb)F_1(Q^2)$$

$$\rho_2(b) = \frac{1}{2\pi}\int QdQJ_0(Qb)F_2(Q^2)$$

$$\rho_m(b) = -b\frac{d}{db}\rho_2(b) = \frac{b}{2\pi}\int Q^2dQJ_1(Qb)F_2(Q^2)$$

FFs and "imaging": transverse densities, II

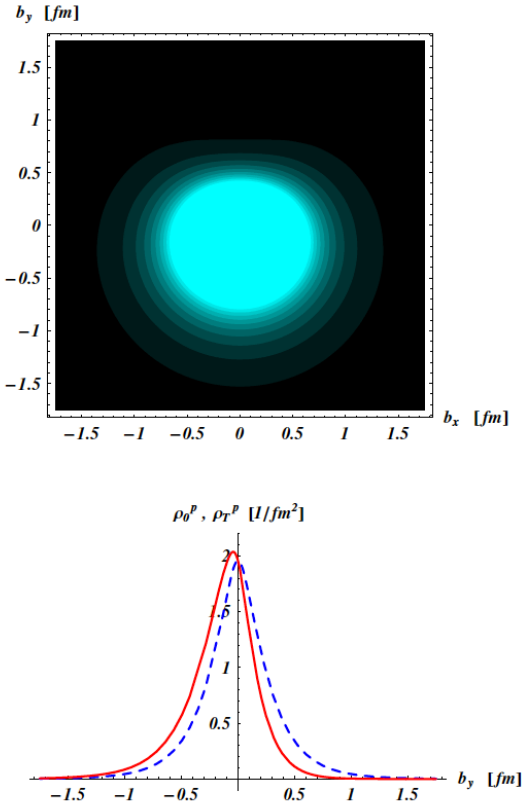

FIG. 1: Quark transverse charge densities in the *proton*. The upper panel shows the density in the transverse plane for a proton polarized along the x-axis. The light (dark) regions correspond with largest (smallest) values of the density. The lower panel compares the density along the y-axis for an unpolarized proton (dashed curve), and for a proton polarized along the x-axis (solid curve). For the proton e.m. FFs, we use the empirical parameterization of Arrington *et al.* [14].

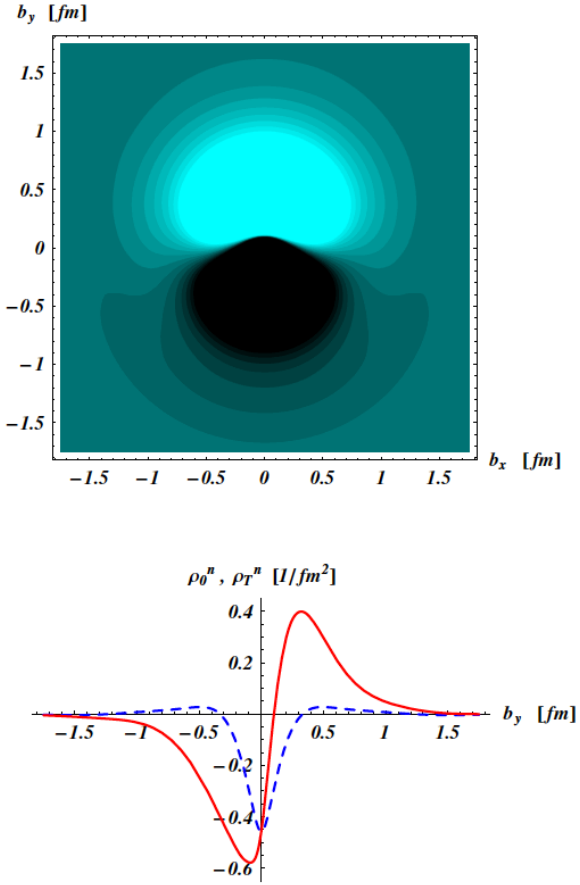

FIG. 2: Same as Fig. 1 for the quark transverse charge densities in the *neutron*. For the neutron e.m. FFs, we use the empirical parameterization of Bradford *et al.* [15].

Proton (left) and neutron (right) 2D polarized transverse charge densities from Carlson and Vanderhaeghen: Phys. Rev. Lett. 100, 032004 (2008)

Measuring Form Factors—Rosenbluth Separation

- The nucleon structure-dependent part of the cross section factorizes from the "point-like" part.
- The "reduced cross section" σ_R depends linearly on ϵ for a given Q^2, with slope G_E^2 and intercept τG_M^2.
- Experimentally, one measures $d\sigma/d\Omega$ while varying the beam energy and scattering angle to change ϵ while holding Q^2 constant

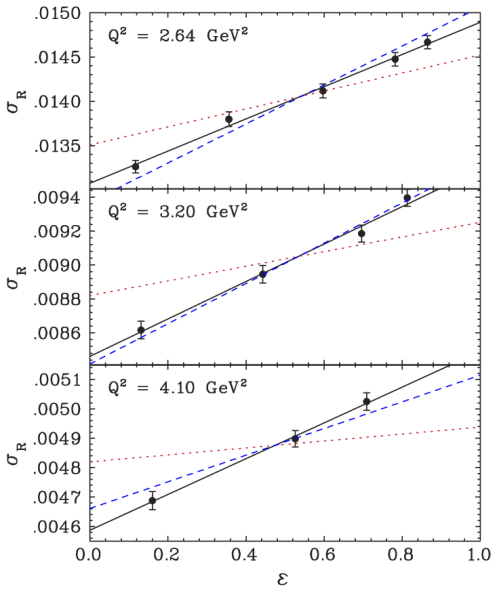

FIG. 2 (color online). Reduced cross sections as a function of ε. The solid line is a linear fit to the reduced cross sections, the dashed line shows the slope expected from scaling ($\mu_p G_E/G_M = 1$), and the dotted line shows the slope predicted by the polarization transfer experiments [6].

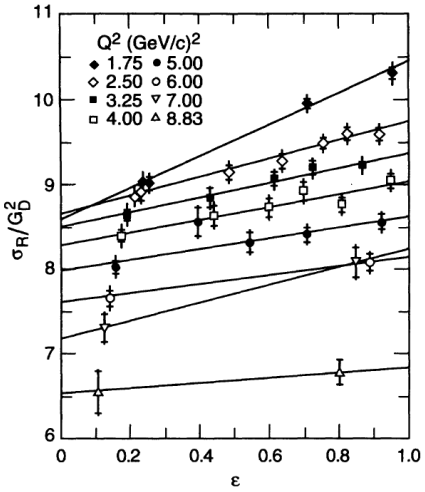

FIG. 22. Reduced cross sections divided by the square of the dipole fit plotted versus ϵ for each value of Q^2. The 1.6 GeV data points correspond to the leftmost point on each line, and the E136 data point is the rightmost point on the $Q^2 = 8.83$ (GeV/c)^2 line. The inner error bars show the statistical error, while the outer error bars show the total point-to-point uncertainty, given by the quadrature sum of the statistical and point-to-point systematic errors. An overall normalization uncertainty of ±1.77% has not been included.

Qattan *et al.*, **Phys. Rev. Lett.** 94, 142301 (2005)

Andivahis *et al.*, **Phys. Rev. D** 50, 5491 (1994)

$$\frac{d\sigma}{d\Omega_e} = \left(\frac{d\sigma}{d\Omega_e}\right)_{Mott} \frac{\epsilon G_E^2 + \tau G_M^2}{\epsilon(1+\tau)}$$

$$\left(\frac{d\sigma}{d\Omega_e}\right)_{Mott} = \frac{\alpha^2 \cos^2\left(\frac{\theta_e}{2}\right)}{4E_e^2 \sin^4\left(\frac{\theta_e}{2}\right)} \frac{E_e'}{E_e}$$

$$\sigma_R = \epsilon G_E^2 + \tau G_M^2$$

$$\tau \equiv \frac{Q^2}{4M_p^2}$$

$$\epsilon \equiv \left[1 + 2(1+\tau)\tan^2\left(\frac{\theta_e}{2}\right)\right]^{-1}$$

Proton FFs—Rosenbluth data

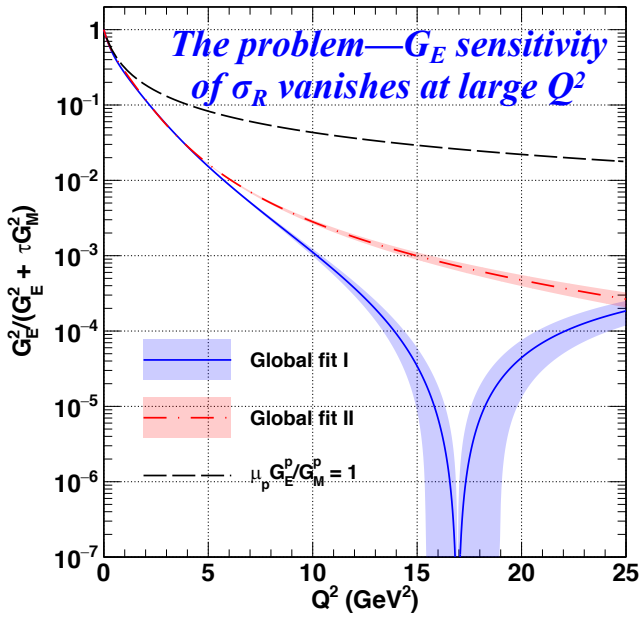

Maximum contribution of G_E^2 term to σ_R vanishes at large τ. Fits to FF data are described in Phys. Rev. C, 96, 055203 (2017)

$$\sigma_R = \epsilon G_E^2 + \tau G_M^2$$

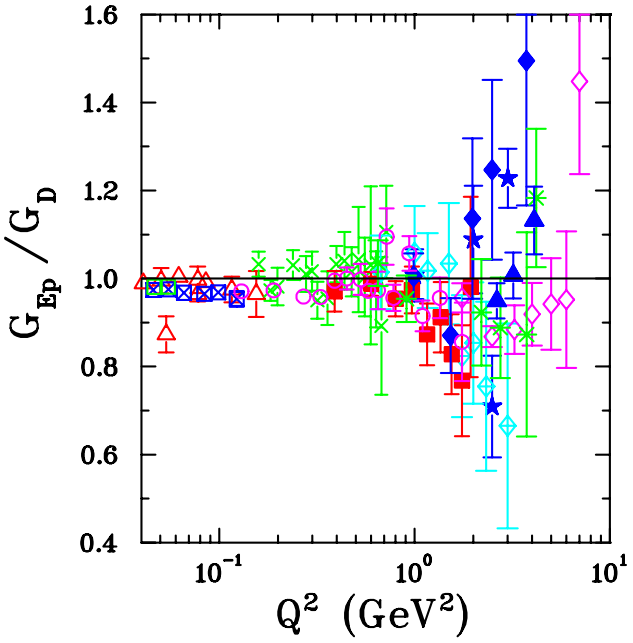

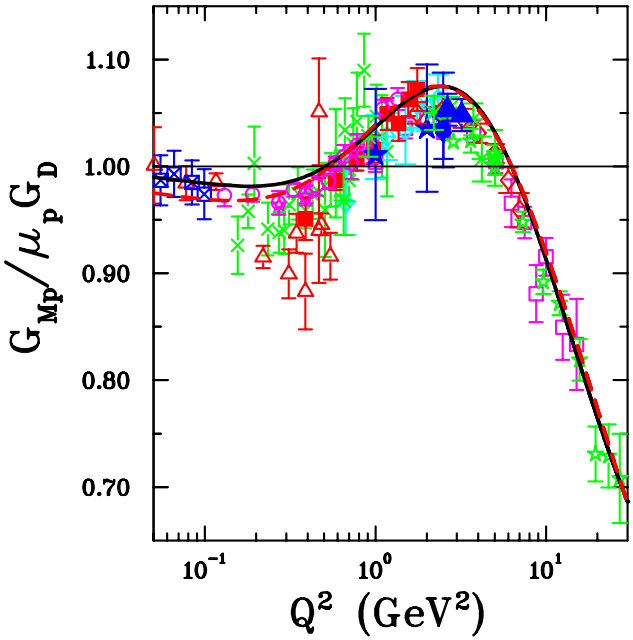

G_E^p and G_M^p Rosenbluth Data: $G_E^p \approx \frac{G_M^p}{\mu_p} \approx G_D$

$$G_D \equiv \left(1 + \frac{Q^2}{\Lambda^2}\right)^{-2}$$

$$\Lambda^2 = 0.71 \text{ GeV}^2$$

- Elastic *ep* cross sections have been measured for $0.003 \leq Q^2 \leq 31.2$ GeV^2.
- Rosenbluth data for G_E^p and G_M^p are qualitatively described by the "dipole" form factor, which is the Fourier transform of a spherically symmetric, exponentially decreasing radial charge/magnetization density.

Polarization Transfer in Elastic *eN* scattering

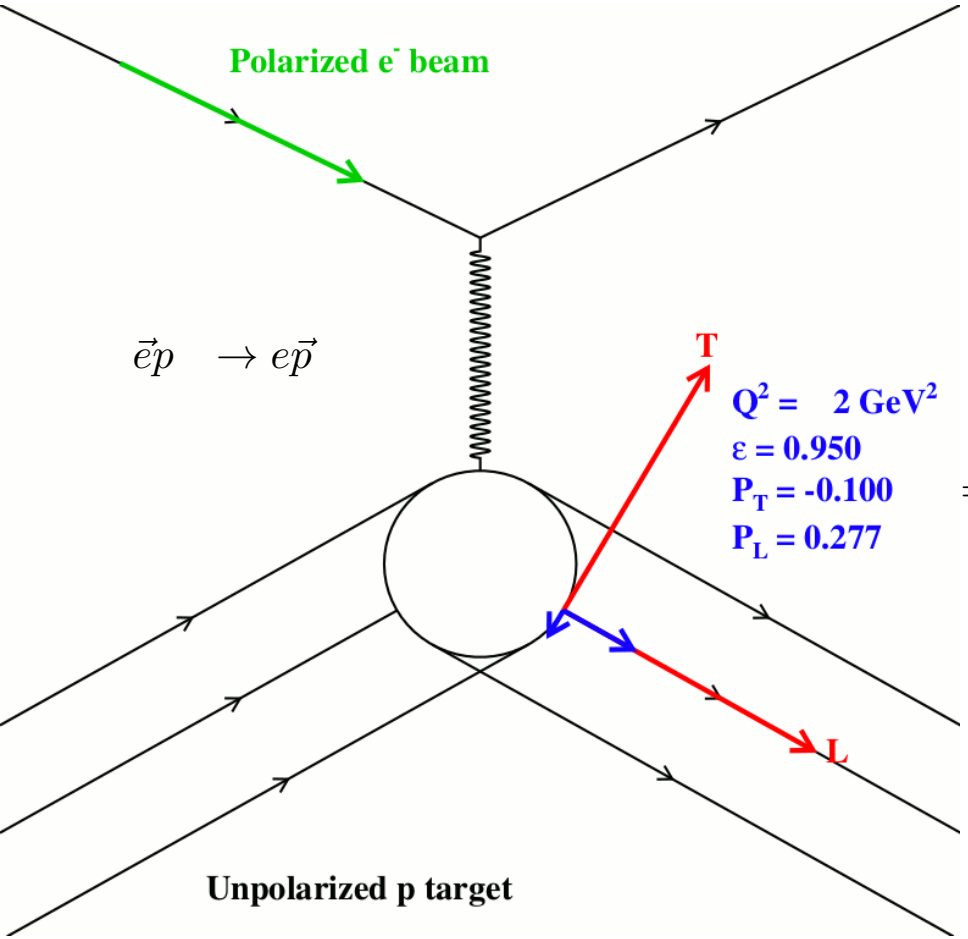

$$P_t = -P_{beam}\sqrt{\frac{2\epsilon(1-\epsilon)}{\tau}}\frac{r}{1+\frac{\epsilon}{\tau}r^2}$$

$$P_\ell = P_{beam}\frac{\sqrt{1-\epsilon^2}}{1+\frac{\epsilon}{\tau}r^2}$$

$$P_n = 0$$

$$r \equiv \frac{G_E}{G_M}$$

$$\Longrightarrow R_p \equiv \mu_p\frac{G_E^p}{G_M^p} = -\mu_p\sqrt{\frac{\tau(1+\epsilon)}{2\epsilon}}\frac{P_t}{P_\ell}$$

- Akhiezer and Rekalo (1968):
  - ***Derived relations between transferred polarization components in elastic eN scattering and the ratio of electromagnetic FFs $R = \mu G_E/G_M$***
- Perdrisat + Punjabi, 1993 proposal to CEBAF PAC: A ***simultaneous*** measurement of the two recoil polarization components in a polarimeter determines the FF ratio while canceling many systematic uncertainties (beam polarization, analyzing power, FPP instrumental asymmetry)

- ***The ratio of transferred polarization components is directly proportional to G_E/G_M, and therefore much more sensitive to G_E at large Q^2 than the cross section***

Recoil Proton Polarimetry: General Principles

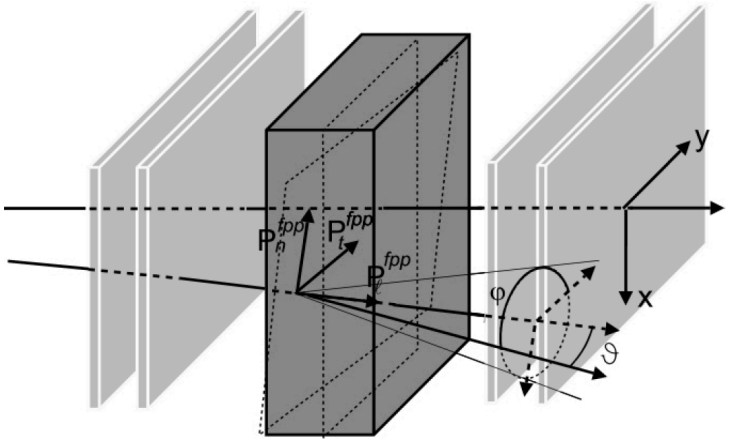

FIG. 9. Principle of the polarimeter, showing a noncentral trajectory through the front chambers, scattering in the analyzer, and a track through the back chambers; ϑ is the polar angle, and φ is the azimuthal angle from the y direction counterclockwise.

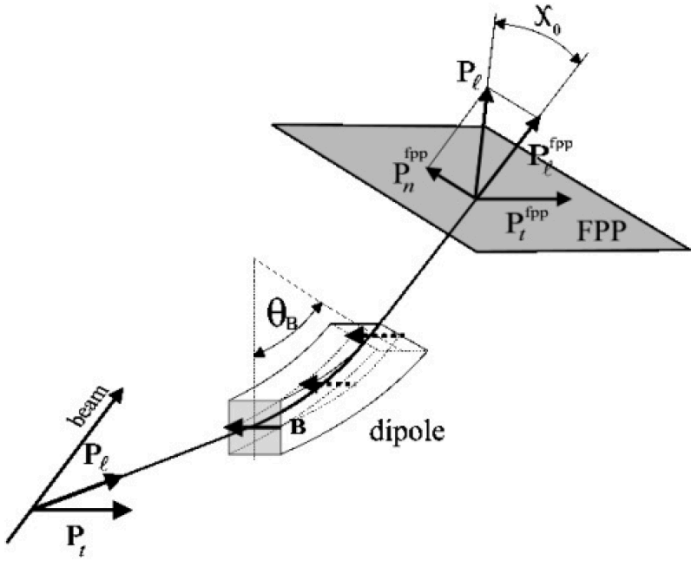

FIG. 15. Precession of the polarization component P_ℓ in the dipole of the HRS by an angle χ_θ.

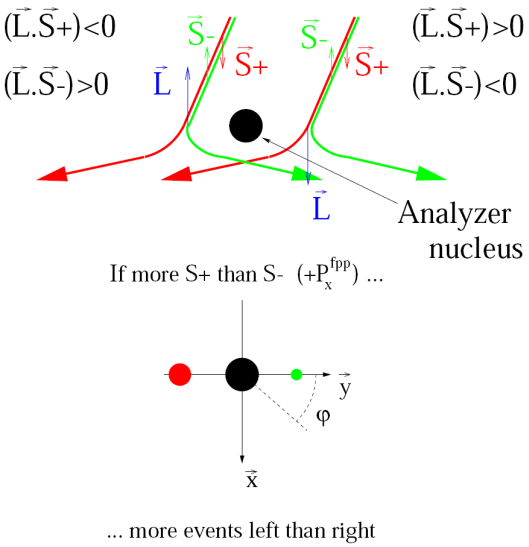

- Proton polarimetry via proton-nucleus scattering is based on the spin-orbit coupling in the nucleon-nucleon force.
- A spin-1/2 particle, such as a proton, is preferentially deflected by a spin-orbit force along the direction of $\vec{p}\times\vec{S}$, where $\vec{p}$ is the incident proton momentum, and $\vec{S}$ is the proton spin.
  - Note that a spin-orbit force is insensitive to longitudinal polarization!
  - Precession in spectrometer dipole field rotates P_L into a transverse component that can be measured
- By tracking the incident and scattered protons and measuring the azimuthal asymmetry in the angular distribution of secondary scatterings, the incident proton's (transverse) polarization is reconstructed

GEp-I in Hall A: $0.5 \leq Q^2 \leq 3.5\ GeV^2$

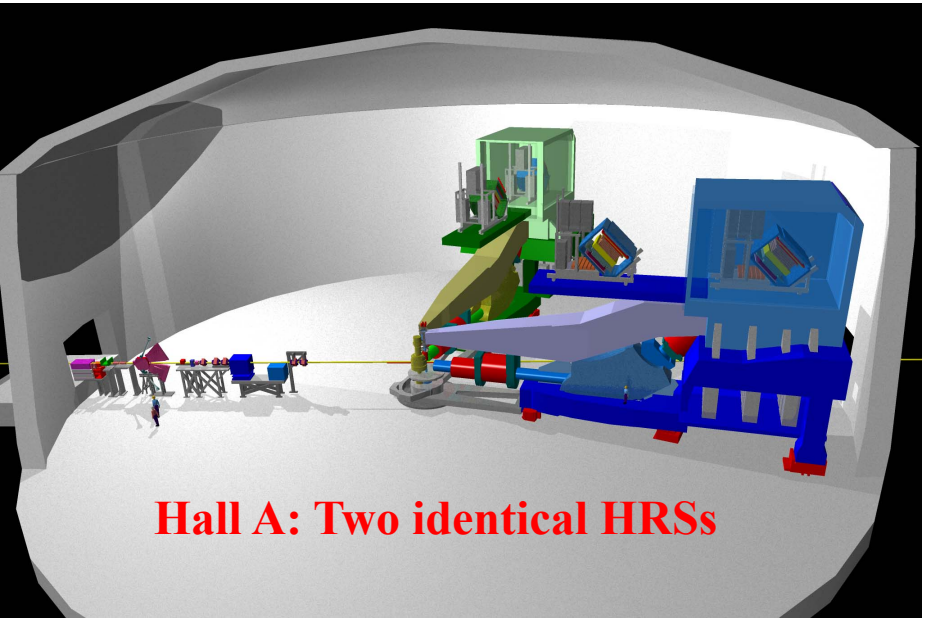

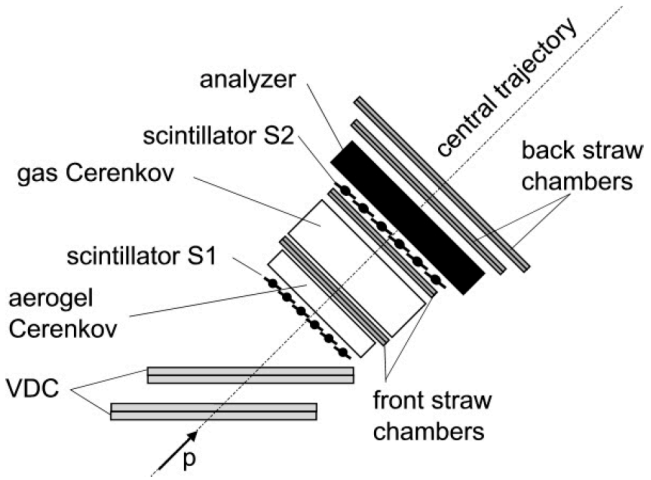

FIG. 2. Side view of the hadron arm detector package including the polarimeter.

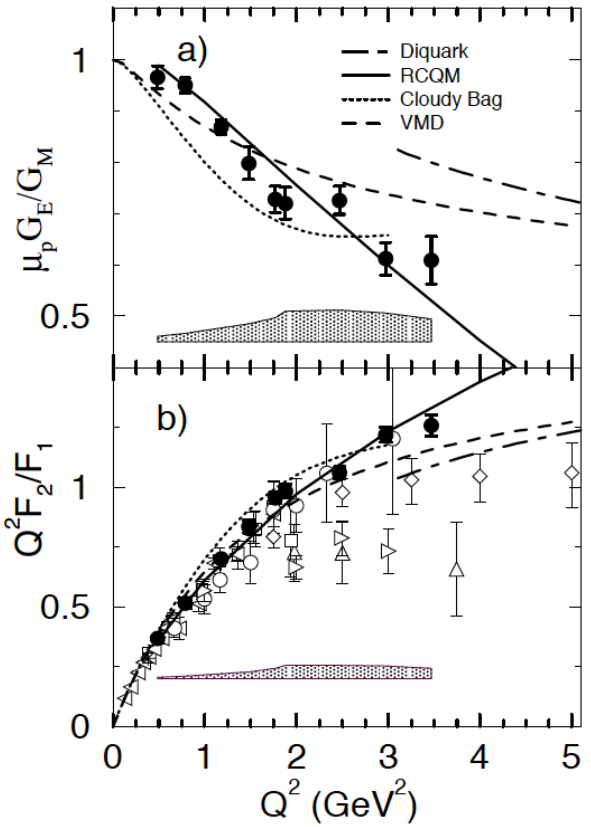

FIG. 2. (a) The ratio $\mu_p G_{Ep}/G_{Mp}$ from this experiment, compared with theoretical calculations. (b) The ratio Q^2F_{2p}/F_{1p} for the same data, compared to the same theoretical models as in (a) and world data; symbols as in Fig. 1. In both (a) and (b) the absolute value of systematic error from this experiment is shown by the shaded area.

Jones *et al.*, Phys. Rev. Lett. 84, 1398 (2000)

GEp-II in Hall A: $3.5 \leq Q^2 \leq 5.6\ GeV^2$

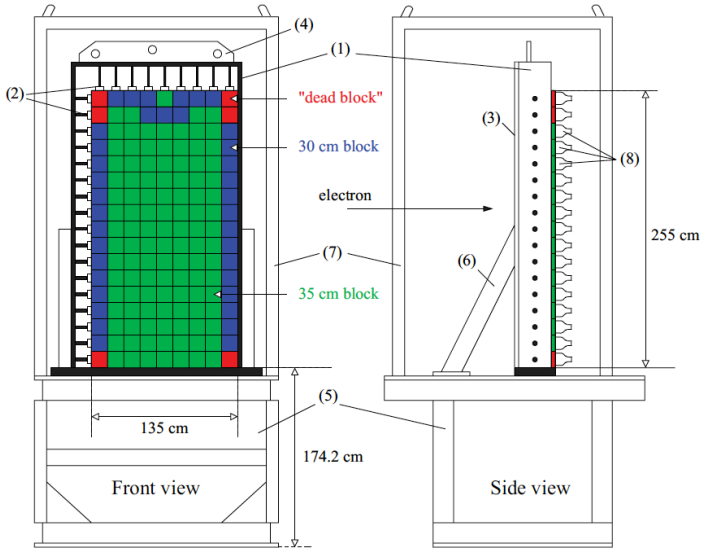

FIG. 4. (Color) Design of the calorimeter used to detect the scattered electron. In the front view, the 2.54-cm-thick aluminum plate in front of the blocks is not shown. See text for details.

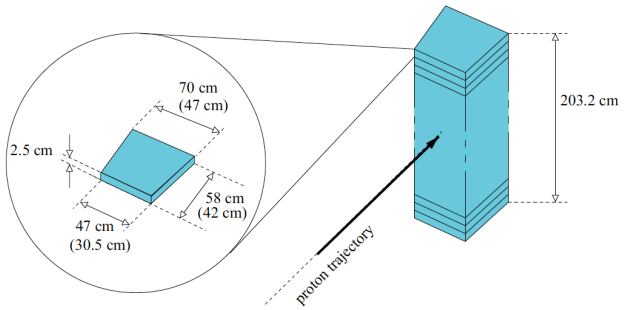

FIG. 3. (Color online) Stack of polyethylene plates for the analyzer. The dimensions shown on the plate are for the 58-cm (42-cm) stack and were chosen to match the envelope of elastically scattered protons in HRSL.

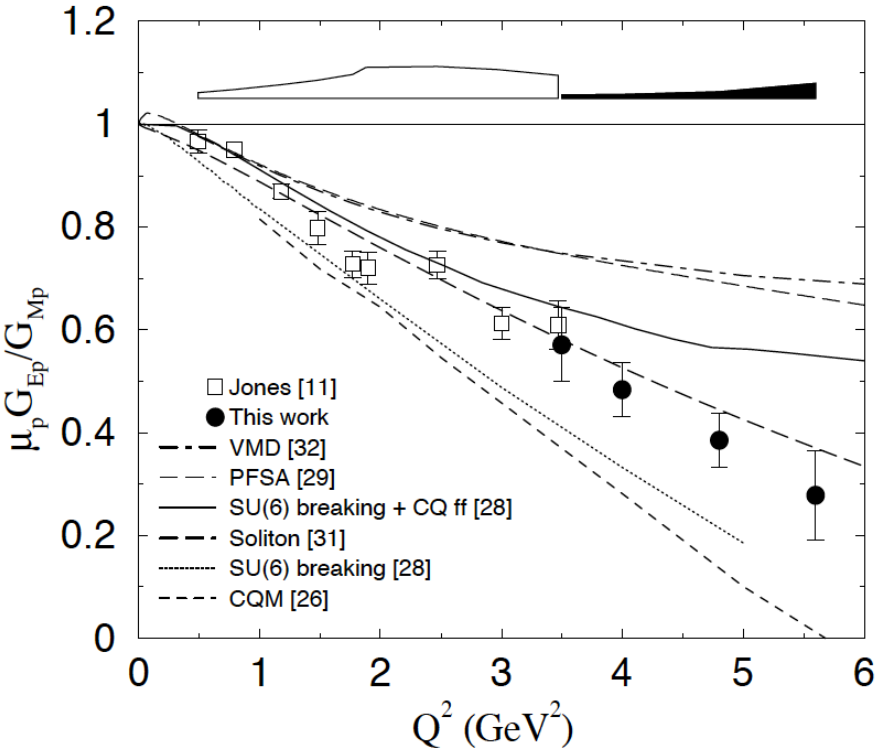

Gayou *et al.*, Phys.Rev. Lett. 88 (2002) 092301

- Relative to GEp-I: increase of analyzer thickness, change of material from carbon to CH_2 (polyethylene)
- Use of large solid-angle lead-glass calorimeter instead of HRS to detect the scattered electron in coincidence

GEp-III and GEp-2γ in Hall C: $2.5 \leq Q^2 \leq 8.5\ GeV^2$

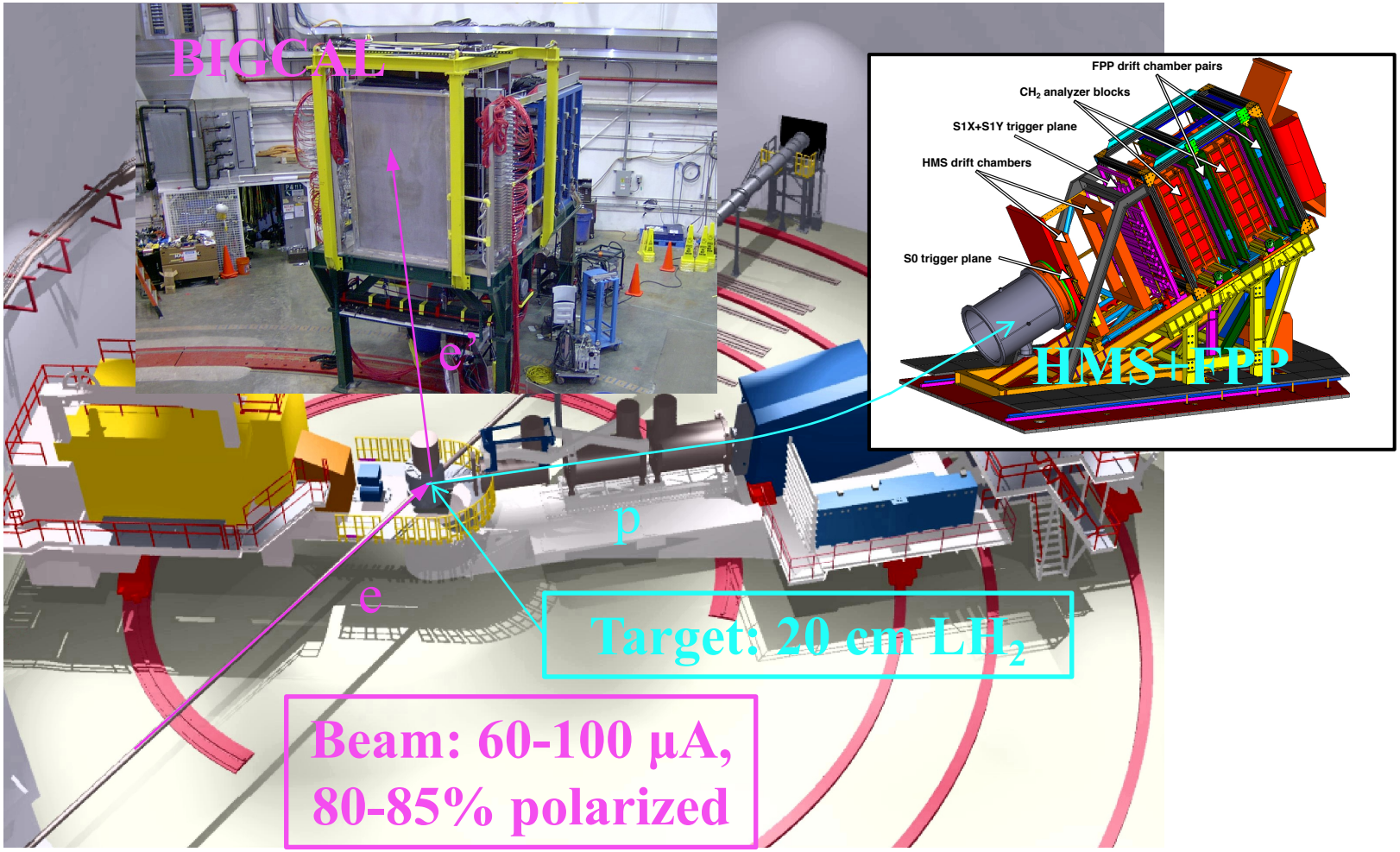

- Polarization transfer in ^{1}H(**e**,e'**p**). Nominal luminosity ~ 4×10^{38} Hz/cm^2
- Changes from Hall A measurements: new double-FPP layout, more finely segmented electron calorimeter, Hall C HMS to detect protons up to p = 5.41 GeV

Hall C GEp Results—PRL 2010 and 2011

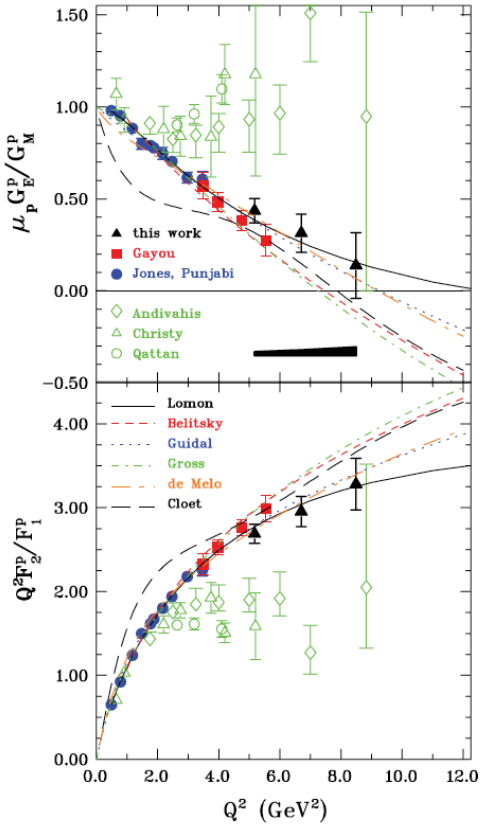

FIG. 3 (color). Upper panel: The proton form factor ratio $\mu_p G_E^p/G_M^p$ from this experiment (filled black triangles), with statistical error bars and systematic error band below the data. Previous experiments are [1] (Jones, Punjabi, Gayou), [3] (Andivahis), [4] (Christy), and [5] (Qattan). Theory curves are [20] (Lomon), [21] (de Melo), [22] (Gross), [23] (Cloët), [24] (Guidal), and [25] (Belitsky). Lower panel: The same data and theory curves as the upper panel, expressed as $Q^2F_2^p/F_1^p$.

Puckett *et al.*, **Phys.Rev.Lett. 104 (2010) 242301**

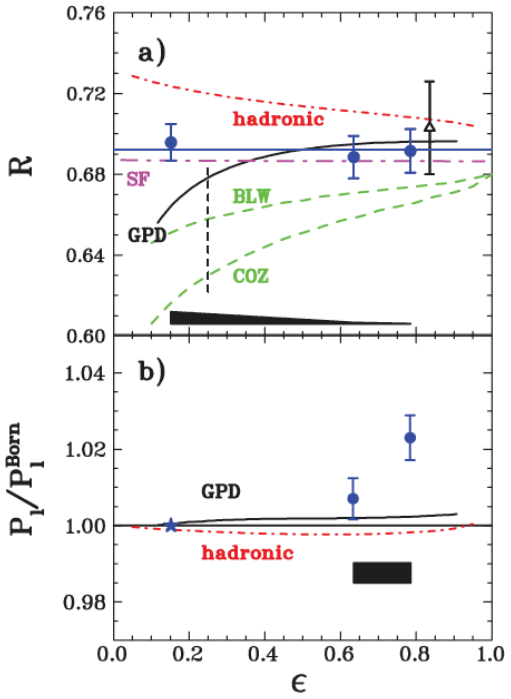

FIG. 2 (color). (a) R as a function of ϵ with statistical uncertainties, filled circles from this experiment and open triangle from [7]. The theoretical predictions are from [14] (hadronic), [13] (GPD), [19] (COZ and BLW), and [17] (SF) offset for clarity by -0.006 with respect to the fit. The one-parameter fit result is $R = 0.6923 \pm 0.0058$. (b) $P_\ell/P_\ell^{\mathrm{Born}}$ as a function of ϵ. The point-to-point systematic uncertainties, shown with a band in both panels, are relative to the largest ϵ kinematic in (a) and relative to the smallest ϵ kinematic in (b). The star indicates the ϵ value at which the analyzing power is determined.

Meziane *et al.*, **Phys.Rev.Lett. 106 (2011) 132501**

GEp-II Reanalysis: PRC 2012

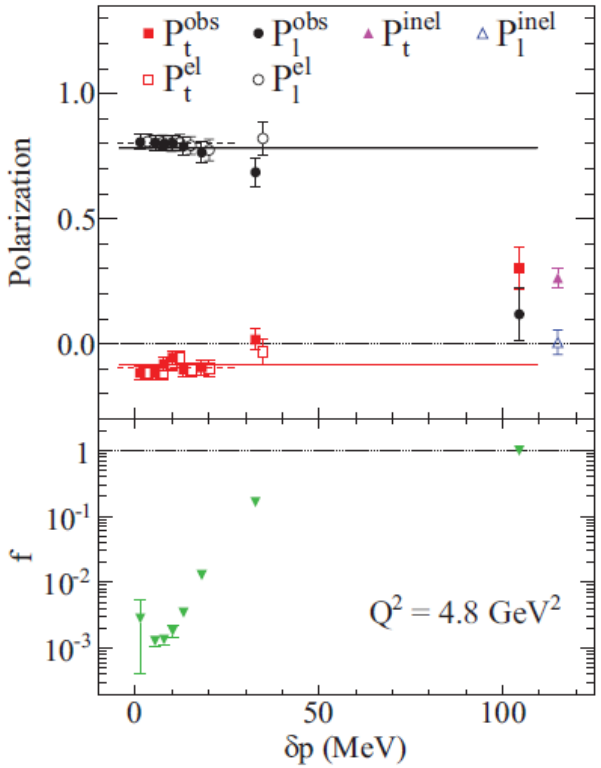

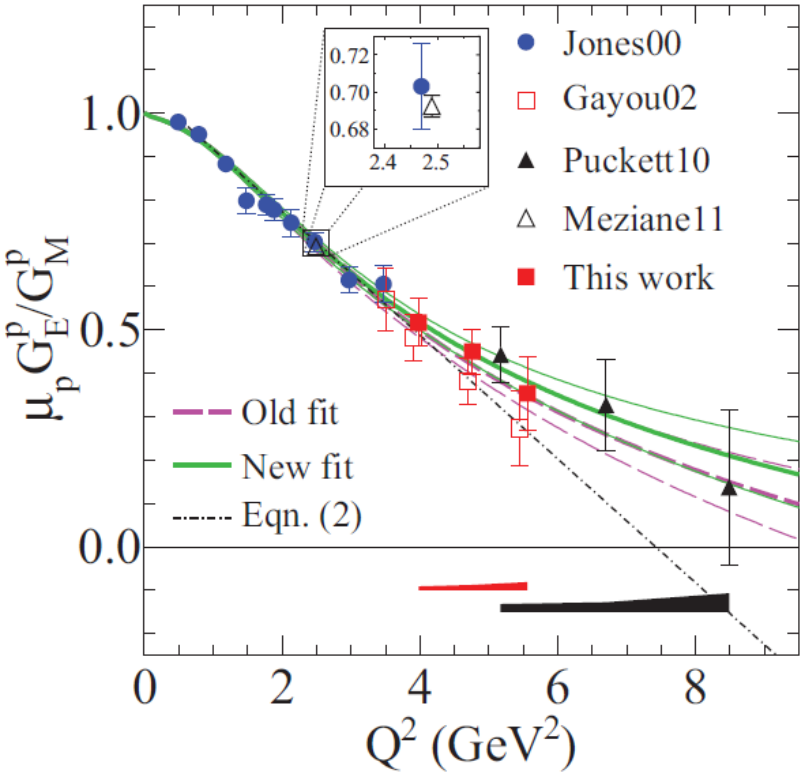

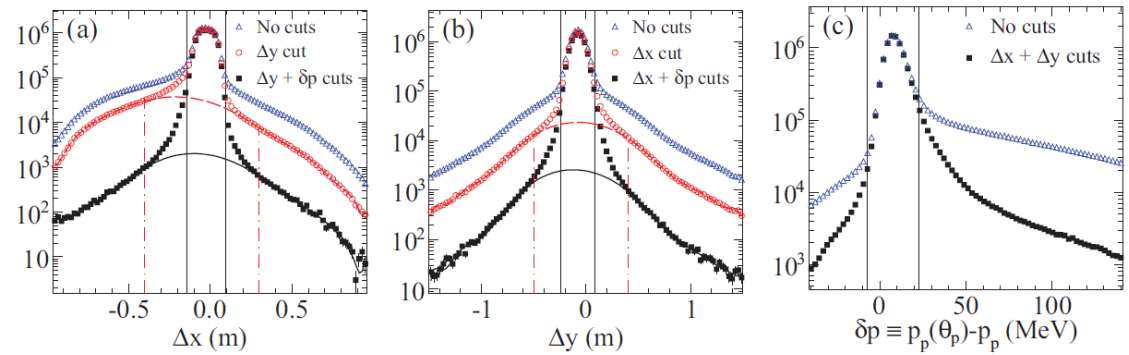

- Improved elastic event selection
- Suppress (previously underestimated) inelastic background
- Increase of $\mu_p G_E^p / G_M^p$, improved consistency with GEp-III

Hall C GEp Final Results—PRC 2017

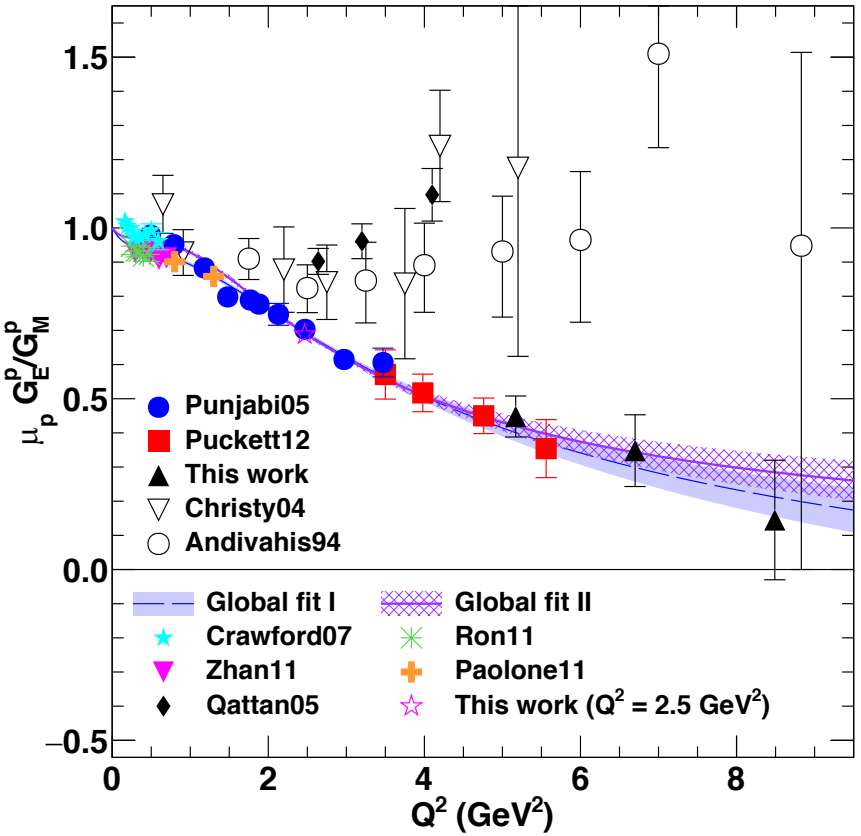

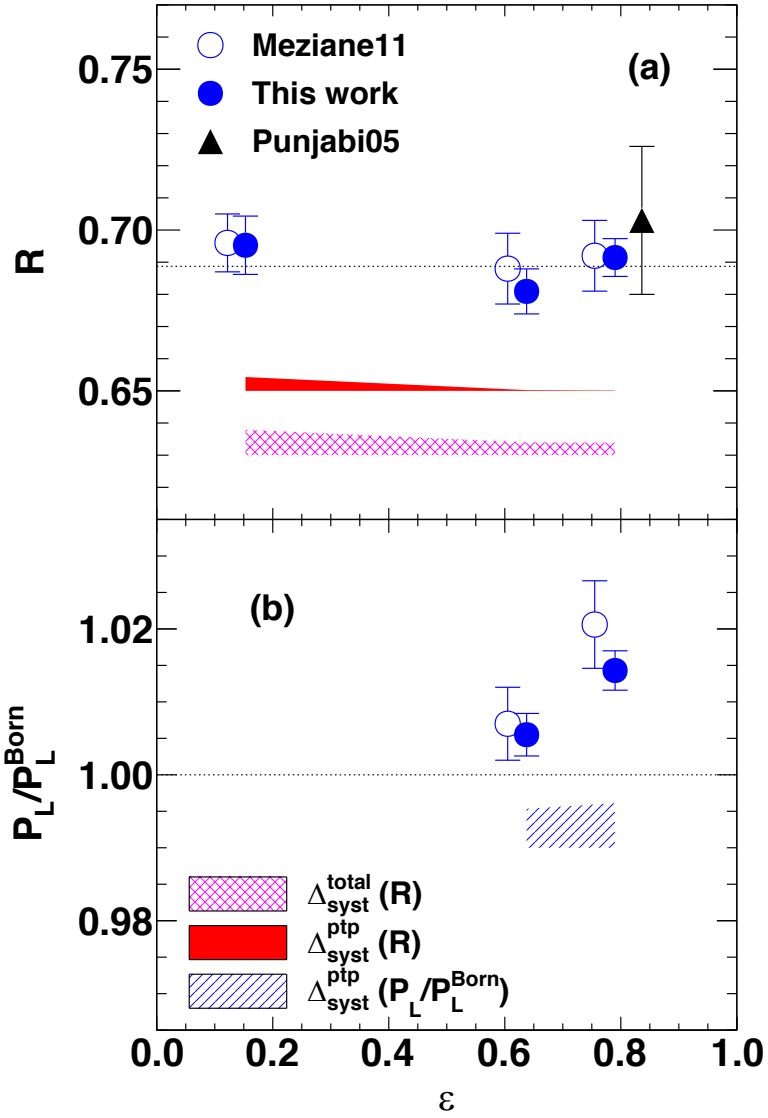

Puckett *et al.*, **Phys.Rev. C96 (2017) no.5, 055203**

- Archival publication with full reanalysis of GEp-III and GEp-2γ data, including previously unpublished full-acceptance dataset of GEp-2γ at 2.5 GeV^2—roughly 2-fold reduction of the statistical uncertainties at $\epsilon = 0.63, 0.78$

Doug Higinbotham's listing of "Hall A" publications by citation count:

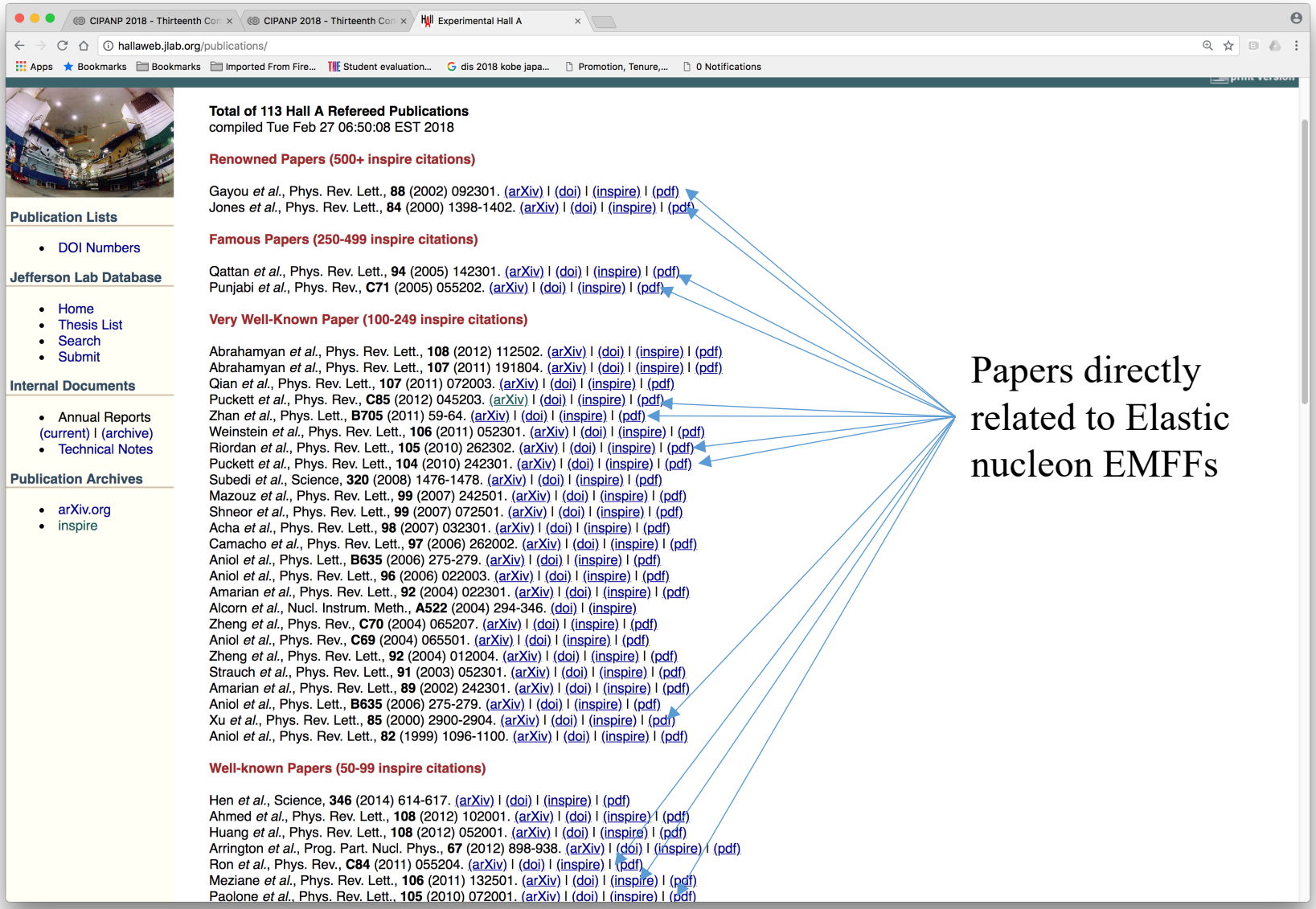

G_E^p/G_M^p polarization transfer data are among the most-cited JLab results: Why?

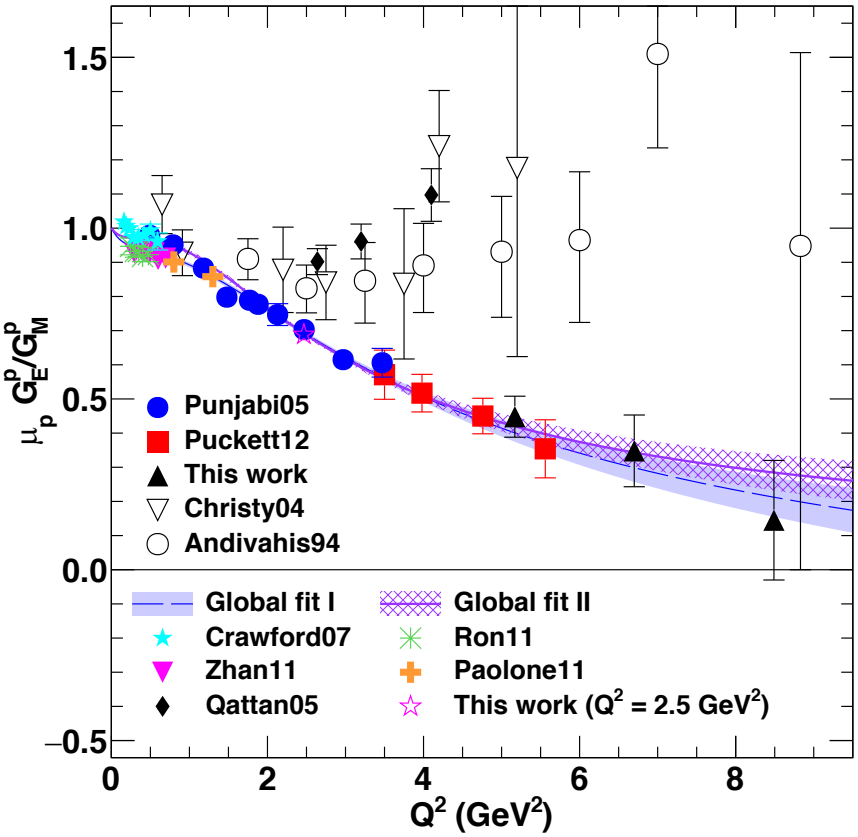

- *Extraction of the same physical property of the proton from different experimental observables yields different results!*
- Guichon and Vanderhaeghen, **PRL** 91, 142303 (2003): *"This discrepancy is a serious problem as it generates confusion and doubt about the whole methodology of lepton scattering experiments."*
- Discrepancy still not yet fully understood
- Unexpected results of GEP experiments have changed our basic notions about proton structure!

- GEp-I:
  - Jones *et al.,* **Phys. Rev. Lett. 84 (2000) 1398-1402: 863 INSPIRE-HEP citations**
  - Punjabi *et al.*, **Phys.Rev. C71 (2005) 055202: 429 INSPIRE-HEP citations**
- GEp-II:
  - Gayou *et al.*, **Phys.Rev.Lett. 88 (2002) 092301: 794 INSPIRE-HEP citations**
  - Puckett *et al.*, **Phys.Rev. C85 (2012) 045203: 136 INSPIRE-HEP citations**
- GEp-III/GEp-2γ:
  - Puckett *et al.*, **Phys.Rev.Lett. 104 (2010) 242301,** 250 **INSPIRE-HEP citations**
  - Meziane *et al.,* **Phys.Rev.Lett. 106 (2011) 132501, 79 INSPIRE-HEP citations**
  - Puckett *et al.*, **Phys.Rev. C96 (2017) no.5, 055203, 22 INSPIRE-HEP citations**
- Low-Q^2 data from JLab:
  - Ron *et al.*, **Phys.Rev.Lett. 99 (2007) 202002**, 69 INSPIRE-HEP citations
  - Ron *et al.*, **Phys.Rev. C84 (2011) 055204,** 93 INSPIRE-HEP citations
  - Zhan *et al.*, **Phys.Lett. B705 (2011) 59-64,** 170 INSPIRE-HEP citations
  - Paolone *et al.*, **Phys.Rev.Lett. 105 (2010) 072001**, 90 INSPIRE-HEP citations

2017 Tom W. Bonner Prize in Nuclear Physics Recipient

Charles F. Perdrisat
College of William and Mary

Citation:

"*For groundbreaking measurements of nucleon structure, and discovering the unexpected behavior of the magnetic and electric nucleon form factors with changing momentum transfer.*"

Background:

Charles F. Perdrisat, Ph.D., was a professor at the College of William and Mary (Williamsburg, Va.) for the last 50 years having retired earlier this year. Throughout his career, Dr. Perdrisat's research focus included nuclear reactions with proton and deuteron beams, both polarized and unpolarized. He conducted research at SATURNE in Saclay, France, TRIUMF in Vancouver, B.C., LAMPF in Los Alamos, New Mexico, Brookhaven National Laboratory in Upton, N.Y., and JINR in Dubna, Russia. During the last half of his career, he was committed to the investigation of the structure of the proton at Jefferson Laboratory, concentrating in obtaining polarization transfer data in the scattering of polarized electrons on unpolarized protons. These data, from 3 distinct experiments organized in close collaboration with Vina Punjabi, Ph.D., Mark K. Jones, Ph.D., Edward J. Brash, Ph.D., and Lubomir Pentchev, Ph.D., have resulted in a significant change of paradigm in the understanding of the structure of the nucleon. After completing his undergraduate training in physics and mathematics at the University of Geneva in 1956, Dr. Perdrisat became an assistant in the physics department at the Swiss Federal Institute of Technology in Zurich) in Switzerland, under Prof. Paul Scherrer; he received his Ph.D. in 1962. He completed a three-year postdoctoral fellowship at the University of Illinois Urbana-Champaign, before heading to William and Mary in 1966.

Selection Committee:

2017 Selection Committee Members: Rocco Schiavilla (Chair), D. Hertzog, P. Jacobs, Kate Jones, I-Y. Lee

Hall A G_M^p preliminary results from 2016 data

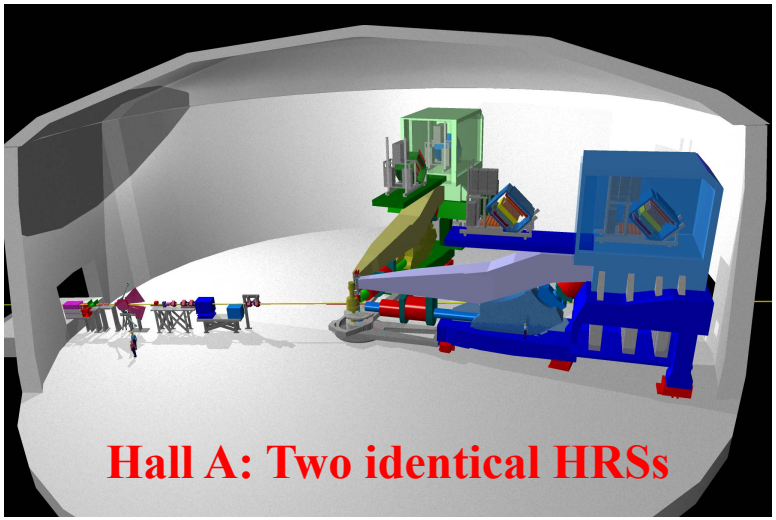

GMp and other High Q^2 data

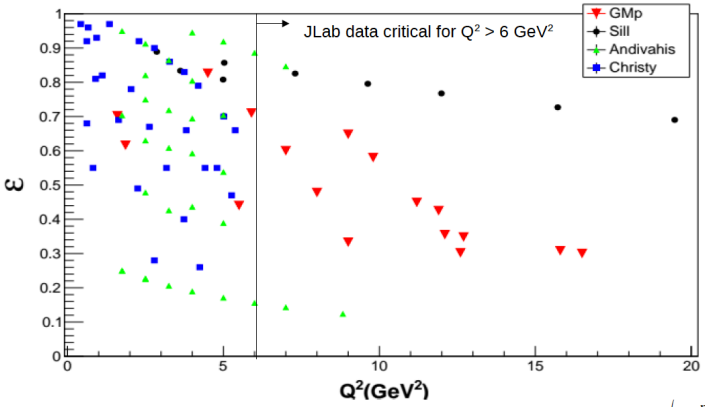

→ GMp12 data at much smaller ε than Sill data

$$\frac{d\sigma}{d\Omega} = \sigma_{Mott} \frac{\epsilon (G_E^p)^2 + \tau (G_M^p)^2}{\epsilon (1+\tau)},$$

- Less sensitivity to G_E in extracting G_M
- Lever arm in ε provides sensitivity to:
  - 2γ from global fit utilizing G_E / G_M from polarization transfer

GMp - E012-07-108 final cross sections

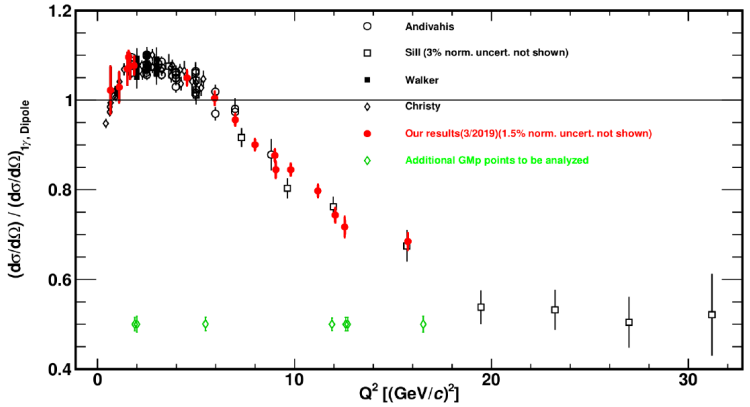

- Cross section relative to 1-γ cross section calculated with $G_E = G_M/\mu = G_{dip}$
- Significant improvement in precision for $Q^2 > 6$.
- Systematic uncertainties on Fall 2016 LHRS data ~1.3% (pt-pt), 1.5% (norm)
  RHRS (additional 2% from optics)

Impact of E12-07-108 data on G_E/G_M at large Q^2

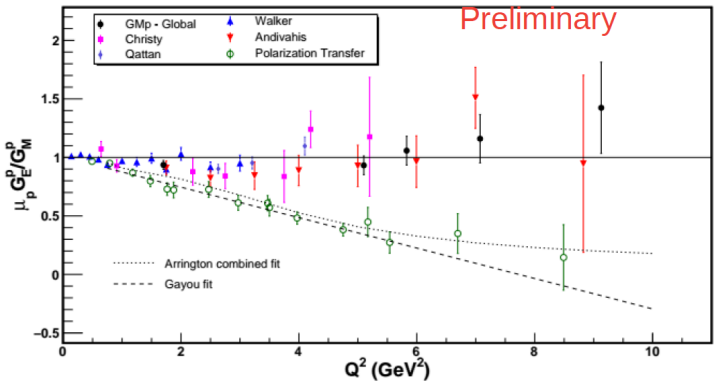

- Lab Hall A GMp12 data significantly reduce uncertainties on G_E/G_M at largest Q^2
  => further highlights discrepancy with P-T data up to $Q^2 > 9$
- Full data set provides significantly more sensitivity than shown in select L/T separations

How to reach higher Q^2?

- Increase beam energy → Increase kinematically accessible Q^2 range; increase cross section for constant Q^2
- Elastic ep cross section scales as $\sigma \approx E^2/Q^{12}$
- FPP efficiency is roughly Q^2-independent
- FPP analyzing power scales roughly as $\frac{1}{p_p} \approx M/Q^2$
- Statistical FOM scales as $NA_y^2 \approx E^2/Q^{16}$
- Increase beam polarization? 80%→100% would only increase FOM by 1.6
- Increase luminosity? Best possible at JLab 12 GeV ~ 10^{39} cm^{-2} s^{-1}; (factor of 2 above 6 GeV expt's).
- Most room for growth? →***Increase solid angle/Q^2 acceptance!***
  - **2X increase in target thickness and solid angle from 6→35 msr leads to ~30X gain in figure-of-merit**
- JLab PAC-approved G_E^p experiment: E12-07-109; 45 days in Hall A
  - $\Delta(\mu G_E/G_M)$ ~ 0.07 @Q^2 = 12 GeV^2
  - "High impact experiment" designation from PAC41 in 2013

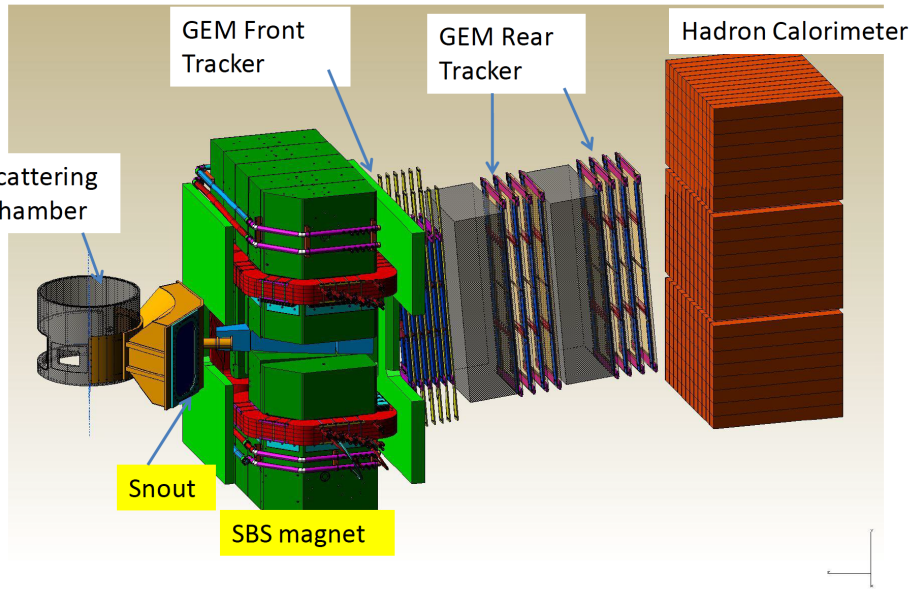

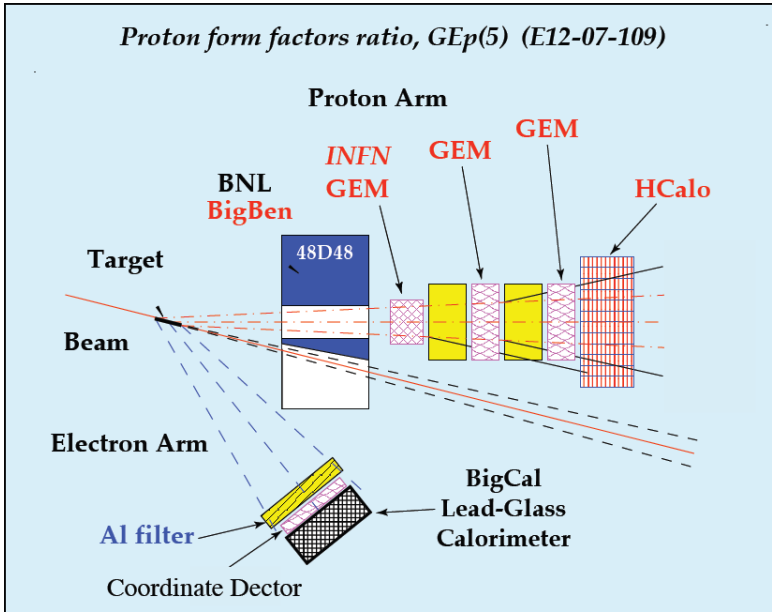

Statistical requirements: asymmetries vs. cross section measurements

Cross sections:

$$\sigma \propto N$$

$$\Longrightarrow \frac{\Delta\sigma}{\sigma} = \frac{1}{\sqrt{N}}$$

To measure a cross section with a relative statistical precision of 1%, you need 10,000 events.

Asymmetries:

$$\Delta A = \sqrt{\frac{1-A^2}{N}}$$

$$\frac{\Delta A}{A} = \sqrt{\frac{1-A^2}{NA^2}}$$

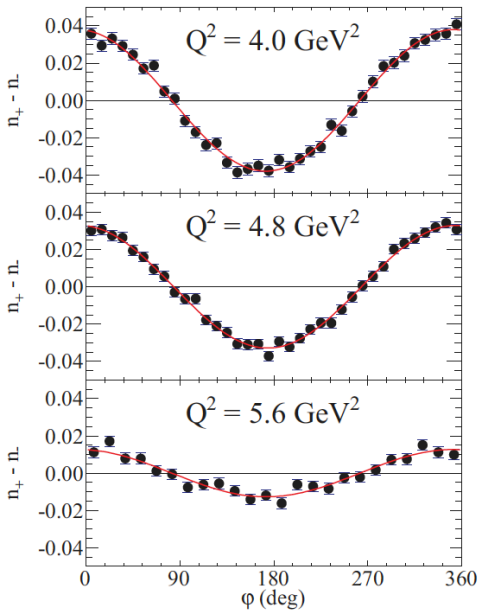

FIG. 6. (Color online) Focal-plane helicity-difference asymmetry $n_+ - n_- \equiv (N_{\text{bins}}/2)[N^+(\varphi)/N_0^+ - N^-(\varphi)/N_0^-]$, where N_{bins} is the number of φ bins and $N^{\pm}(\varphi)$, $N_0^{\pm}$ are defined as in Eq. (4), for the three highest Q^2 points from GEp-II. Curves are fits to the data. See text for details.

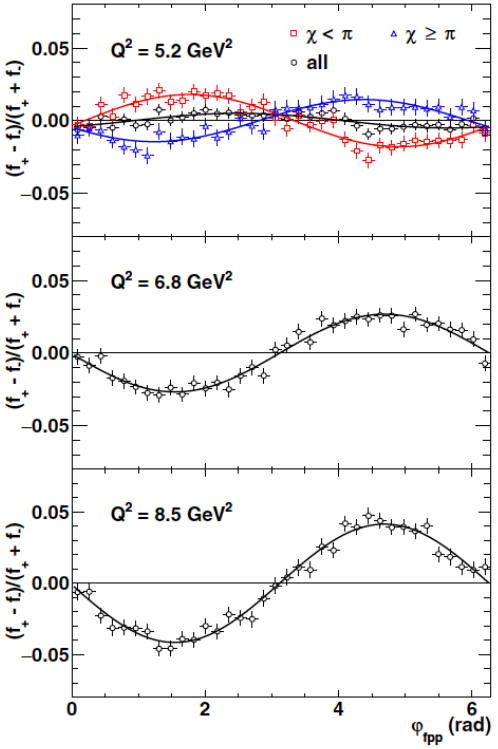

FIG. 10. Focal plane helicity difference/sum ratio asymmetry $(f_+ - f_-)/(f_+ + f_-)$, defined as in Eq. (20), for the GEp-III kinematics, for FPP1 and FPP2 data combined, for single-track events selected according to the criteria discussed in Sec. III B 2. Asymmetry fit results are shown in Table V. The asymmetry at $Q^2 = 5.2$ GeV^2 is also shown separately for events with precession angles $\chi < \pi$ and $\chi \geq \pi$, illustrating the expected sign change of the $\sin(\varphi)$ term.

- Typical asymmetry magnitude in a recoil proton polarimeter at ”high” momentum is ~few percent.
- For example: to measure a 5% asymmetry with a relative precision of 1%, one needs $N = 10{,}000 \times \frac{1-A^2}{A^2} \approx 4\times10^6$ events!

→ Asymmetry measurement must maximize beam and/or target polarization, and luminosity × acceptance!

The 12 GeV Upgrade of CEBAF

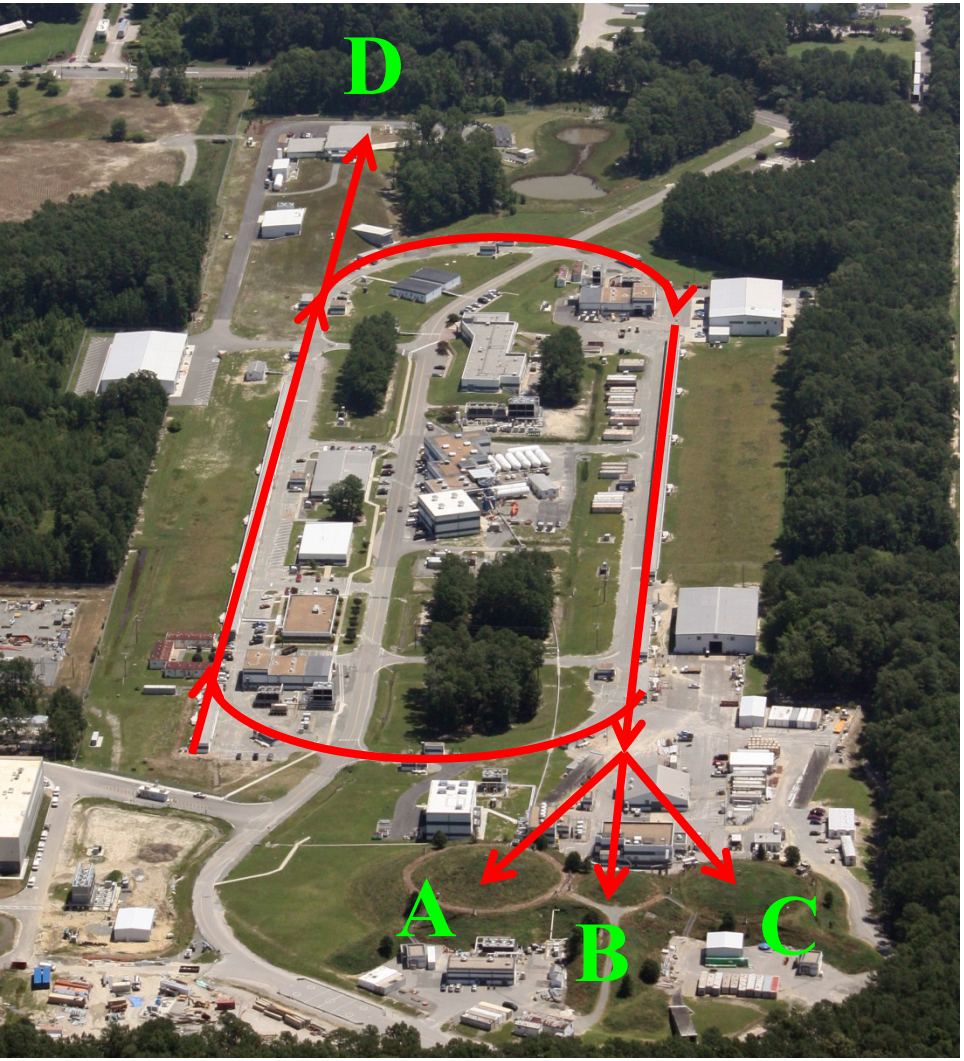

Site Aerial, June 2012

JLab 12 GeV Upgrade

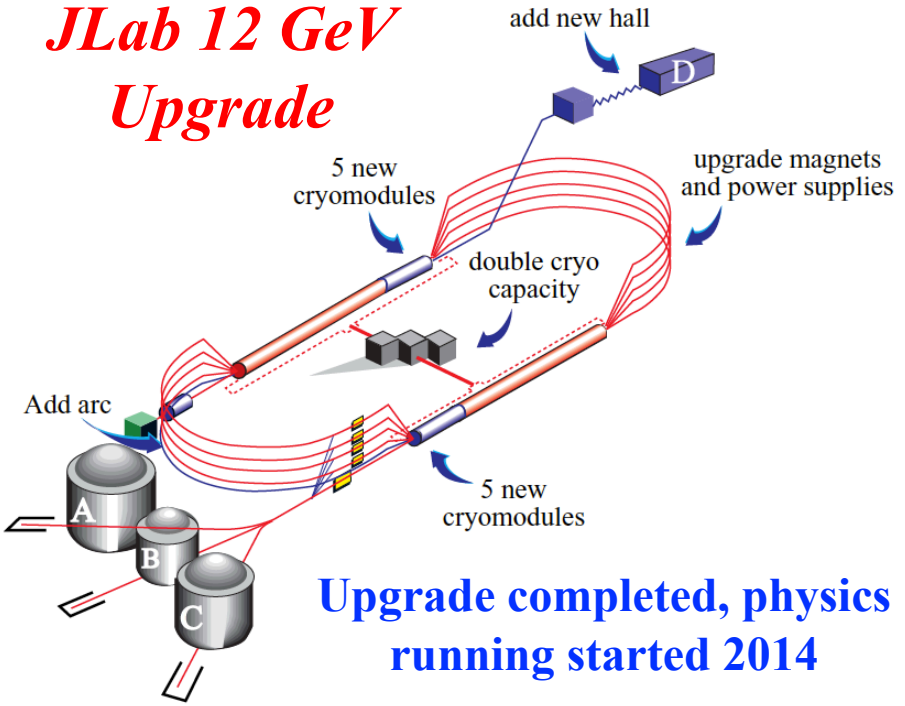

Upgrade completed, physics running started 2014

Seven-cell, High-Gradient Niobium SRF cavity for 12 GeV Upgrade

Electron Scattering Kinematics @11 GeV

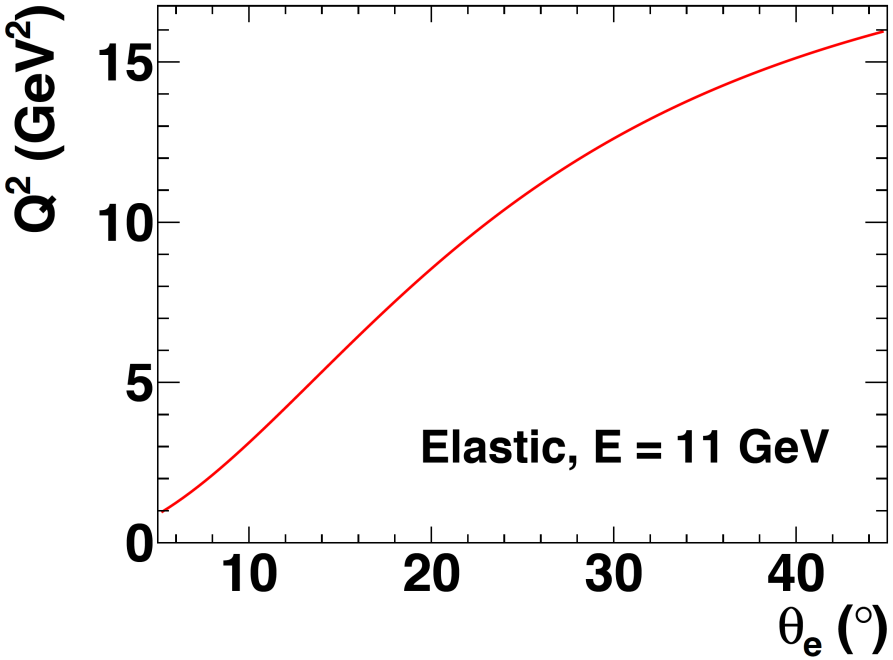

- Measurements of elastic FFs, SIDIS, DVCS, etc., involve coincidence N(e,e'X) (electroproduction) reactions, where X =
  - N' (elastic or quasi-elastic)
  - h (SIDIS or DVMP)
  - γ (DVCS)
- Virtual photon angle decreases as "inelasticity" increases:

$$Q^2 = 2M\nu x_{Bj}$$

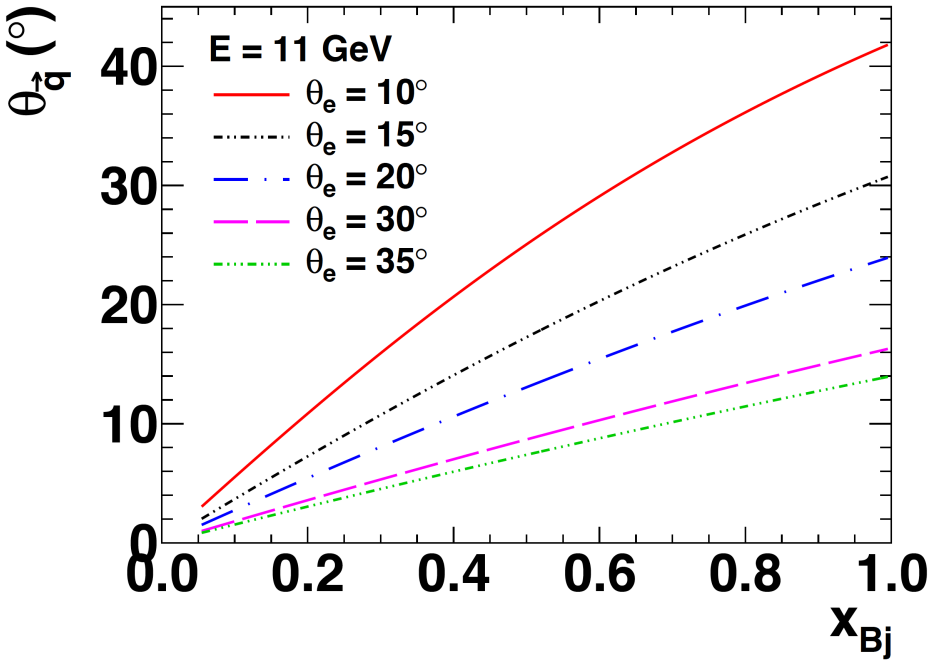

- Particles associated with the partonic (or other) degree of freedom that absorbed the virtual photon are found predominantly near the direction of the momentum transfer **q**
- ***Partonic interpretation of electron scattering data is accessible at large Q^2 → particles of interest are located at forward angles and high momentum***

The Super BigBite Spectrometer in Hall A

Proton form factors ratio, GEp(5) (E12-07-109)

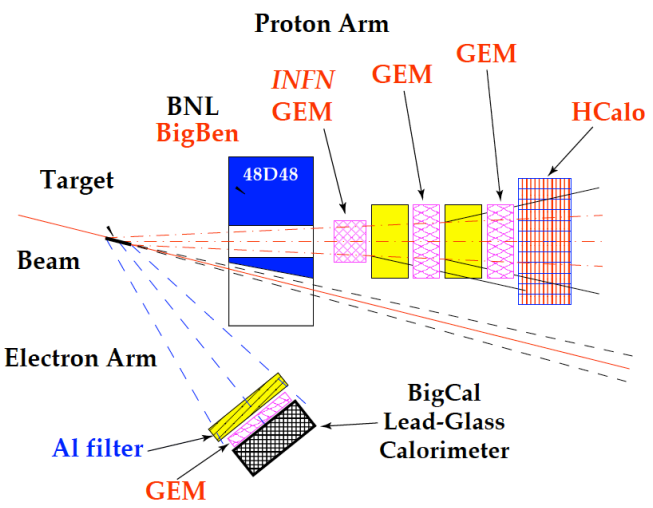

Neutron form factors, E12–09–016 and E12–09–019

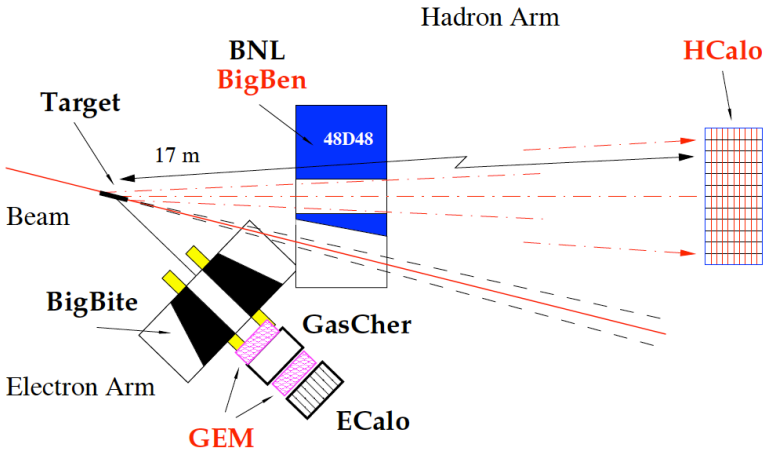

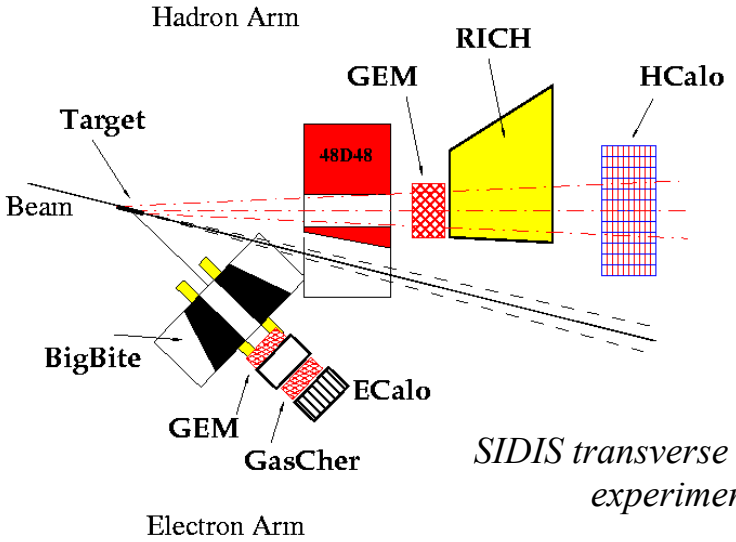

SIDIS transverse single-spin asymmetry experiment: E12-09-018

- What is SBS? → A 2.5 T*m dipole magnet with vertical bend, a cut in the yoke for passage of the beam pipe to reach forward scattering angles, and a flexible/modular configuration of detectors.
- Designed to operate at luminosities up to 10^{39} cm^{-2} s^{-1} with large momentum bite, moderate solid angle
- Time-tested "Detectors behind a dipole magnet", two-arm coincidence approach—historically most productive in fixed-target expts.
- ***Large solid-angle + high luminosity @ forward angles = most interesting physics!***

SBS Form Factor Program—Summary

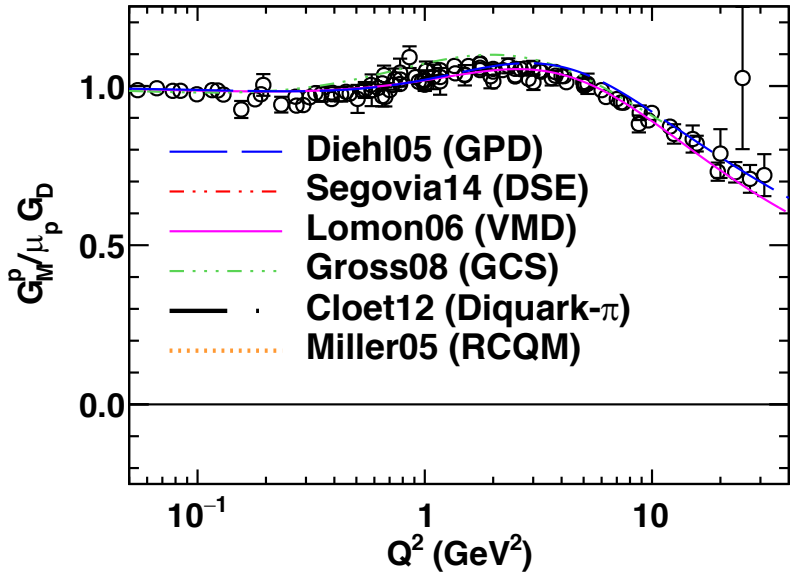

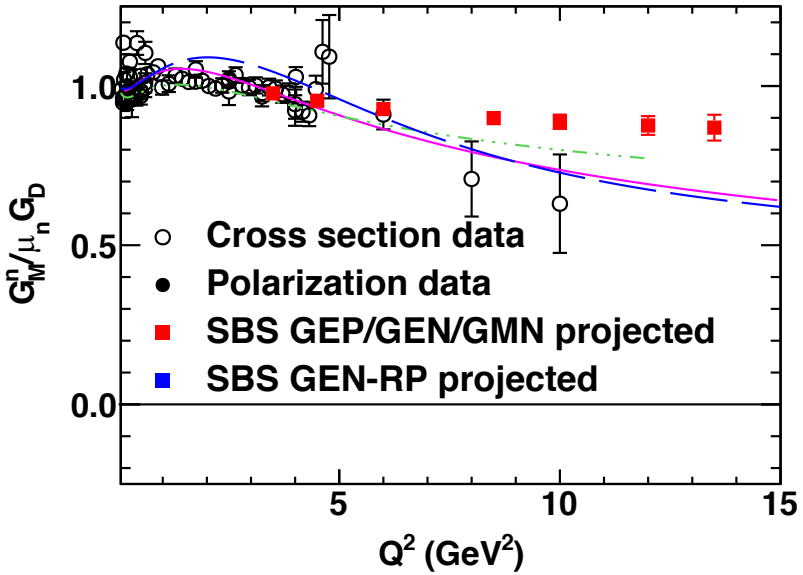

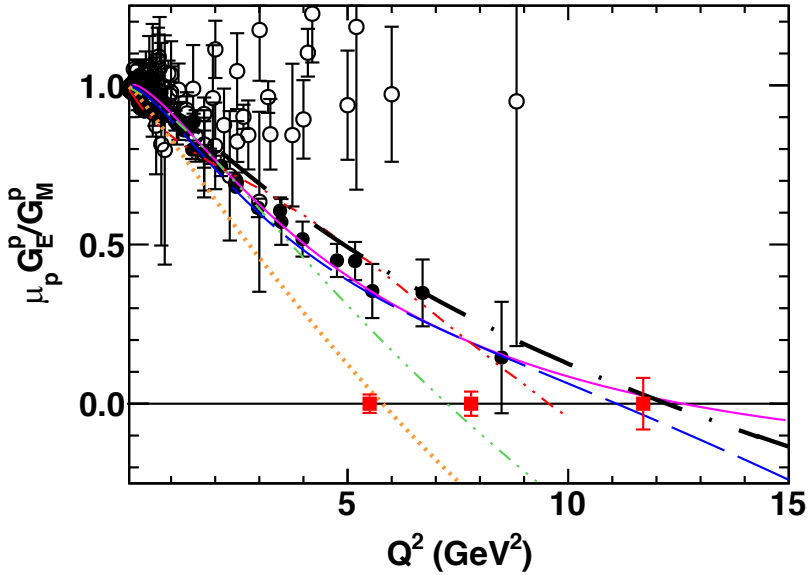

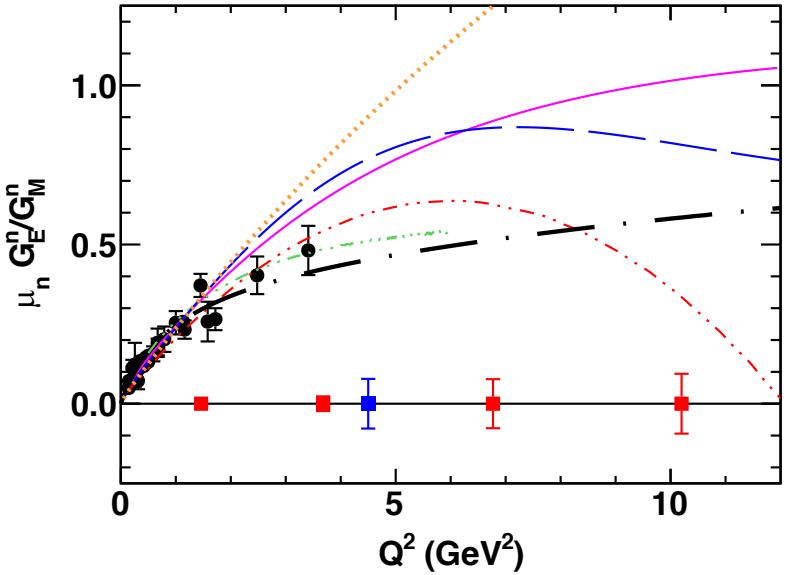

Experiment E12-07-109 (G_{Ep}/G_{Mp} at large Q^2)

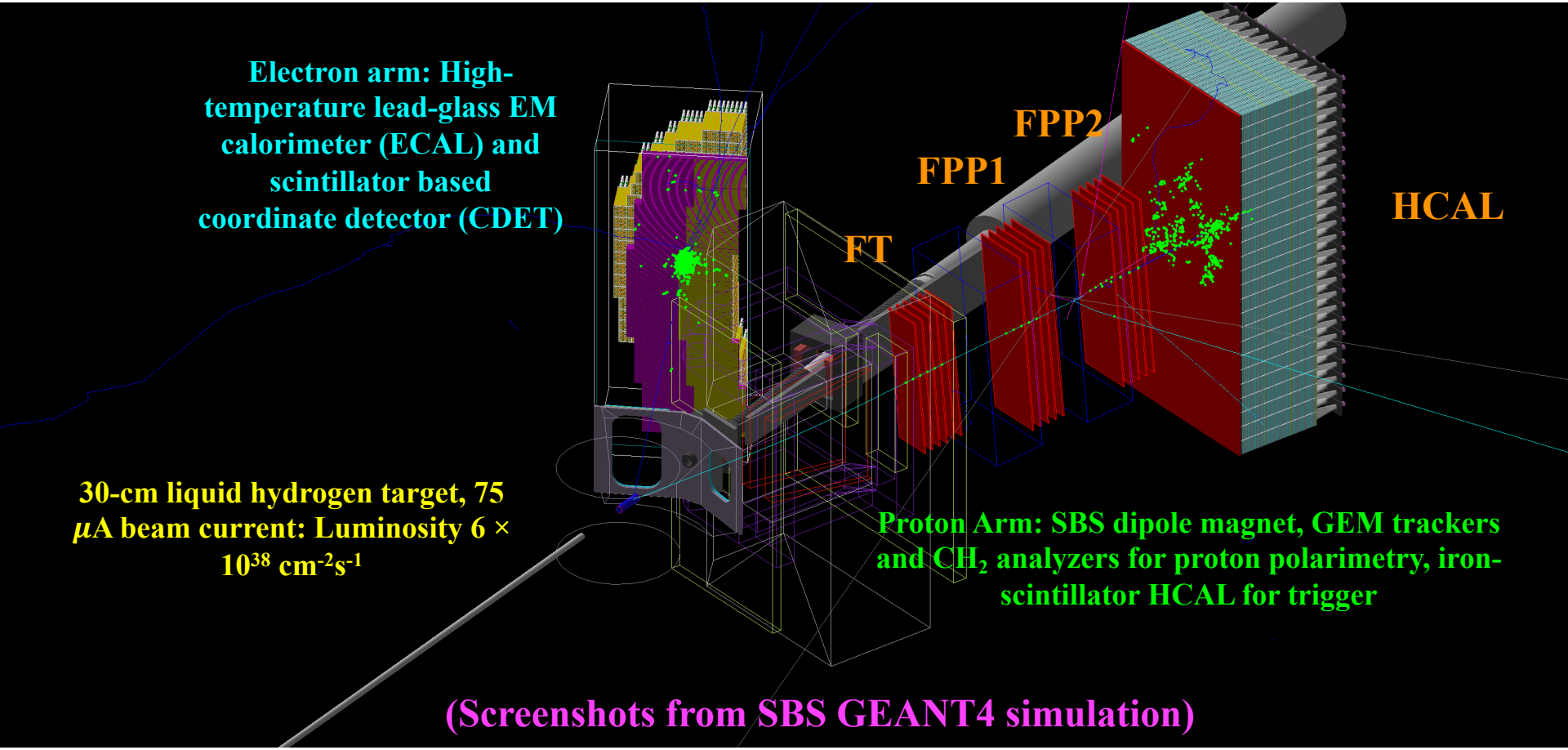

- Original motivation for SBS concept. Need large solid angle to overcome rapidly falling cross section at large Q^2 in elastic *ep* scattering.
- Lead-glass electromagnetic calorimeter to detect the scattered electron in coincidence; suppress inelastic backgrounds offline and also provide a selective trigger for high-energy electrons.
- **What's new (everything!): G_E^p recoil polarization firsts: a) "open geometry" spectrometer b) hadron calorimeter based trigger located *behind* proton polarimeter**

The SBS Hadron Calorimeter

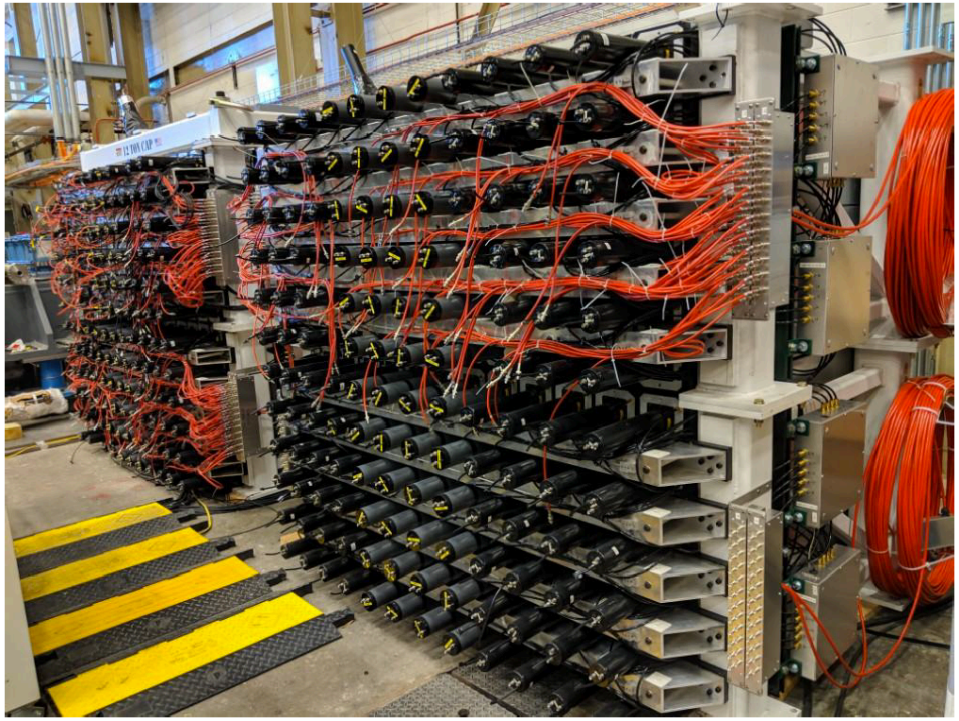

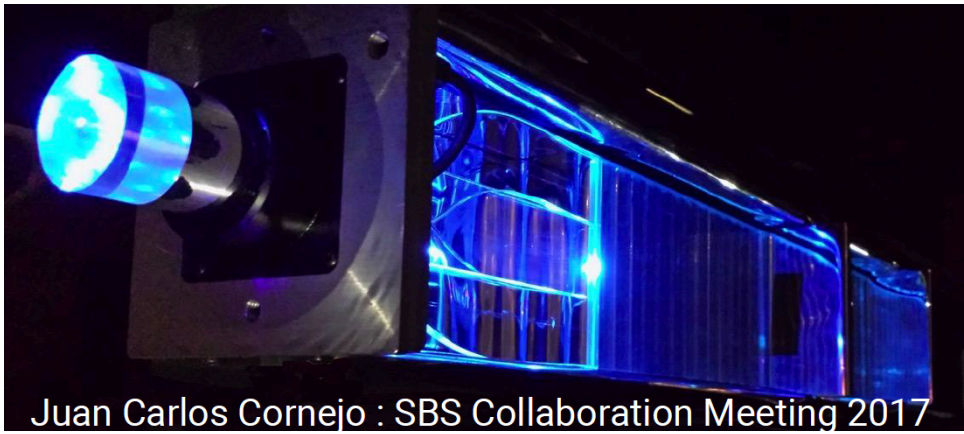

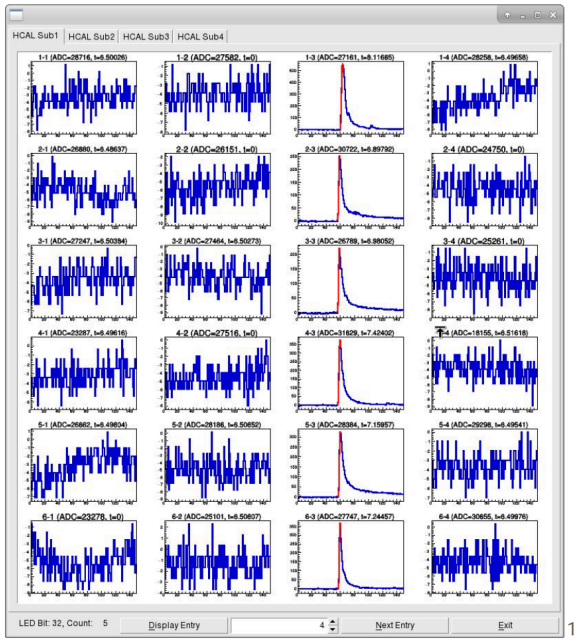

- Iron-Scintillator sampling calorimeter with high (and similar) efficiency for protons and neutrons, and other high-energy hadrons
- Threshold ~50% of mean elastic proton signal
- Used in all SBS experiments
- Important for trigger and constraining high-rate tracking in GEP

Cosmic ray tracks through HCAL

The High-Temperature ECAL (Proof of Concept)

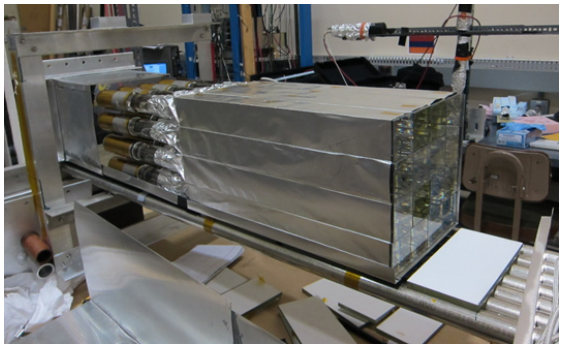

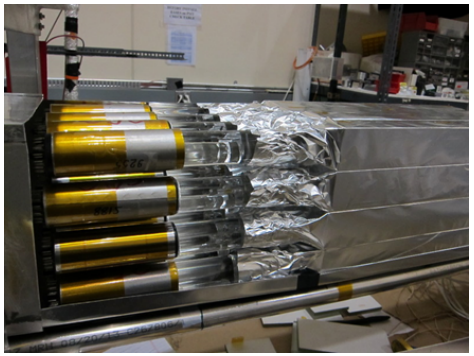

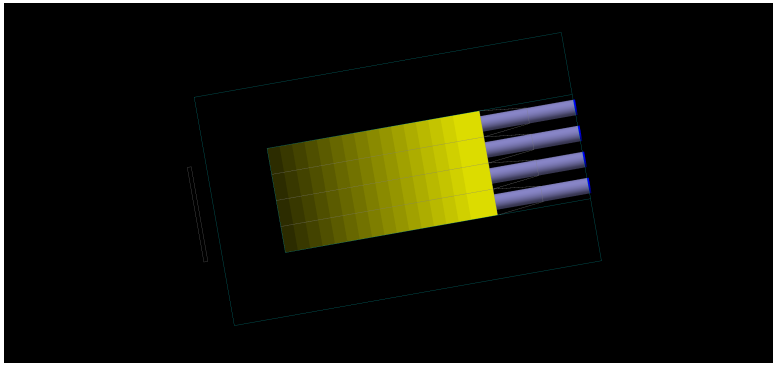

Figure 1 Photo of C16 lead glass blocks, light guide and PMTs.

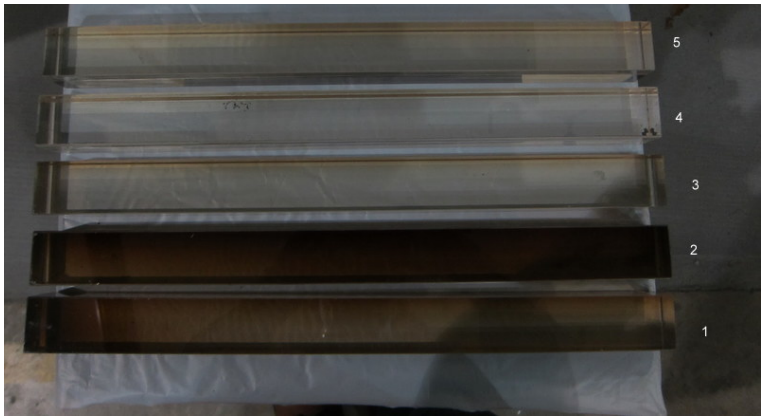

Figure 6 The lead glass blocks used to monitor the radiation dose after the C16 was placed at 10° and there was 20uA beam on the 15cm LH2 target. Block 1 was placed parallel to the C16 along the beamline side of the C16. Block 1 has damage at the front (left side of photo) and along the side. Block 2 was placed in front of the C16 and perpendicular to the front face. Blocks 3,4 and 5 were located at different locations on the spectrometer platform that was near 30°. These blocks show only moderate damage.

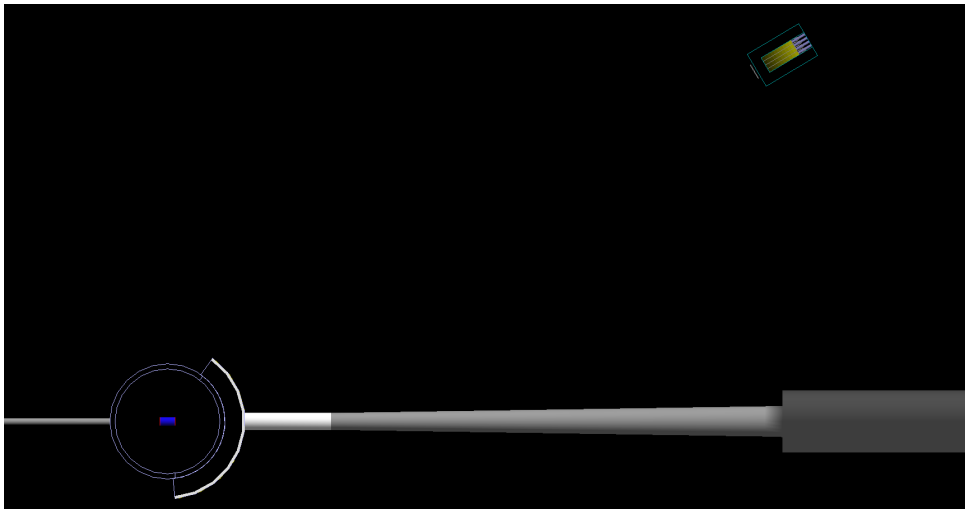

- 16-block thermal annealing prototype test in Hall A with 250 °C oven, 2015
- GEANT4 simulation with model for radiation-induced transparency reduction

Benchmarking Thermal Annealing Model

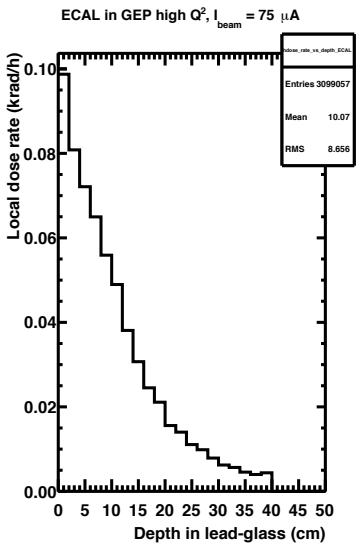

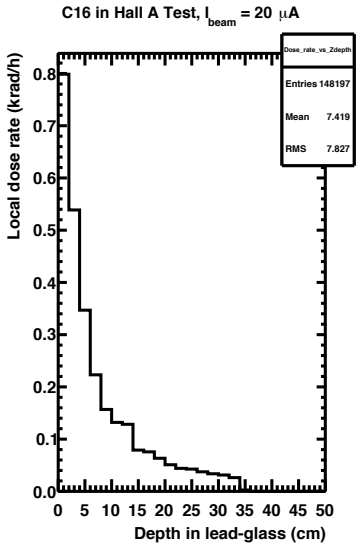

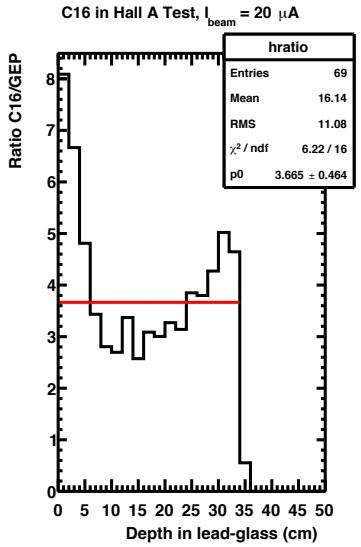

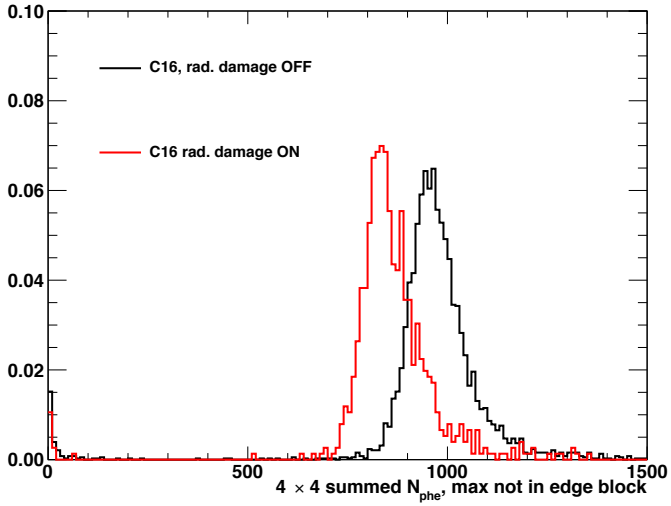

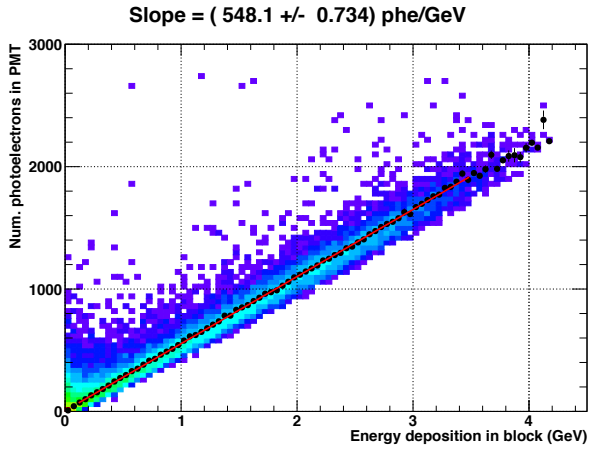

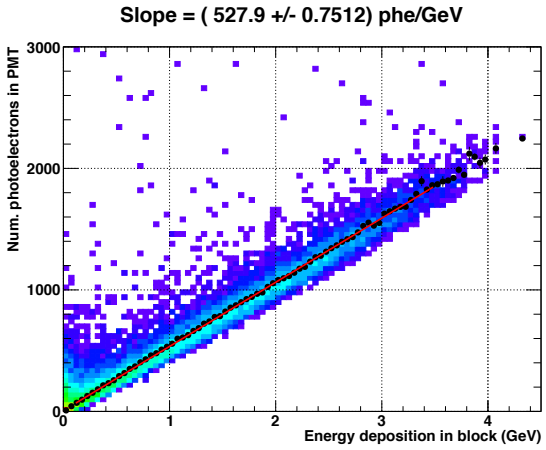

- Radiation dose rate during C16 test ~8X higher (at front of glass) than expected in GEP ECAL
- Radiation damage model calibrated to reproduce C16 test data.
- **Predicts equilibrium state during GEP of (96.3 ± 0.2)% of undamaged signal**

The High Temperature ECAL, I

Electron arm calorimeter in the model

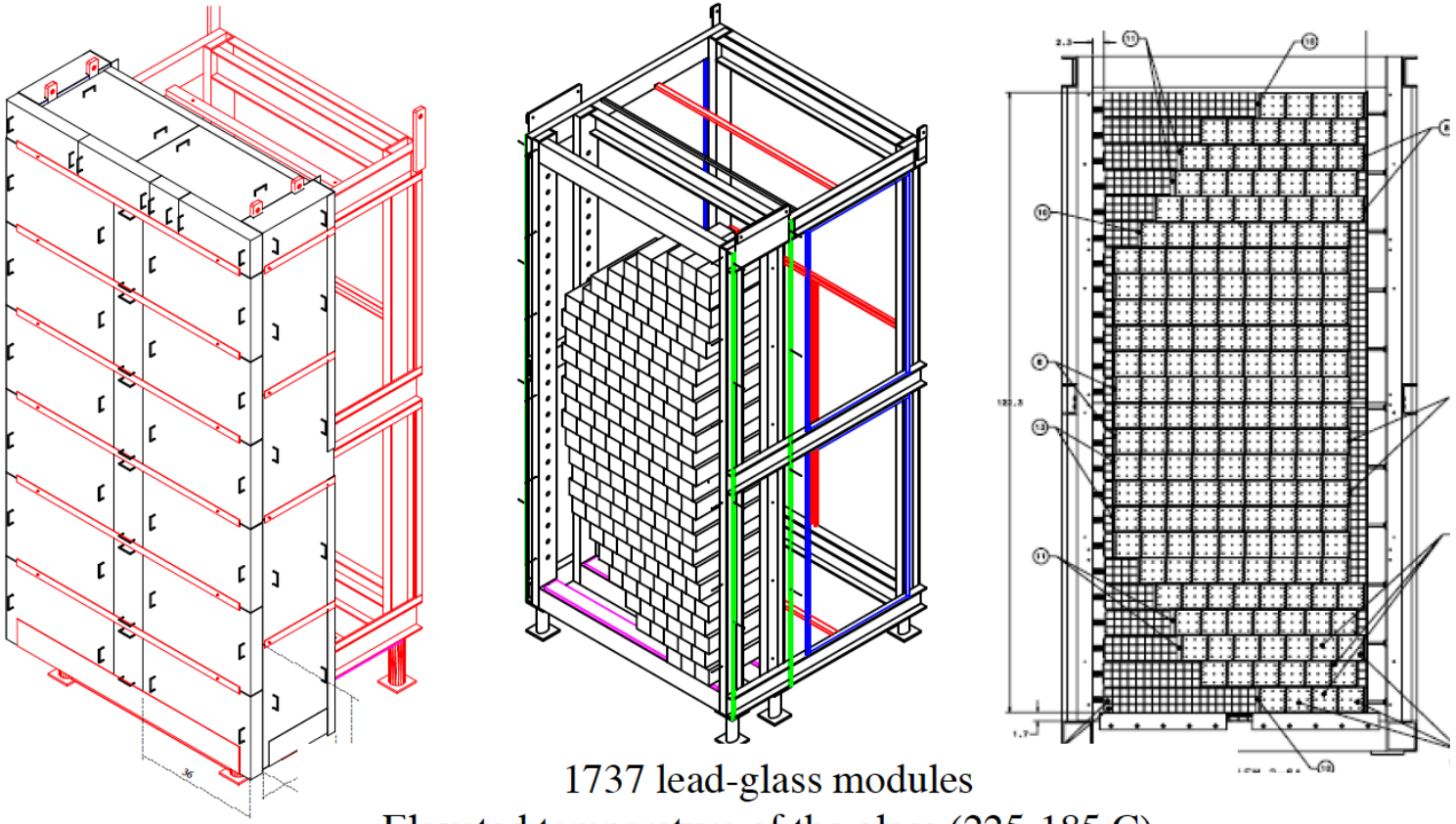

1737 lead-glass modules

Elevated temperature of the glass (225-185 C)

provides continuous annealing of radiation damage

The High Temperature ECAL, II

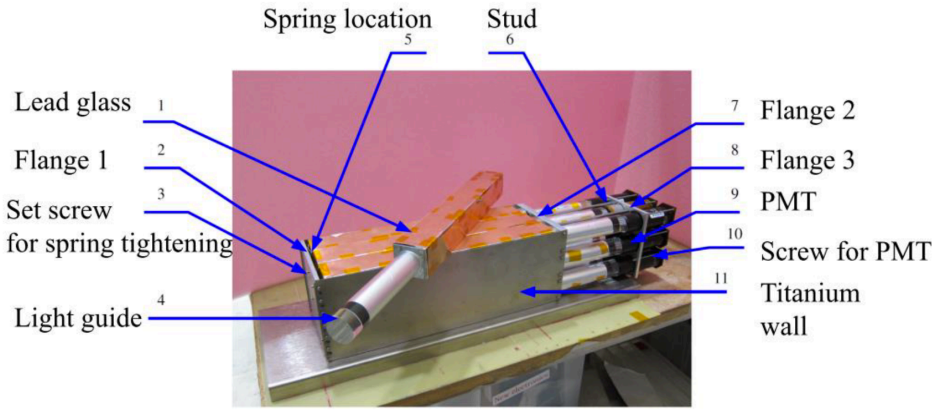

Work since Feb SBS meeting

- 126 of out 191 supermodules have been assembled
- JLab Detector Support Group is contributing manpower to assembling supermodules.

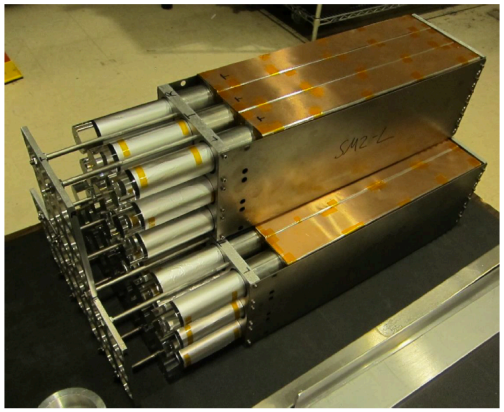

7

Electron arm: Calorimeter's temperature, 3x3 group

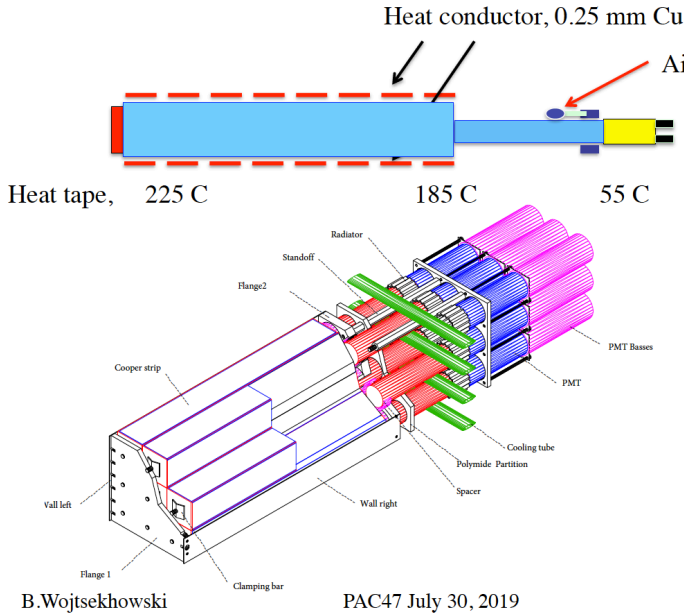

GEp/SBS B.Wojtsekhowski PAC47 July 30, 2019 23

- Contributions from: NCCU, JLab, YerPhi, SBU, UVA, JMU, UConn, Glasgow, INFN, CMU, NCAT
- NCCU received large NSF grant to design and construct ECAL oven

Logic of the GEp Trigger/DAQ, I: ECAL

- Trigger for GEP is based on exclusive two-body final state and total absorption calorimeters for both final-state particles, with high threshold
- Raw data rate dominated by ~150,000 individual GEM readout strips, each firing at high rate ("online" occupancy approaching 100%)
- Need as-selective-as-possible trigger, for inelastic background suppression but especially for data rate management.
- ECAL trigger is based on overlapping sums of 32 (4 horizontal x 8 vertical)
- High-temperature ECAL maintains stable energy resolution of lead-glass at $\frac{\sigma_E}{E} \approx 6\%$
  - →Trigger threshold as high as 80-85% of elastic electron energy (equivalent) at efficiency $\geq 95\%$
- Singles rate ~100 kHz

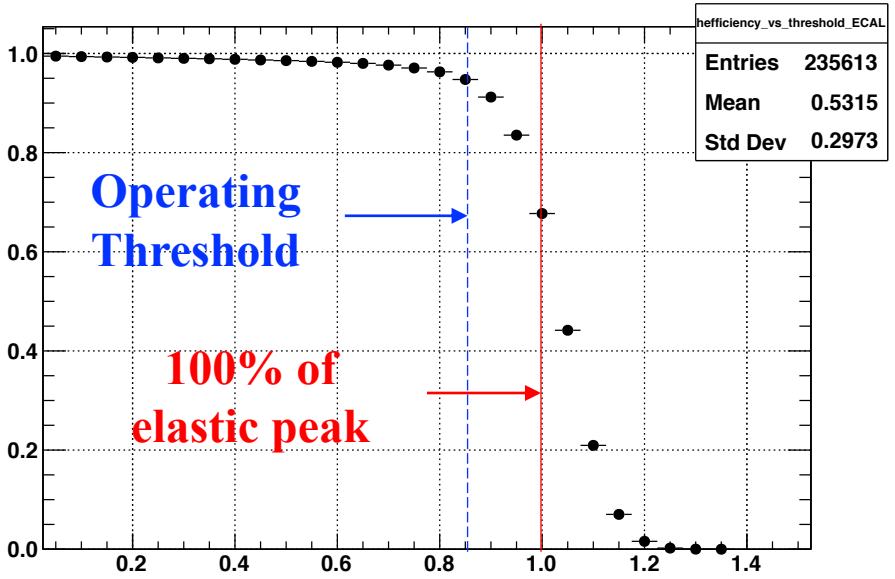

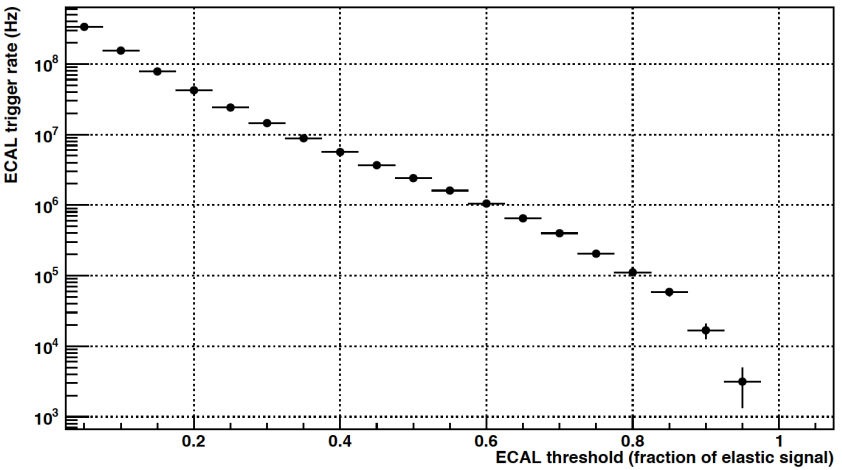

Logic of the GEP Trigger/DAQ, II: HCAL

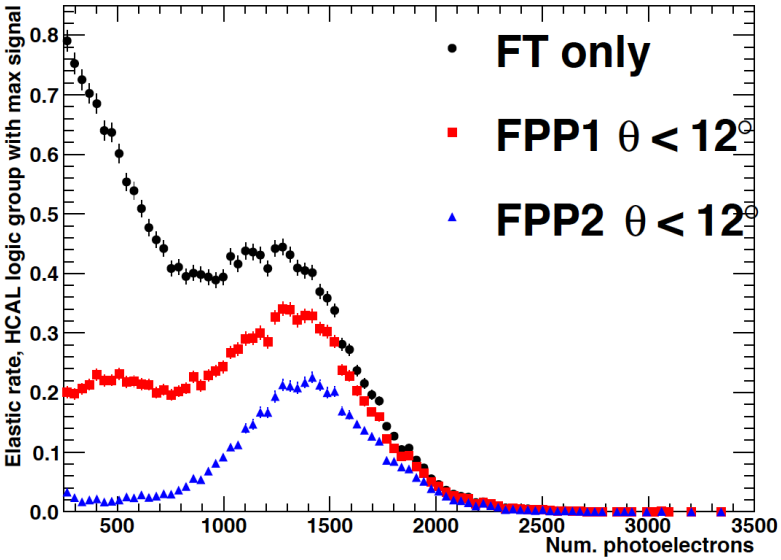

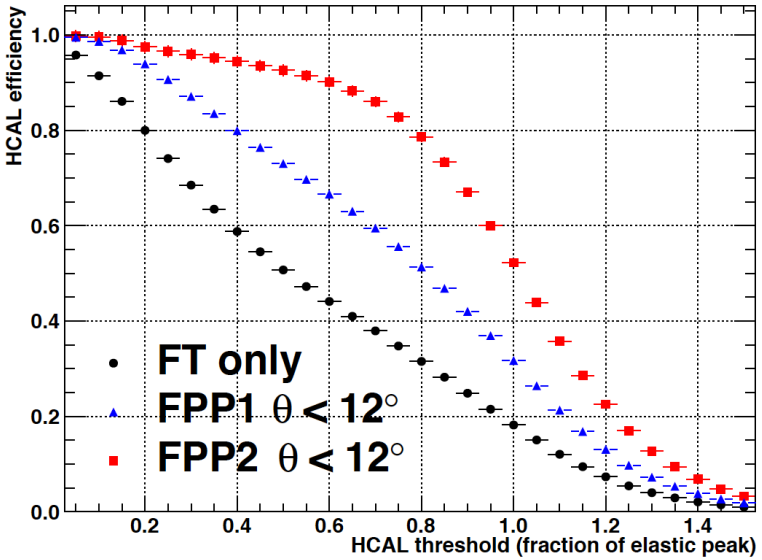

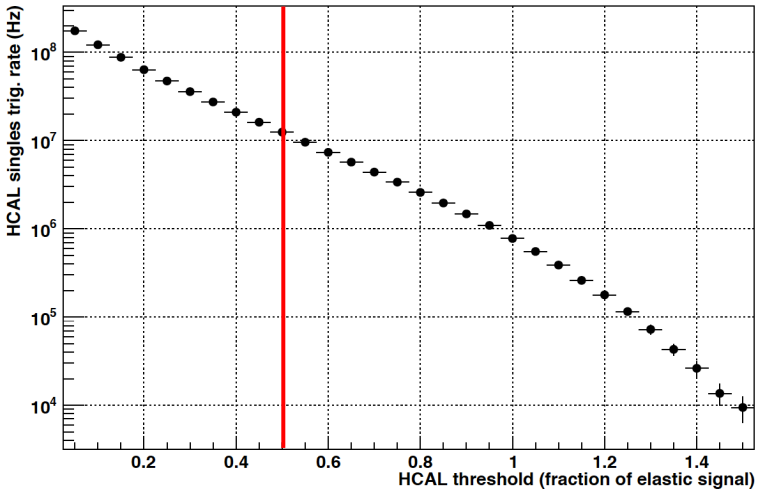

- HCAL single-arm trigger is formed from an "OR" of all possible (overlapping) sums of 4×4 modules (rate vs threshold below, left), ~10 MHz at threshold approximately 50% of average elastic proton signal (above, left)
- "Efficiency" for HCAL trigger (above, right) is complicated because it is located *behind* the proton polarimeter (GEM chambers plus CH_2 analyzers)
- Efficiency of HCAL trigger for events of interest for polarimetry is high (≥ 90%)
- HCAL trigger *may* actually *increase* polarimeter FOM by preferentially selecting events with high analyzing power:
  - See https://arxiv.org/abs/1908.06159

Logic of the GEP Trigger/DAQ, III: ”Level 2” coincidence

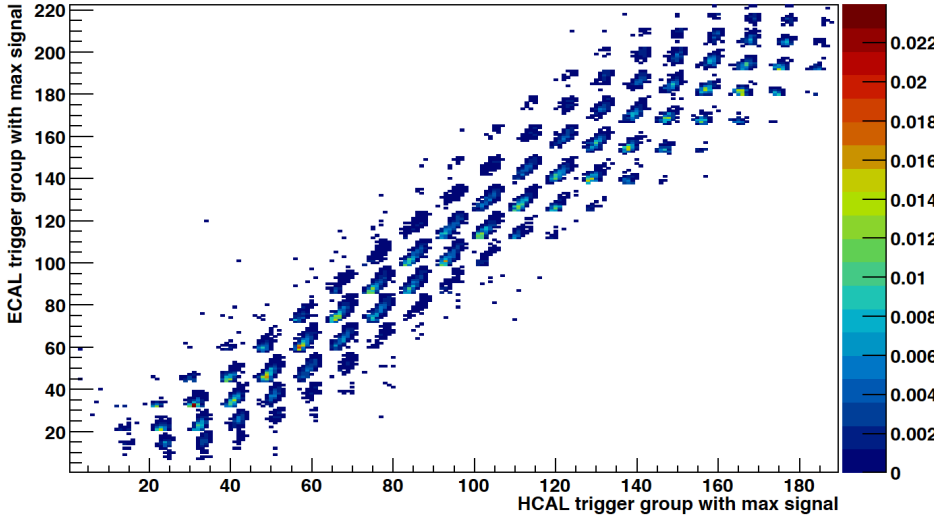

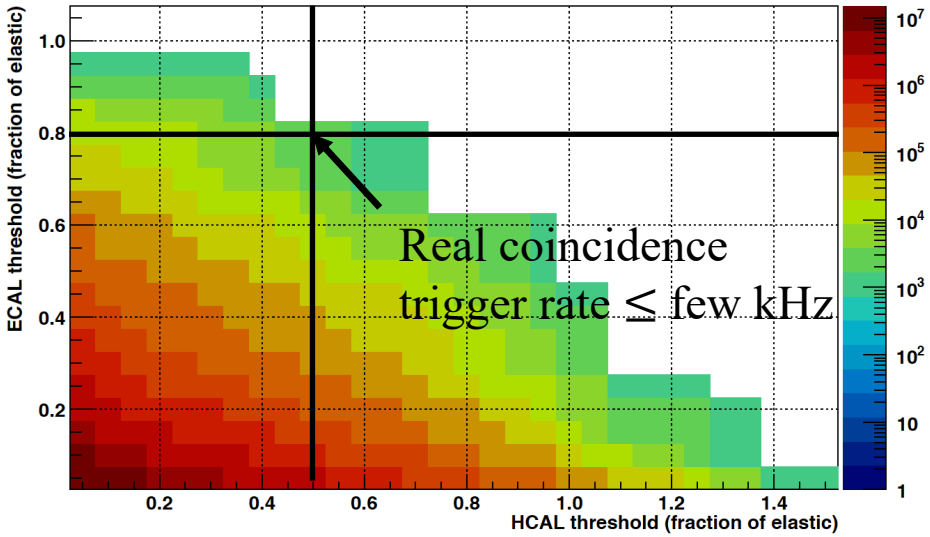

- To get from ~100 kHz ECAL single-arm trigger rate to <5 kHz event rate to disk/tape, we implement *ep* angular correlation in the coincidence trigger.
- To define the coincidence trigger logic, we simulate the single-arm trigger logic with elastic *ep* scattering events, and plot the correlation between the respective HCAL and ECAL sums with largest signals.
- We then create a look up table consisting of a list for each HCAL sum of all ECAL sums containing at least 0.1% of the total elastic yield (for that HCAL sum).
- The ”level 2” coincidence trigger then requires at least one ECAL-HCAL “match” above threshold within this lookup table.
- The “real” coincidence rate due to inelastic events with this logic is ~3 kHz at the nominal thresholds, with another 1-2 kHz of accidental coincidences for a 30-ns coincidence timing window

Gas Electron Multipliers (GEMs): High-Rate, High Resolution Charged-Particle Tracking

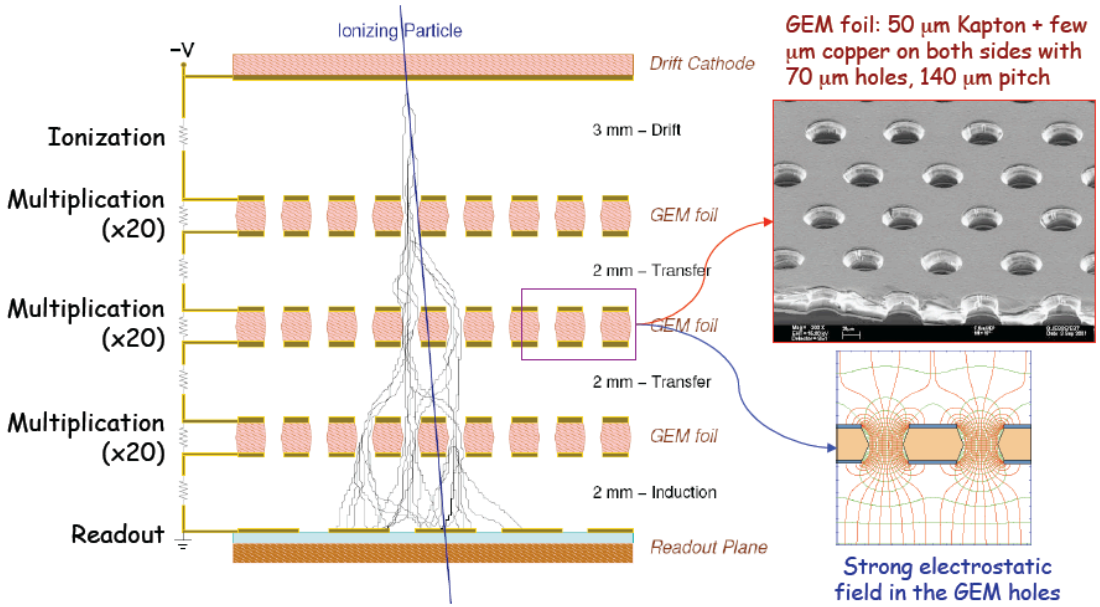

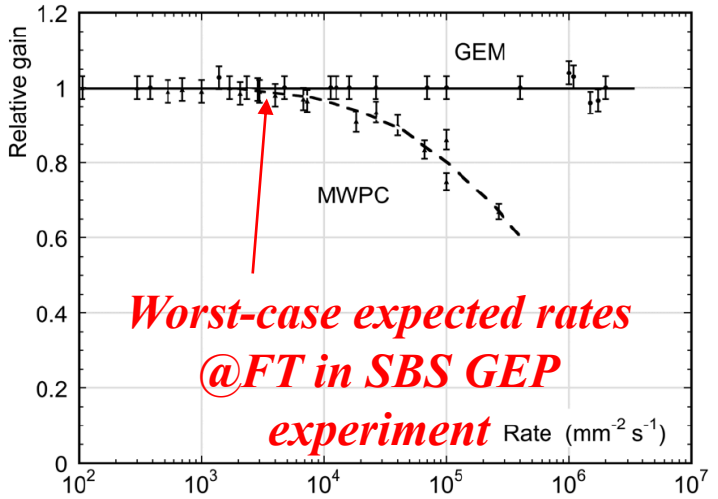

Figure 28.9: Normalized gas gain as a function of particle rate for MWPC [70] and GEM [84].

Stable gain up to very high rates

Recent technology: F. Sauli, NIM A 386, 531 (1997)

- High spatial granularity
- Ability to cascade several foils: higher gain at lower voltage, reduced discharge risk
- Readout and amplification stages decoupled—XY and/or UV readout strips—pitch 400 μm
- Spatial resolution ~70 μm
- "Fast" signals (for gas ionization detector): intrinsic time resolution <10 ns; arrival time spread ≈ 60 ns for 3-mm gap
- **Enabling technology for SBS physics program!**

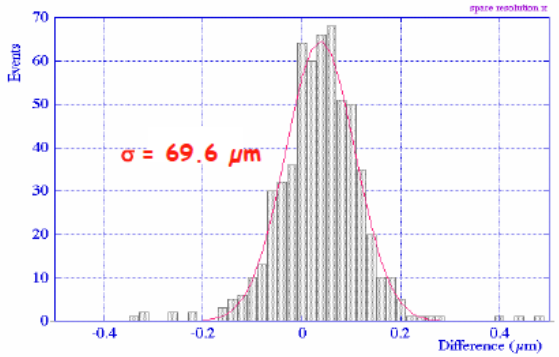

Space resolution

Front Tracker and Polarimeter GEMs (INFN+UVA, others)

SBS trackers/polarimeters:
Front tracker: INFN/UVa

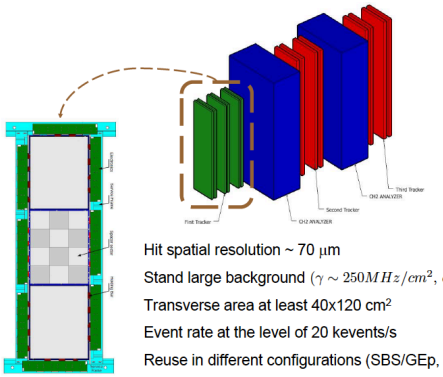

Hit spatial resolution ~ 70 μm
Stand large background ($\gamma \sim 250 MHz/cm^2$, $e + \pi \sim 160 kHz/cm^2$)
Transverse area at least 40x120 cm^2
Event rate at the level of 20 kevents/s
Reuse in different configurations (SBS/GEp, BigBite/GEn …)

GEp/SBS B.Wojtsekhowski PAC47 July 30, 2019 13

SBS trackers/polarimeters:
Rear tracker: UVa/INFN

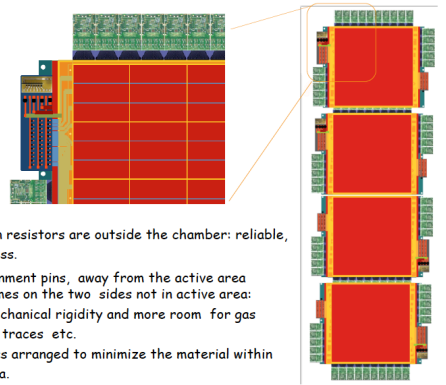

- Protection resistors are outside the chamber: reliable, easy access.
- Large alignment pins, away from the active area
- Wide frames on the two sides not in active area: better mechanical rigidity and more room for gas inlets, HV traces etc.
- Electronics arranged to minimize the material within active area.

14

GEM Front Tracker / Cosmic Setup

Nov/18 →

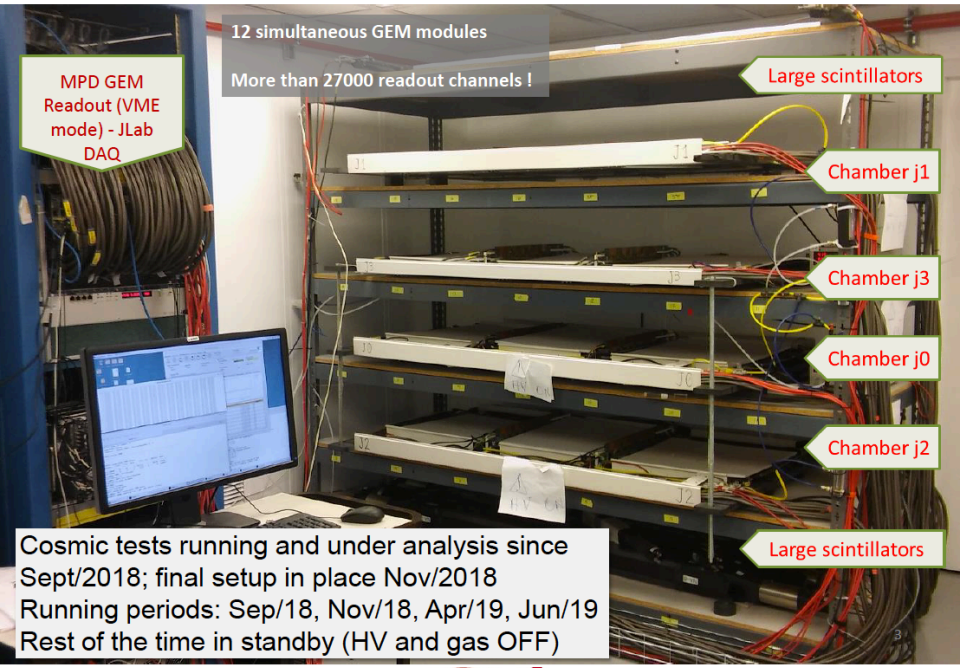

UVa GEMs: Cosmic Setup in EEL124

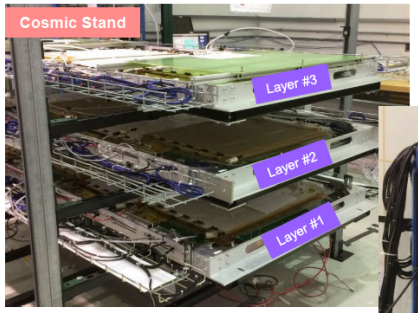

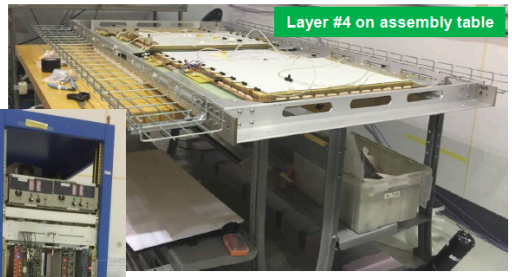

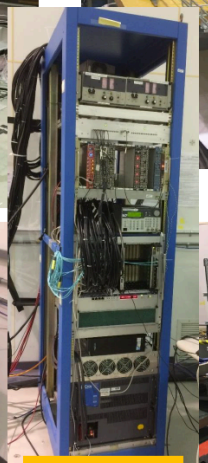

8/6/2019 SBS Coll. Meeting @ JLab 6

The tracking challenge at high-luminosity in open geometry: a taste

Reminder: GEM analysis software

* Primary deployed algorithm using recursive TreeSearch (raw combinatorics also employed for some analyses)
* GEMs provide six time samples over 25ns bins with jitter
* Hits are differentiated by fitting to spatial and temporal components
* Require amplitude matching between x-y components to obtain full 3D reconstruction
* General restrictions are placed on search areas based on other detector knowledge
* Basic multithreading implemented

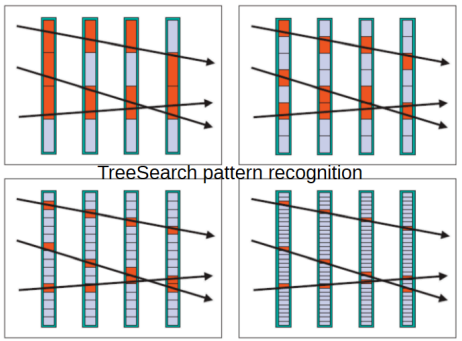

TreeSearch pattern recognition

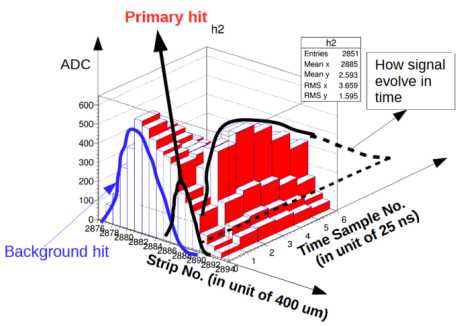

Plot credit : Danning Di

Presented at Nov Review

GEM Tracking – GMn

- Since 2016
  - Improved GEM response and validation based on data from constructed GEMs
  - Observe larger and wider background response
- Event reconstruction at
  - 70% tracking efficiency (2020 goal 80%)
  - 3 Hz (2020 goal 8Hz)
- Continuing to evaluate better separation of broad ADC clusters

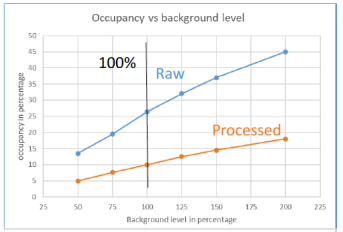

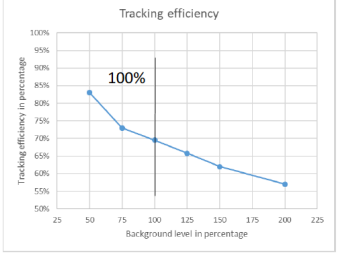

11

- In all the SBS experiments, detectors are located in field-free regions behind large dipole magnets with vertical bend*.
- Magnets shield detectors from low-energy *charged* backgrounds, BUT:
- Large flux of low-energy photons into GEMs—can convert in GEMs via Compton/photoelectric effects, pair production.
  - Secondary electrons from soft photon interactions ionize GEM gas, give high rate of background hits: ~0.4 MHz/cm^2 at $Q^2 = 12\ GeV^2$ in the GEP measurement
- *--except GEP electron calorimeter, which is mainly sensitive to high-energy particles

Logic of the High-Rate Tracking in GEP

- Random soft photon background hit rate of ~400 kHz/cm^2 leads to high "raw" occupancy of GEM readout strips due to ~200 partially overlapping background hits/GEM module/event within 150 ns sampling window
- Six ADC samples/strip at 25 ns/sample, with APV25 pulse shaping electronics:
  - Intrinsic GEM timing resolution ~10 ns
  - Intrinsic GEM spatial resolution ~70 μm
- The charge from primary signal hits is collected in an area of approximately 3 mm^2 and produces signals on 2-3 readout strips in both X and Y directions:
  - Within this 2D area, the probability for a random background hit to overlap with a signal hit within the acquisition window of an event is ~0.2%
  - **However, because we have strip readout and not pixel readout, a large fraction of strip signals will be partially contaminated/distorted by background hits in other areas of the GEM→ biggest challenge in reconstruction!**
  - Exploit pulse shape from six-sample readout and XY ADC correlation to suppress background hits
  - Machine learning application?

Exploiting the electron arm information

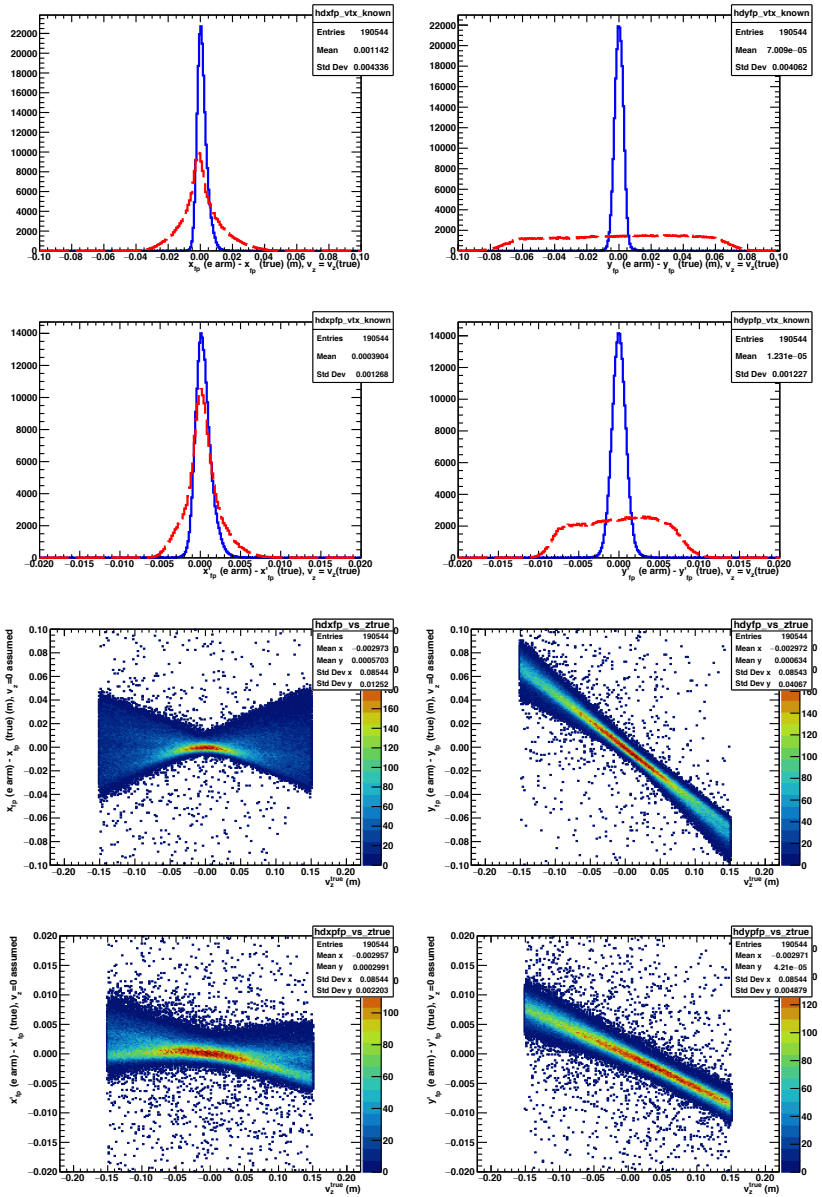

- Measurement of electron kinematics drastically narrows the allowed search region for proton tracks
- Because our ECAL has no magnets/tracking, it does not constrain the interaction vertex directly.
- Precise vertical coordinate determination with "CDET" constrains azimuthal angle of the reaction plane very well.
- Without knowing the interaction vertex *a priori*, the ECAL+CDET defines an allowed search region at the front tracker of $\mathbf{4\ cm\ (vertical)}\times$ $\mathbf{8\ cm\ (horizontal)}$, and determines the slope of the proton track to within $\mathbf{\pm 10\ mrad}$ in both directions (minimum horizontal size limited by the 30-cm target thickness)
- If the vertex is known, ECAL+CDET confines the proton track to within a $\mathbf{\sim 1\ cm^2}$ area and the direction to within $\mathbf{\pm\ 3\ mrad}$ in both directions.
- Tracking strategy involves scanning the assumed vertex location along the target thickness and searching for tracks in a restricted area within each z bin consistent with elastic kinematics. Kinematic fitting is also being evaluated to enhance signal/background ratio

Elastic event selection—Rejecting inelastic backgrounds

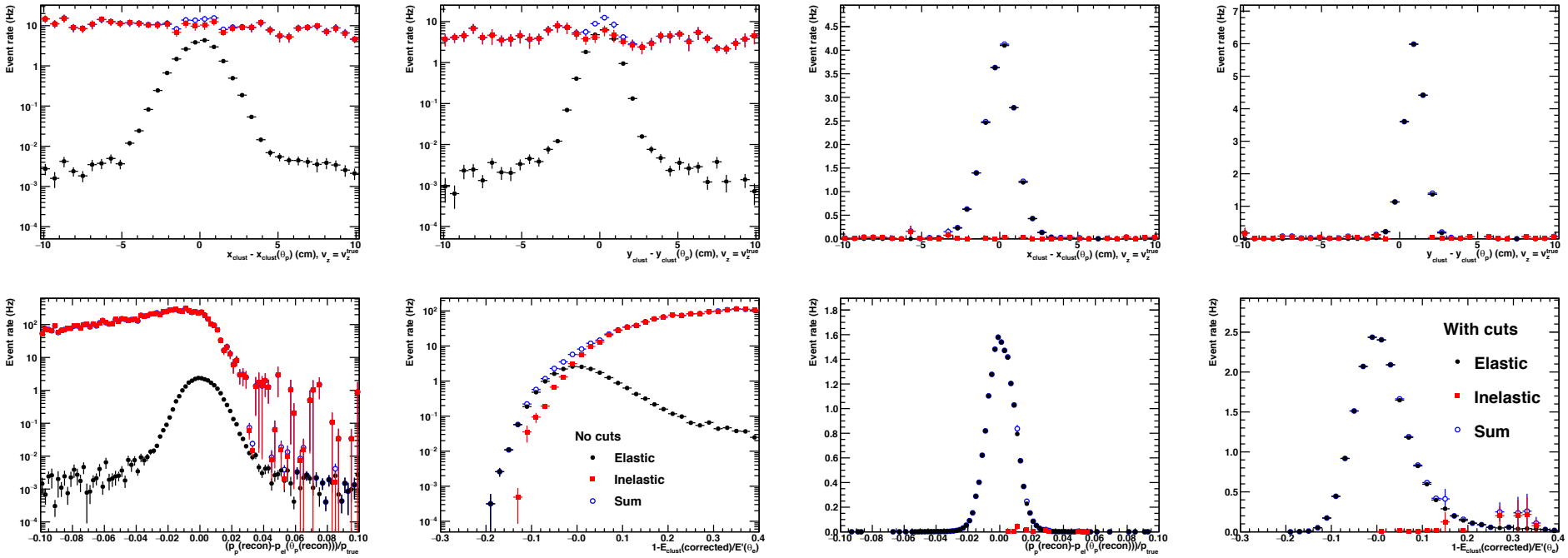

- High rate of inelastic background events will be present in the data, even at high thresholds
- Not many of these inelastic events will actually be reconstructed, since tracking will only even be attempted within a narrow region consistent with elastic kinematics for the detected electron
- Even if these events *were* reconstructed, the combined SBS+ECAL resolution plus exclusivity cuts would suppress inelastic background to <1% (less if kinematic fitting used).

Polarimetry—Spin Transport

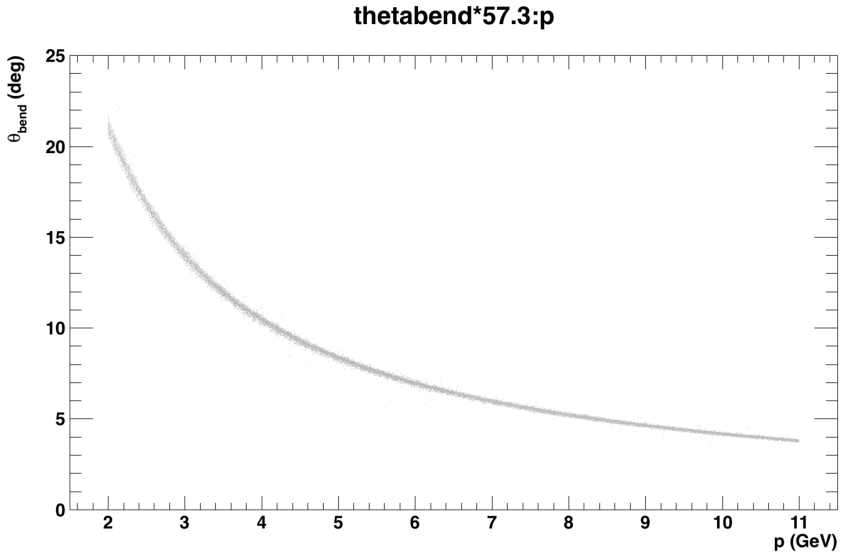

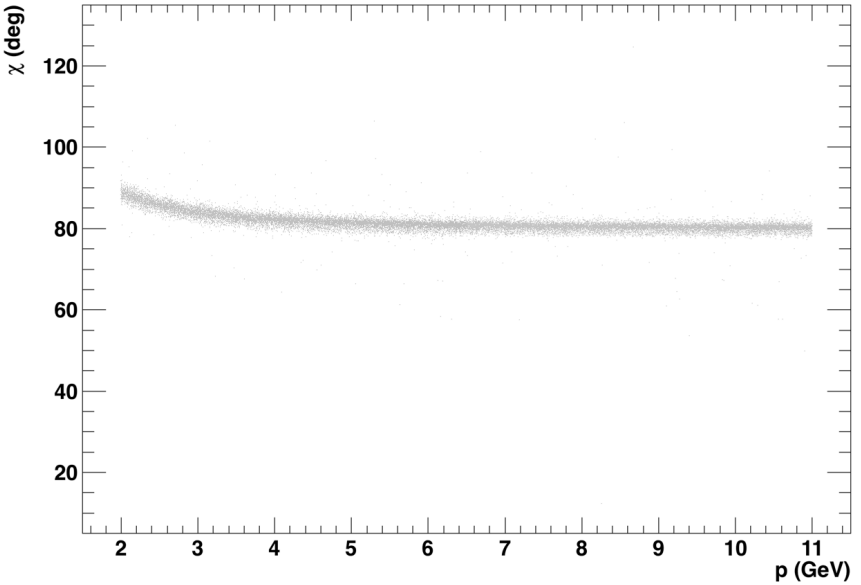

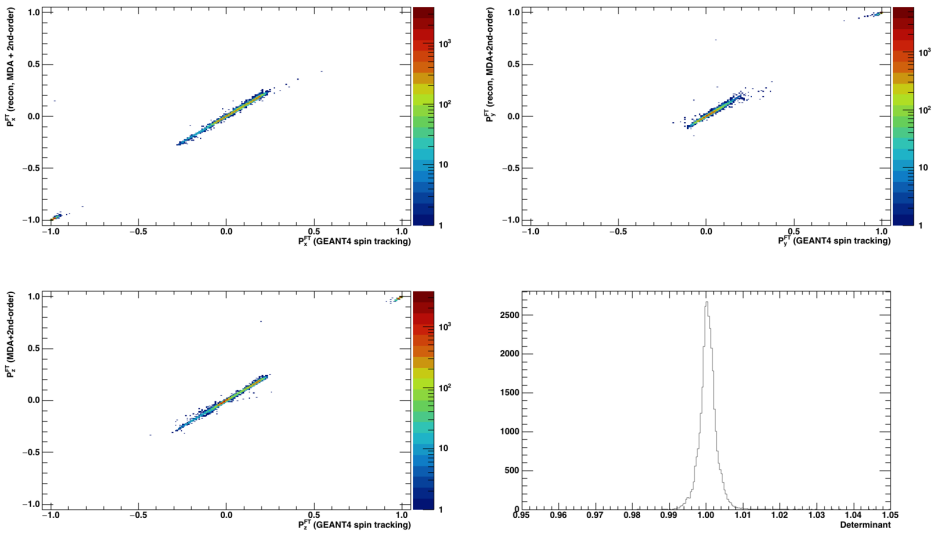

- SBS spin transport is much simpler than in previous experiments—simple, non-focusing dipole magnet
- Precession angle $\chi = \gamma \kappa_p \theta_{bend}$ is approximately constant within acceptance
- Fit of full spin tracking to 2nd-order expansion of the deviations from ideal dipole approximation converges—only 15 parameters per rotation matrix element

Polarimetry—Efficiency and Angular Distribution

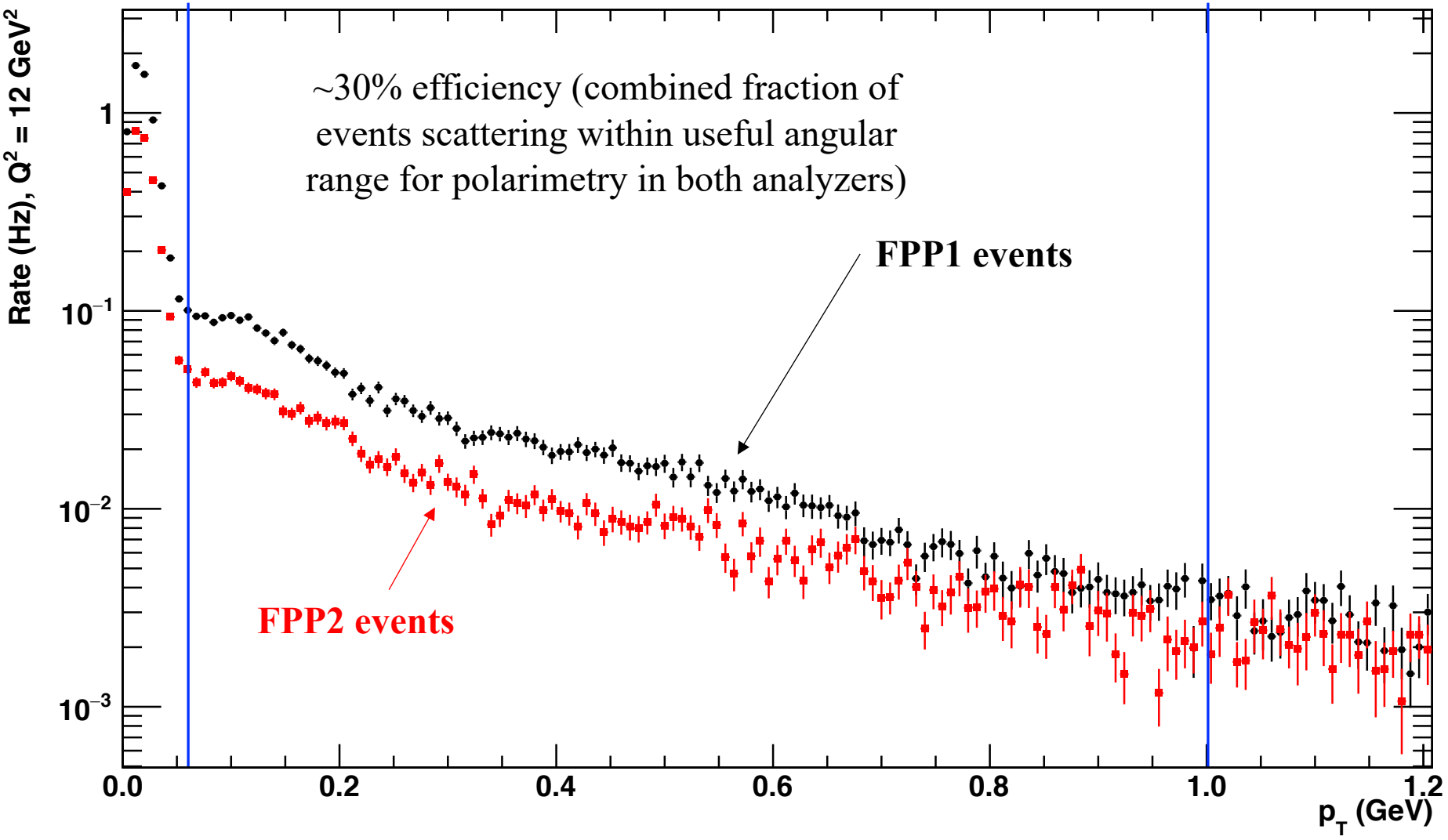

$$p_T = p_p \sin \vartheta_p$$

Polarimetry– $p + CH_2$ analyzing power

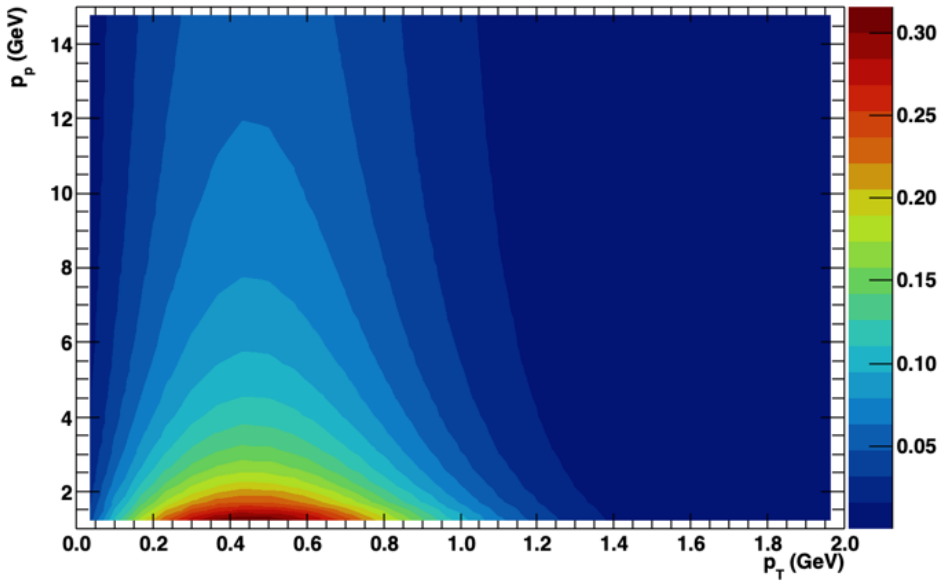

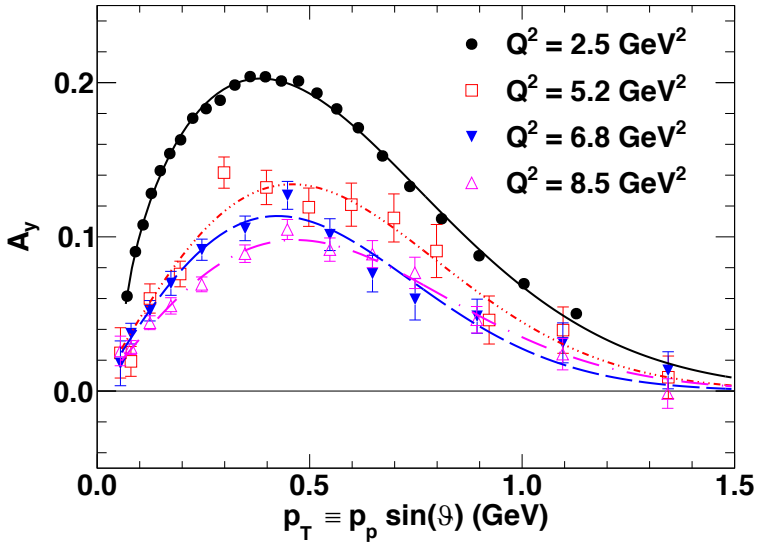

- From previous experiments, we know that the analyzing power angular distribution has roughly the same shape as a function of $p_T = p_p \sin\vartheta$, with the maximum and average analyzing power decreasing as p_p^{-1}.
- Expected average analyzing power based on modest extrapolation to SBS proton momentum from GEp-III results (shown at right) is ~5.6%
- Analyzing power in elastic *ep* scattering is ”self-calibrating

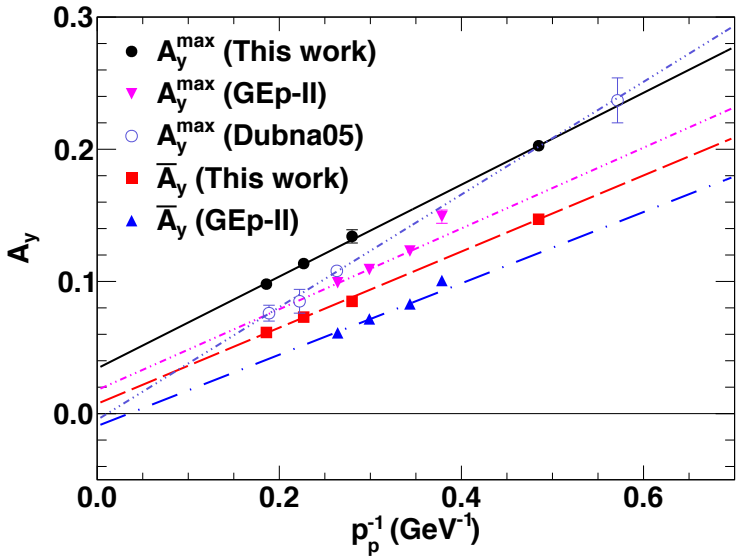

Polarimetry—Figure-of-Merit Assumptions

- 75 μA beam
- 30 cm LH_2 target
- 85% beam polarization
- SBS dipole field strength scaled with proton momentum
- Analyzing power based on parametrized angular and momentum dependence from GEp-III data (modest extrapolation in momentum)

$$\mathcal{F} \equiv \sum_{i=1}^{N_{event}} \left(P_e A_y(p_p, p_T)\right)^2$$

$$\Delta P_{x,y}^{FPP} = \sqrt{\frac{2}{\mathcal{F}}}$$

$$\left(\frac{\Delta R}{R}\right)^2 = \left(\frac{\Delta P_t}{P_t}\right)^2 + \left(\frac{\Delta P_\ell}{P_\ell}\right)^2$$

$$P_t \approx P_x^{FPP}$$

$$P_\ell \approx \frac{P_y^{FPP}}{\sin\chi}$$

SBS G_E^p Projected Results

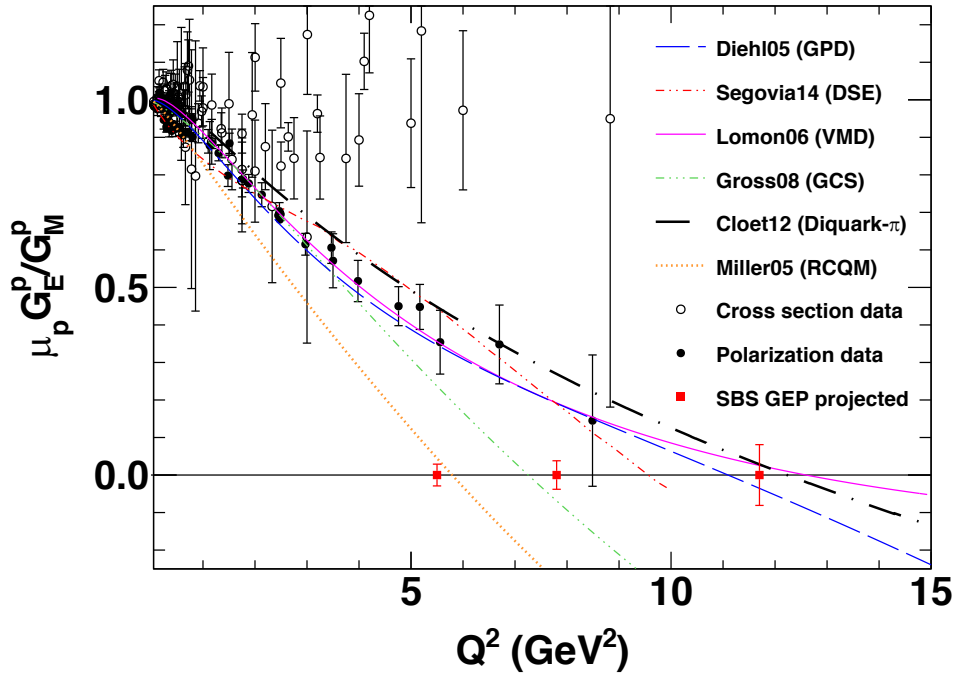

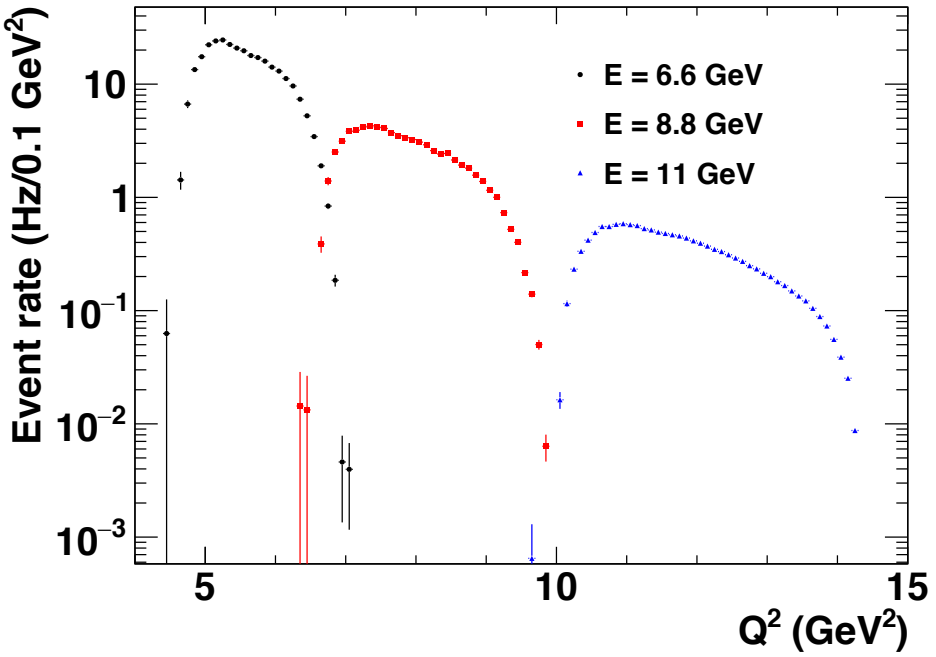

E12-07-109 Jeopardy update re-approved by JLab PAC47, no change in beam time, scientific rating A-

TABLE I. Kinematics, projected accuracy and beam time allocations. The projected statistical uncertainties in the form factor ratio include the assumption of 70% overall event reconstruction efficiency due to the combined efficiencies of the individual detectors, including DAQ dead-time.

E_{beam}, GeV	Q^2 range, GeV^2	$\langle Q^2 \rangle$ GeV^2	θ_{ECAL} degrees	$\langle E'_e \rangle$, GeV	θ_{SBS} degrees	$\langle P_p \rangle$ GeV	$\langle \sin\chi \rangle$ degrees	Event rate Hz	Days	$\Delta(\mu G_E/G_M)$
6.6	4.5-7.0	5.5	29.0	3.66	25.7	3.77	0.72	291	2	0.029
8.8	6.5-10.0	7.8	26.7	4.64	22.1	5.01	0.84	72	11	0.038
11.0	10.0-14.5	11.7	29.0	4.79	16.9	7.08	0.99	13	32	0.081

SBS Status

- Unofficial projected Hall A schedule places E12-07-109 (GEP) run in late 2022.
- All major components exist, assembly, testing and commissioning is underway
- First SBS experiment, GMN, will be installed in Hall A next year
- Start of SBS experiments ~Jan. 2021

Prospects for future proton FF measurements at an EIC (JLEIC concept as of May 2018)

JLEIC Design Update (Apr. 2017)

energy range:

E_e: 3 to 12 GeV

E_p: 40 to 100-400 GeV

$\sqrt{s}$: 20 to 65- 140 GeV

(upper limit depends on magnet tech. choice)

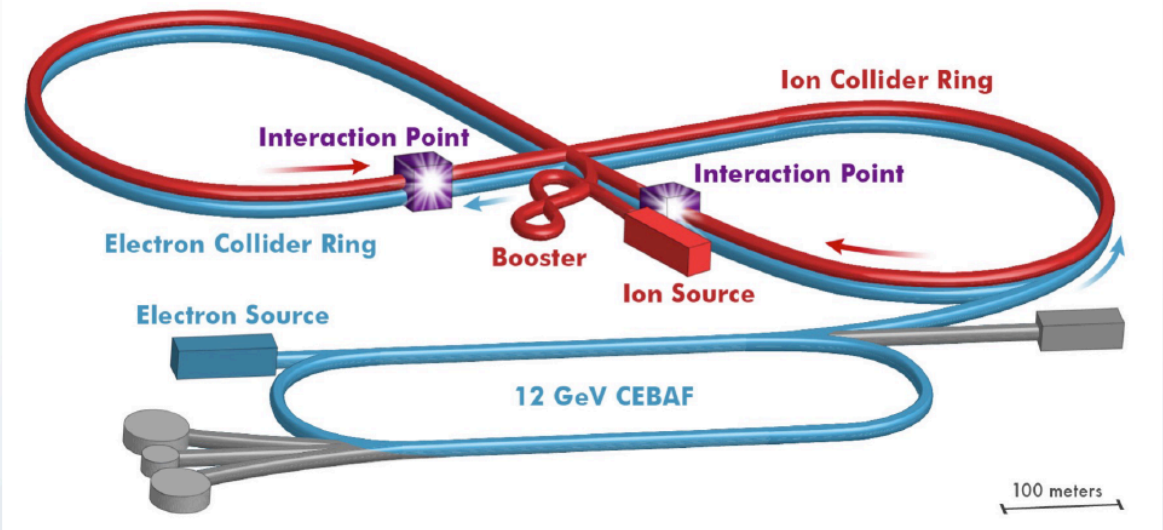

- **Electron complex**
  - CEBAF
  - Electron collider ring
- **Ion complex**
  - Ion source
  - SRF linac
  - Booster
  - Ion collider ring
- Fully integrated IR and **detector**
- DC and bunched beam **coolers**

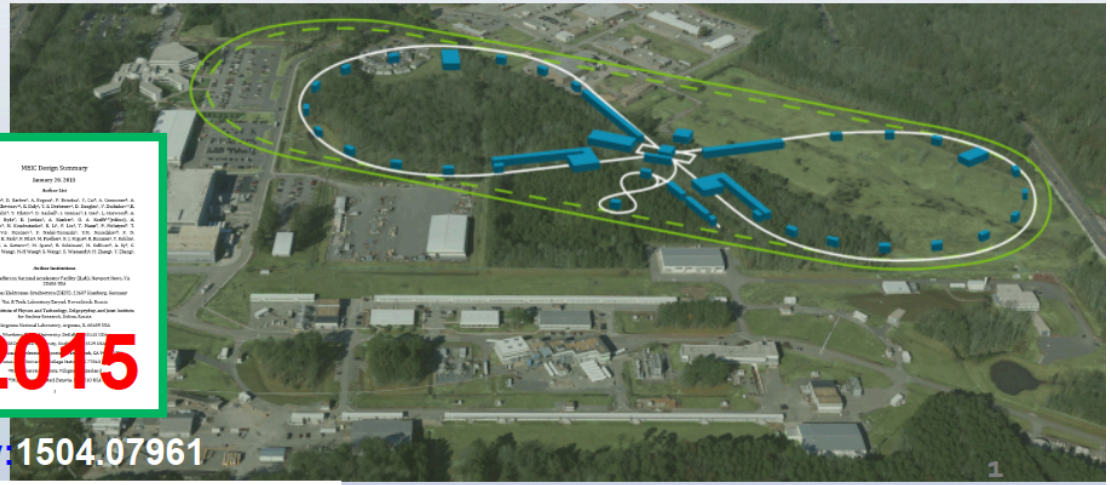

JLEIC energy reach and luminosity (log)

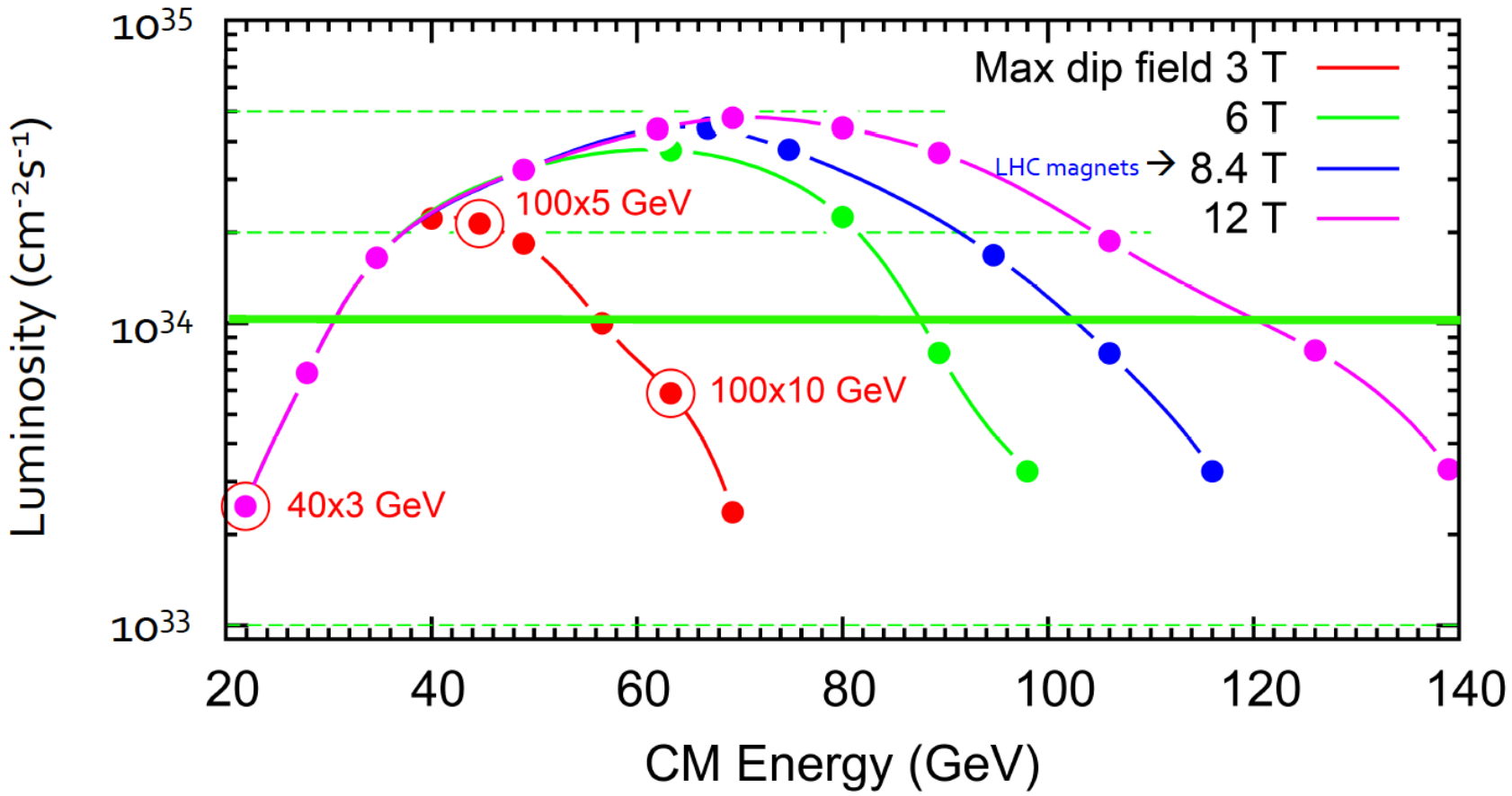

High polarization: Figure-8

- **Figure-8** concept: spin precession in one arc is exactly cancelled in the other
- **Spin stabilization by small fields**: ~3 Tm vs. ~ 400 Tm for **deuterons** at 100 GeV
  - Criterion: induced spin rotation >> spin rotation due to orbit errors
- **Polarized deuterons possible**
- **3D spin rotator**: combination of small rotations about different axes provides any polarization orientation at any point in the collider ring
- No effect on the orbit
- Adiabatic spin flips
- **Spin tracking** in progress

Electron polarization

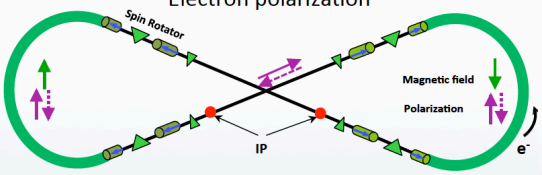

E- energy (GeV)	3	5	7	9	10
Estimated Pol. Lifetime (hours)	66	5.2	2.2	1.3	0.8

Ion polarization

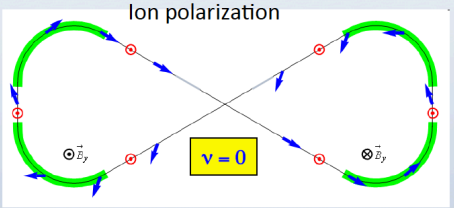

Integration IR: total acceptance

Possible to get ~100% acceptance for the whole event

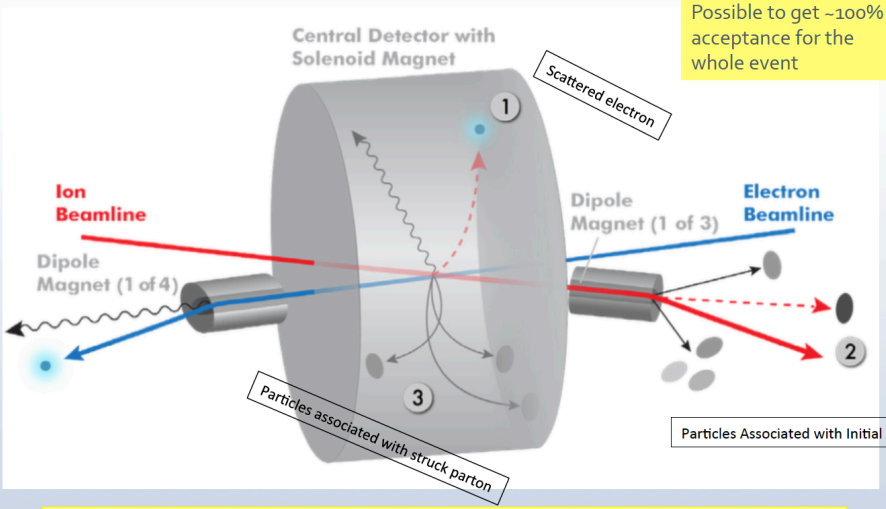

Relatively large crossing angle (**50 mr**) combined with large aperture final focus magnets, and forward dipoles are keys to this design.

High luminosity: electron cooling

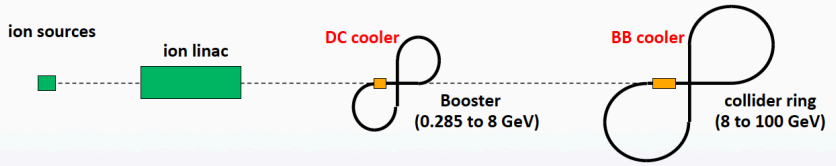

Ring	Cooler	Function	Ion energy	Electron energy
			GeV/u	MeV
Booster ring	DC	Injection and accumulation of positive ions	**0.11 ~ 0.19** (injection)	**0.062 ~ 0.1**
		Emittance reduction	**2**	**1.1**
Collider ring	Bunched Beam Cooling (BBC)	Maintain emittance during stacking	**7.9** (injection)	**4.3**
		Maintain emittance	Up to **100** (3T option)	**Up to 55**

- DC cooling for emittance reduction
- BBC cooling for emittance preservation against intra-beam scattering

JLEIC Parameters (3T option)

CM energy	GeV	21.9 (low)		44.7 (medium)		63.3 (high)	
		p	e	p	e	p	e
Beam energy	GeV	40	3	100	5	100	10
Collision frequency	MHz	476		476		476/4=119	
Particles per bunch	10^{10}	0.98	3.7	0.98	3.7	3.9	3.7
Beam current	A	0.75	2.8	0.75	2.8	0.75	0.71
Polarization	%	**80%**	**80%**	**80%**	**80%**	**80%**	**75%**
Bunch length, RMS	cm	3	1	1	1	2.2	1
Norm. emittance, hor / ver	μm	0.3/0.3	24/24	0.5/0.1	54/10.8	0.9/0.18	432/86.4
Horizontal & vertical β*	cm	8/8	13.5/13.5	6/1.2	5.1/1.0	10.5/2.1	4/0.8
Ver. beam-beam parameter		0.015	0.092	0.015	0.068	0.008	0.034
Laslett tune-shift		0.06	$7x10^{-4}$	0.055	$6x10^{-4}$	0.056	$7x10^{-5}$
Detector space, up/down	m	3.6/7	3.2/3	3.6/7	3.2/3	3.6/7	3.2/3
Hourglass(HG) reduction		1		0.87		0.75	
Luminosity/IP, w/HG, 10^{33}	$cm^{-2}s^{-1}$	**2.5**		**21.4**		**5.9**	

Elastic *ep* Scattering in JLEIC Kinematics (neglecting crossing angle)

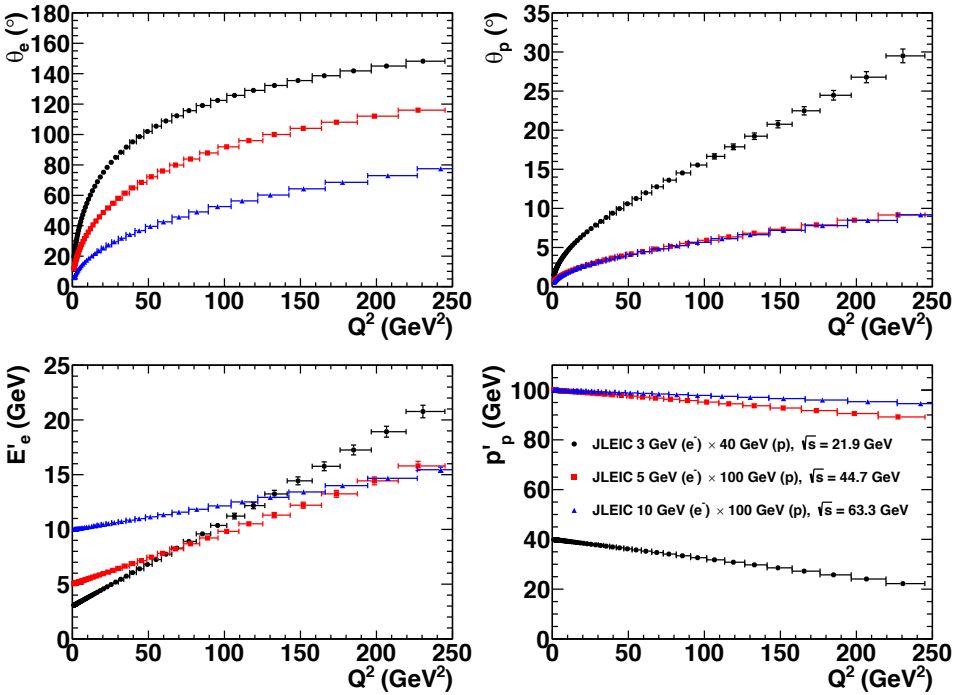

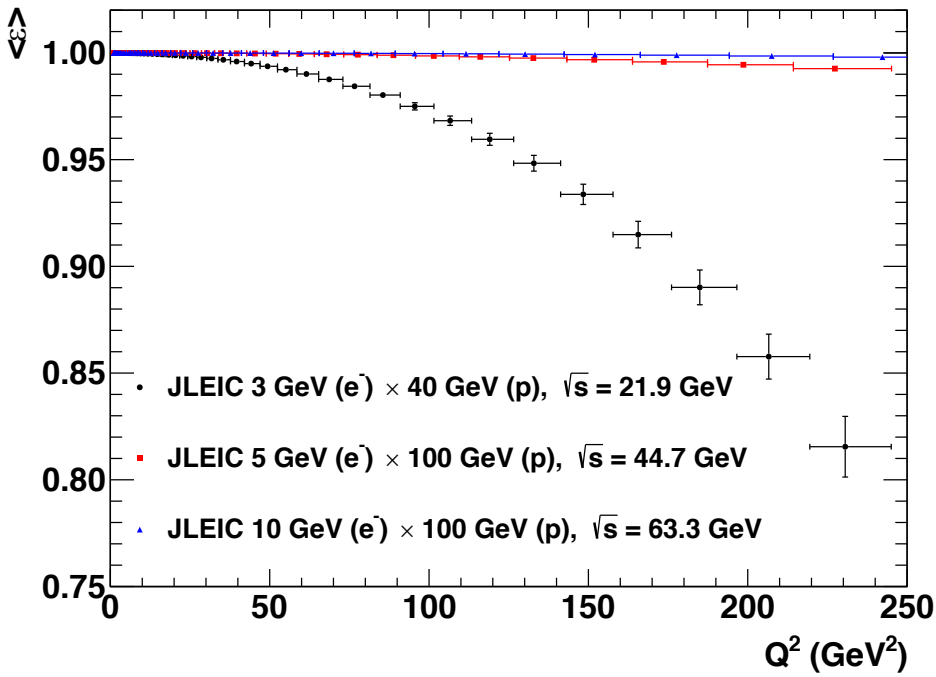

Electron and proton polar scattering angles and outgoing energies vs. Q², for various JLEIC energy scenarios:

- For asymmetric energy configuration ($E_p \gg E_e$), electron actually gains energy in collision (think bowling-ball ping-pong ball collision)
- Outgoing proton and electron are detectable in JLEIC "100% acceptance" IR design over a wide range of Q².
- Angular/momentum resolution requirements for the identification of elastic *ep* channel in the presence of dominant inelastic backgrounds needs to be evaluated
- For "reasonable" Q² values (unfortunately), $\epsilon \approx 1$ since $|s|, |u| \gg |t|$

$$E'_e = \frac{E_e}{1 + \frac{E_e - p_p}{E_p + p_p}(1 - \cos\theta_e)} = E_e + \frac{Q^2(p_p - E_e)}{2E_e(E_p + p_p)}$$

$$\epsilon = \frac{su - M^4}{su - M^4 + 2M^2 t - \frac{t^2}{2}}$$

Estimated elastic *ep* event rates (Born xsec.) for JLEIC scenarios

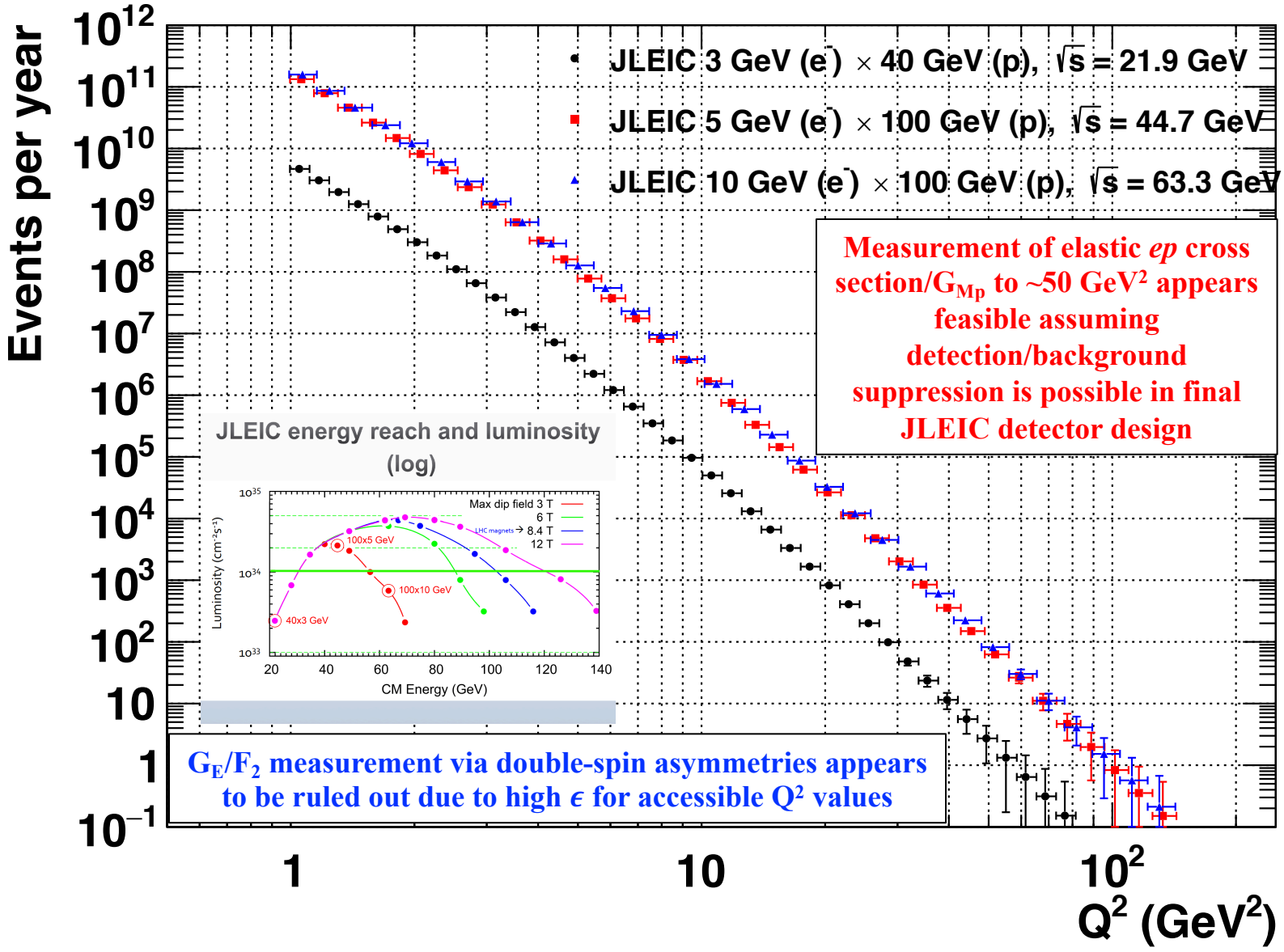

Polarized Beam-Polarized Target Asymmetry

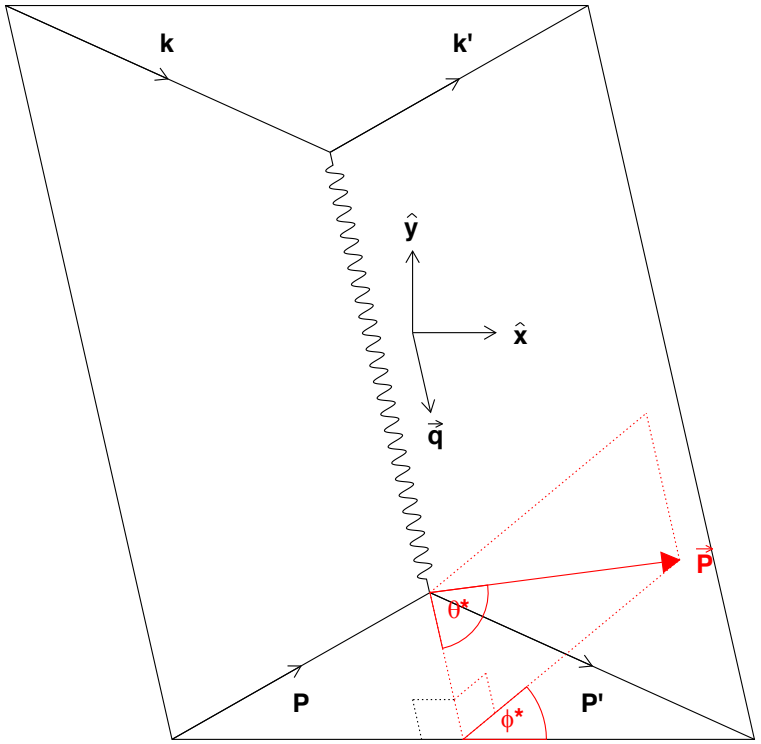

- The beam helicity asymmetry in elastic *eN* scattering from a polarized target is related to the transferred polarization by time reversal symmetry.
- The asymmetry A_t for target polarization perpendicular to the momentum transfer but parallel to the scattering plane ($\theta^* = 90°, \phi^* = 0$) equals the transverse component P_t of the transferred polarization.
- The asymmetry A_ℓ for target polarization along the momentum transfer direction ($\theta^* = 0$) is equal in magnitude but opposite in sign to the longitudinal transferred polarization P_ℓ.
- The sign change between A_ℓ and P_ℓ is due to the proton spin flip required for the absorption of the transversely polarized virtual photon

$\vec{\mathbf{P}}$ $\equiv$ Target polarization

$$
\begin{aligned}
A_{eN} &= -\frac{P_{beam}P_{target}}{1+\frac{\epsilon}{\tau}r^2}\left[\left(\sqrt{\frac{2\epsilon(1-\epsilon)}{\tau}}\sin\theta^*\cos\phi^*\right)r+\sqrt{1-\epsilon^2}\cos\theta^*\right] \\
&\equiv P_{target}\left[A_t\sin\theta^*\cos\phi^*+A_\ell\cos\theta^*\right] \\
A_t &= P_t \\
A_\ell &= -P_\ell \\
A_n &= P_n = 0
\end{aligned}
$$

On Measuring G_E^p, F_2^p at an EIC

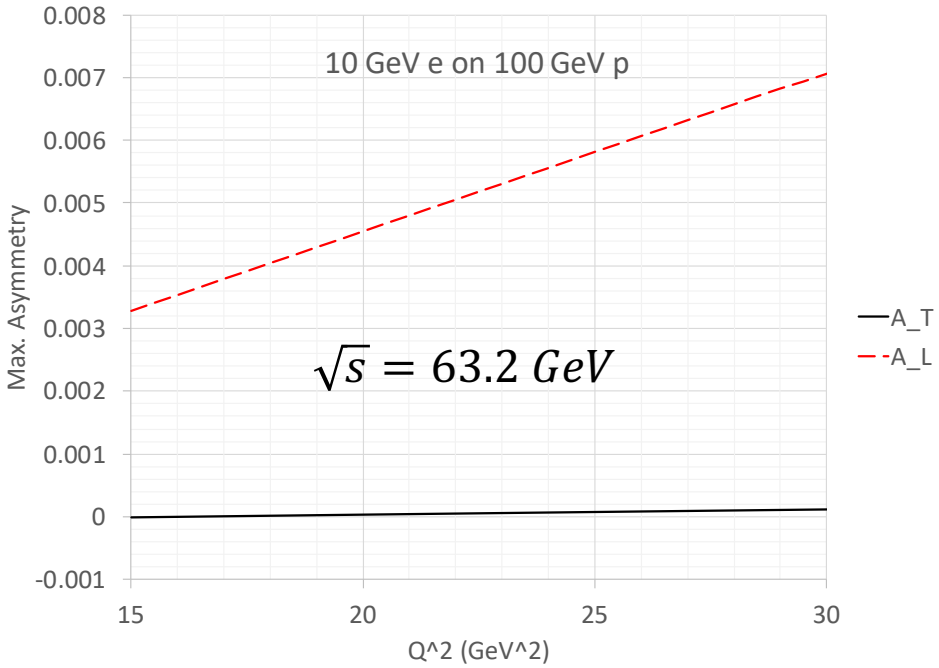

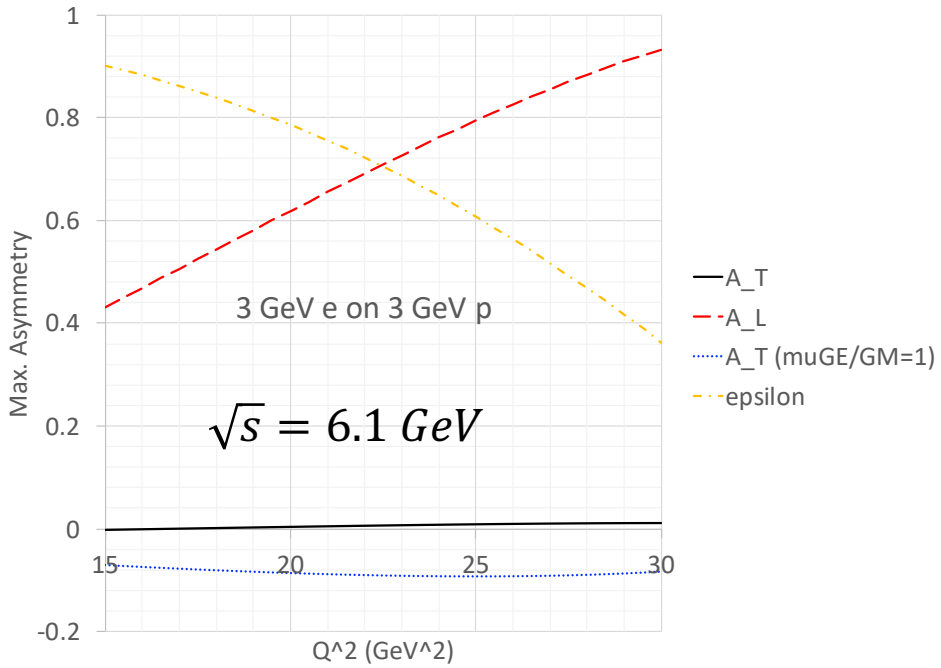

- To measure G_E^p at large Q^2 in a polarized EIC, one must measure the beam-target double-spin asymmetry (equations shown on the previous slide).
- Sensitivity to G_E^p is maximized approximately when $\epsilon = 0.5$:
  - $A_T = -P_{beam}P_{targ}\sqrt{\frac{2\epsilon(1-\epsilon)}{\tau}}\frac{\frac{G_E}{G_M}}{1+\frac{\epsilon}{\tau}\left(\frac{G_E}{G_M}\right)^2}\sin\theta^*\cos\phi^*$
- To go significantly beyond SBS/CEBAF 11 GeV, we look at the range $15 \leq Q^2 \leq 30\ GeV^2$
- To produce sufficiently large asymmetries to measure in a reasonable time, we would need a much lower *cms* energy than is being contemplated

Summary and Conclusions

- Near-future SBS high-Q^2 FF program will dramatically sharpen the precision with which we can make inferences about the relevant degrees of freedom for understanding the structure and dynamics of the nucleon at short distances, by precisely mapping proton and neutron FFs to at least 10 GeV^2
- **Questions?**

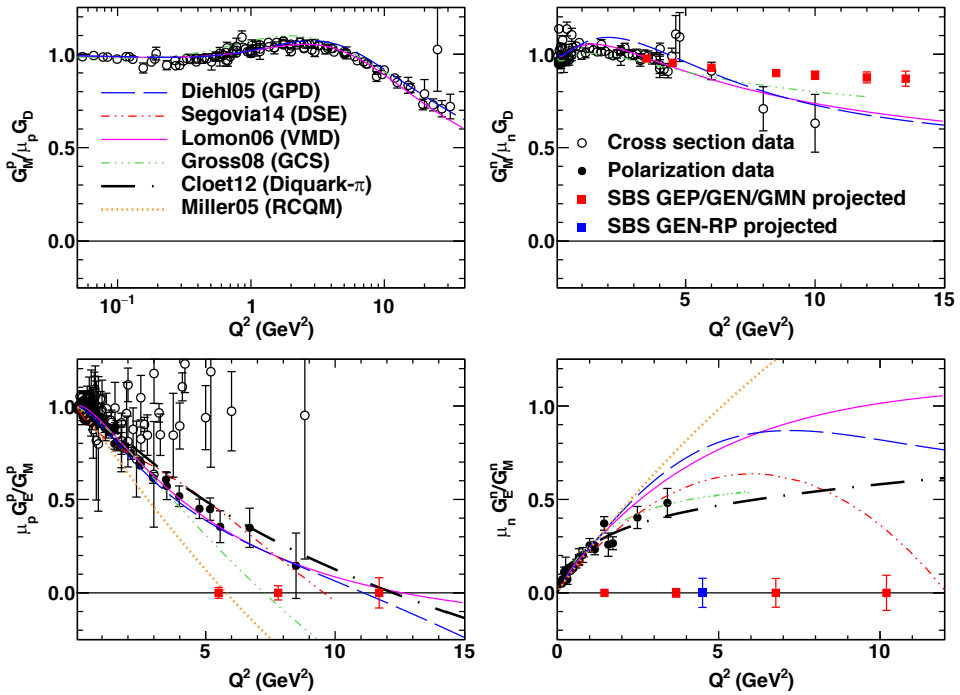

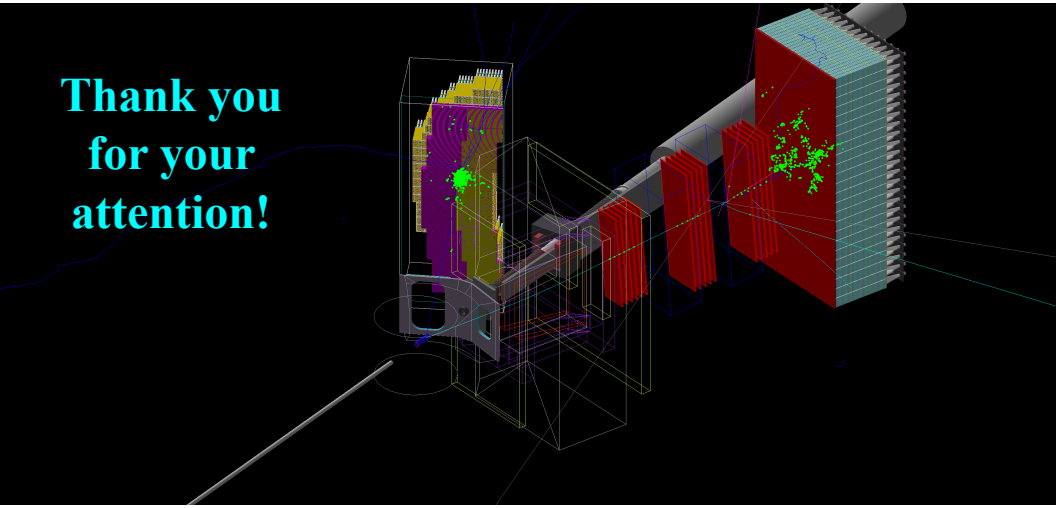

- SBS program projected start: 2021
- GEP projected run: 2022
- Future EIC could measure *ep* elastic cross sections to ~50-60 GeV^2 (and perhaps higher) IFF luminosity $\geq 10^{34}\ Hz/cm^2$

Backup Slides

Exposing the dressed-quark mass function

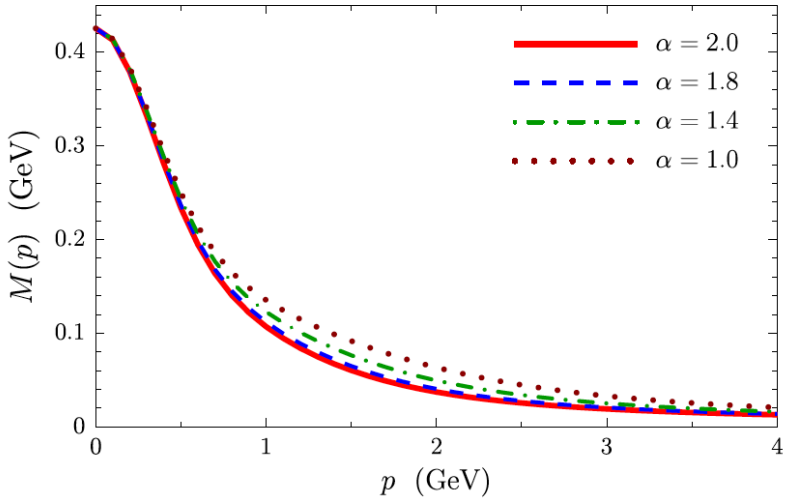

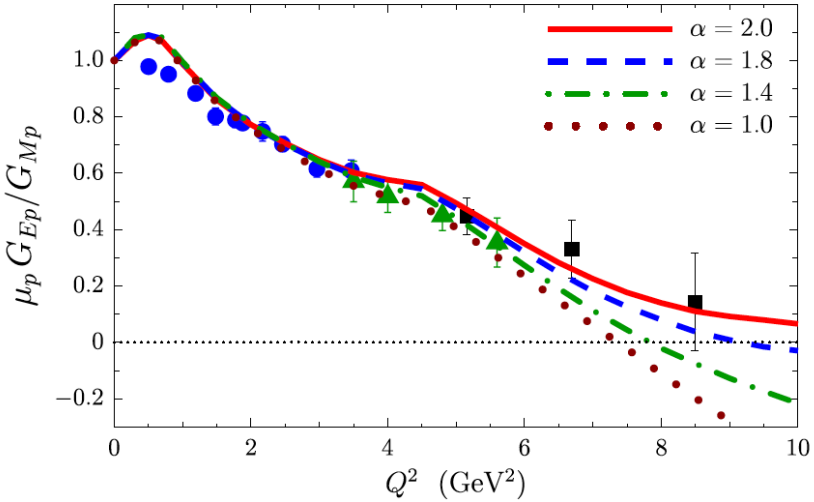

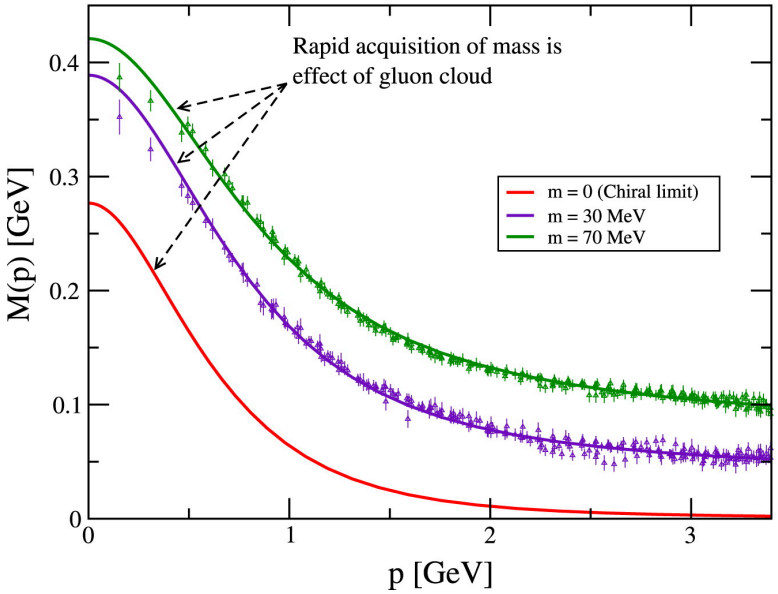

In the framework of Dyson-Schwinger equations, the high-Q^2 nucleon FFs ($Q^2 > 5$ GeV^2) are especially sensitive to momentum-dependent dressed-quark mass function in the few-GeV region, see e.g.,:

- I. Cloet, C. Roberts, A. Thomas: "Revealing Dressed Quarks via the Proton's Charge Distribution", **PRL 111, 101803 (2013)**
- I. Cloet and C. Roberts: "Explanation and Prediction of Observables Using Continuum Strong QCD", arxiv:1310.2651v2 (2013), **PPNP 77 (2014), 1-69**

"Role of diquark correlations and the pion cloud in nucleon elastic form factors"

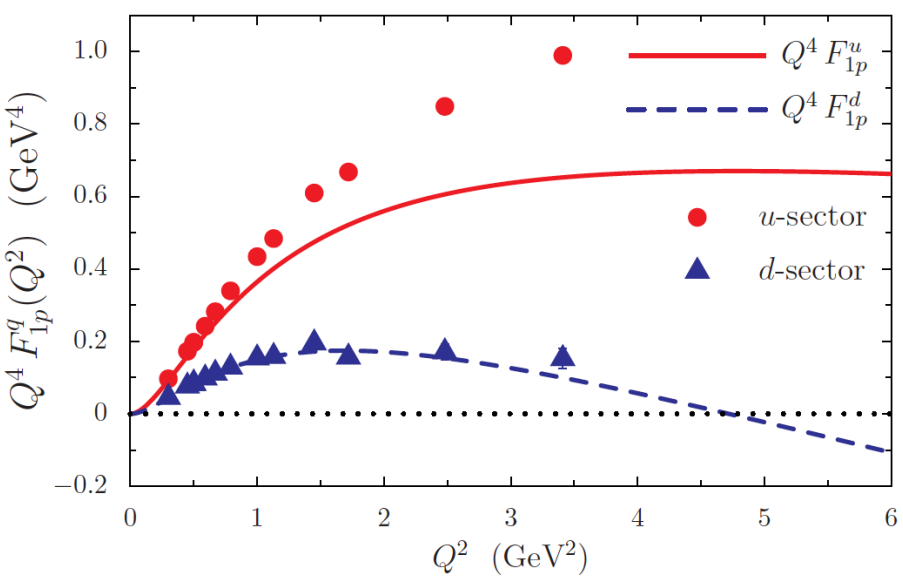

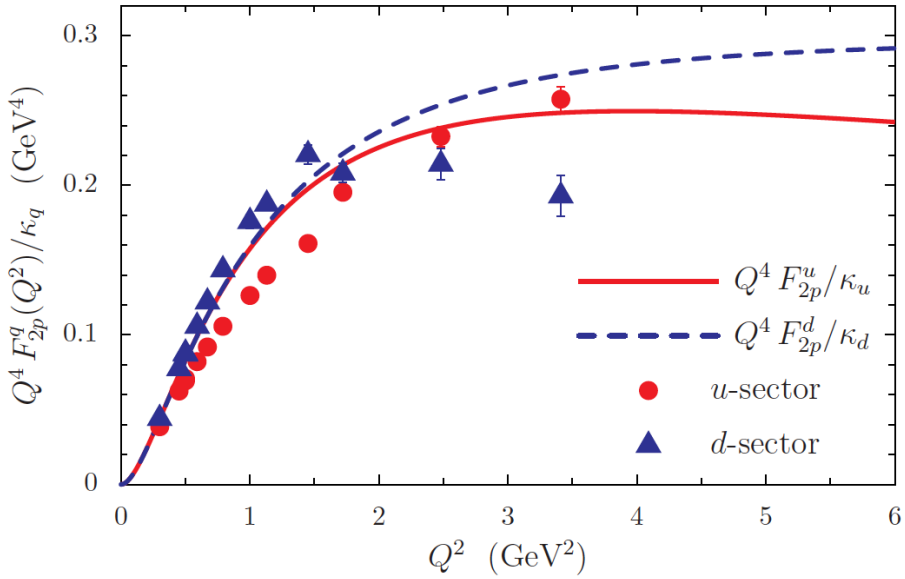

I. Cloet, W. Bentz and A. Thomas: Phys. Rev. C 90, 045202 (2014)

- Nucleon EMFF calculation in covariant, confining NJL model
- Parameter-free calculation (no fit to form factors)
- Softness of d-quark Dirac FF a consequence of dominance of scalar diquark correlations in nucleon wavefunction
- Axial vector diquark correlations and pion cloud effects play a more significant role in the Pauli form factors

Dyson-Schwinger Equations, diquark correlations, and zero crossings of G_{Ep}, G_{En}

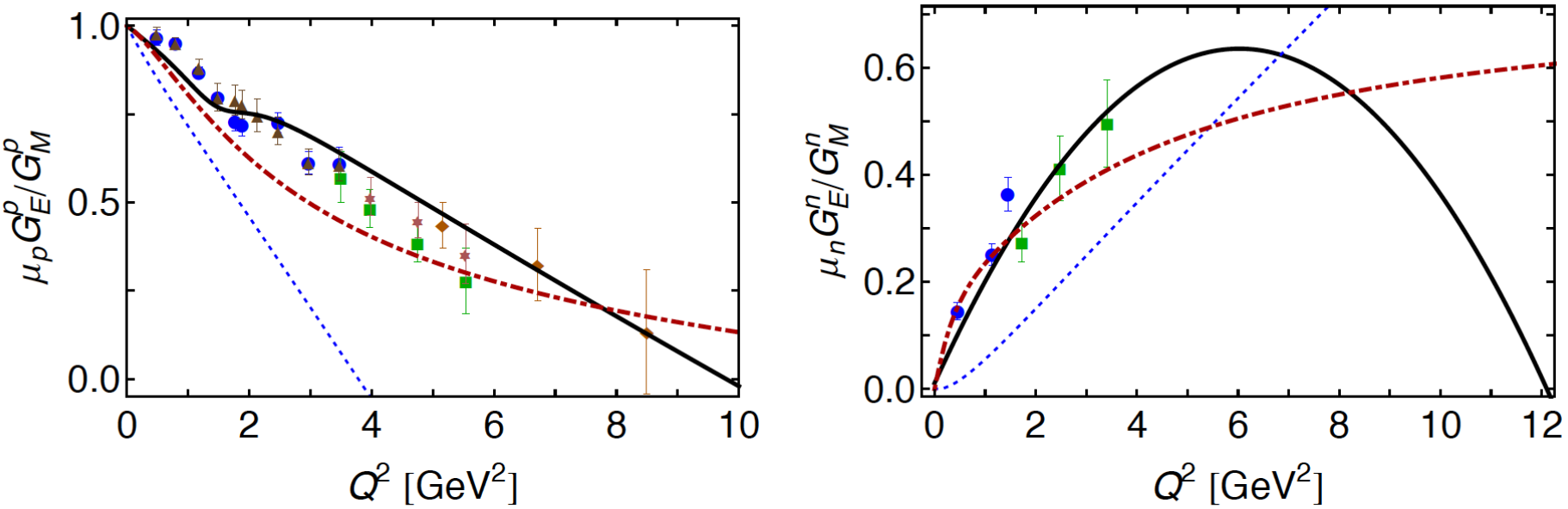

Fig. 3 *Left panel*: normalised ratio of proton electric and magnetic form factors. Curves: *solid, black* – result obtained herein, using our QCD-kindred framework; *Dashed, blue* – CI result [18]; and *dot-dashed, red* – ratio inferred from 2004 parametrisation of experimental data [65]. Data: blue circles [68]; green squares [69]; brown triangles [70]; purple asterisk [71]; and orange diamonds [72]. *Right panel*: normalised ratio of neutron electric and magnetic form factors. Curves: same as in left panel. Data: blue circles [73]; and green squares [74].

J. Segovia, I. Cloet and C. Roberts: Few-Body Syst. 55, 1185 (2014)

Quote from the abstract:

of dynamical chiral symmetry breaking in the bound-state problem. Amongst the results we describe, the following are of particular interest: $G_E^p(Q^2)/G_M^p(Q^2)$ possesses a zero at $Q^2 = 9.5\,\mathrm{GeV}^2$; any change in the interaction which shifts a zero in the proton ratio to larger Q^2 relocates a zero in $G_E^n(Q^2)/G_M^n(Q^2)$ to smaller Q^2; there is likely a value of momentum transfer above which $G_E^n > G_E^p$; and the presence of strong diquark correlations within the nucleon is sufficient to understand empirical extractions of the flavour-separated form factors. Regarding the $\Delta(1232)$-baryon, we find that, *inter*

Reaching high Q^2 in Lattice QCD

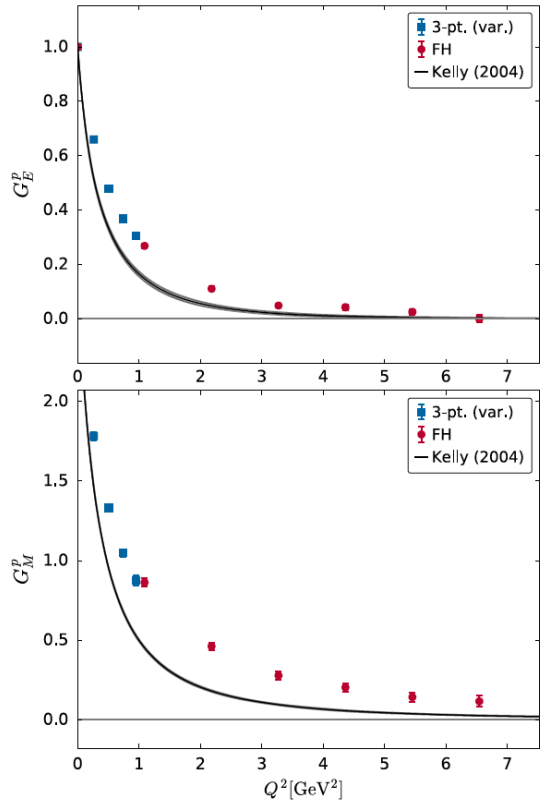

FIG. 3. G_E and G_M for the proton from the Feynman-Hellmann method and from a variational method described in Ref. [29] employed on the same ensemble. The experimental parametrization is from Ref. [49].

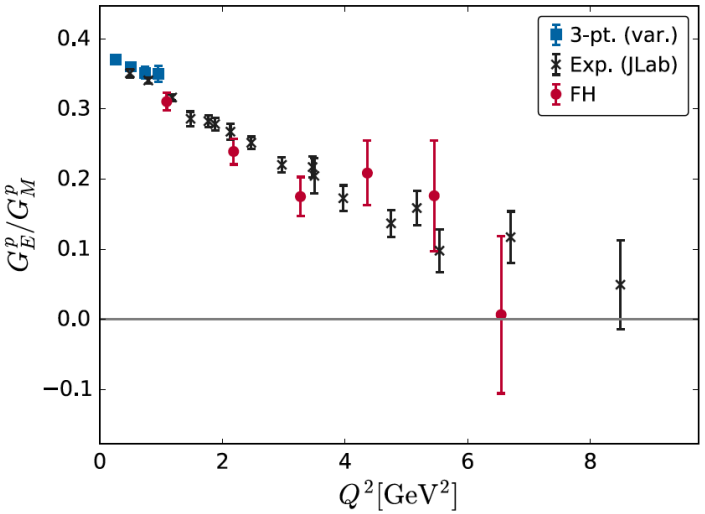

FIG. 4. Ratio G_E/G_M for the proton from the application of the Feynman-Hellmann method, from a variational analysis of three-point functions [29], and from experiment [5–7]. Note this is not scaled by the magnetic moment of the proton μ_p, as this would require phenomenological fits to the low-Q^2 data, which is not the focus of this work.

A. J. Chambers *et al.*, (QCDSF/UKQCD/CSSM Collaborations) Phys. Rev. D 96, 114509 (2017)

$$\frac{\partial E_\psi}{\partial \lambda} = \left\langle \psi \left| \frac{\partial H}{\partial \lambda} \right| \psi \right\rangle$$

- Novel application of the Feynman-Hellman method: relates hadronic matrix elements to energy shifts, allowing access to form factors via two-point correlators as opposed to more complicated three-point functions; improves signal-to-noise ratio for high-momentum states

FFs and "imaging": transverse densities, I

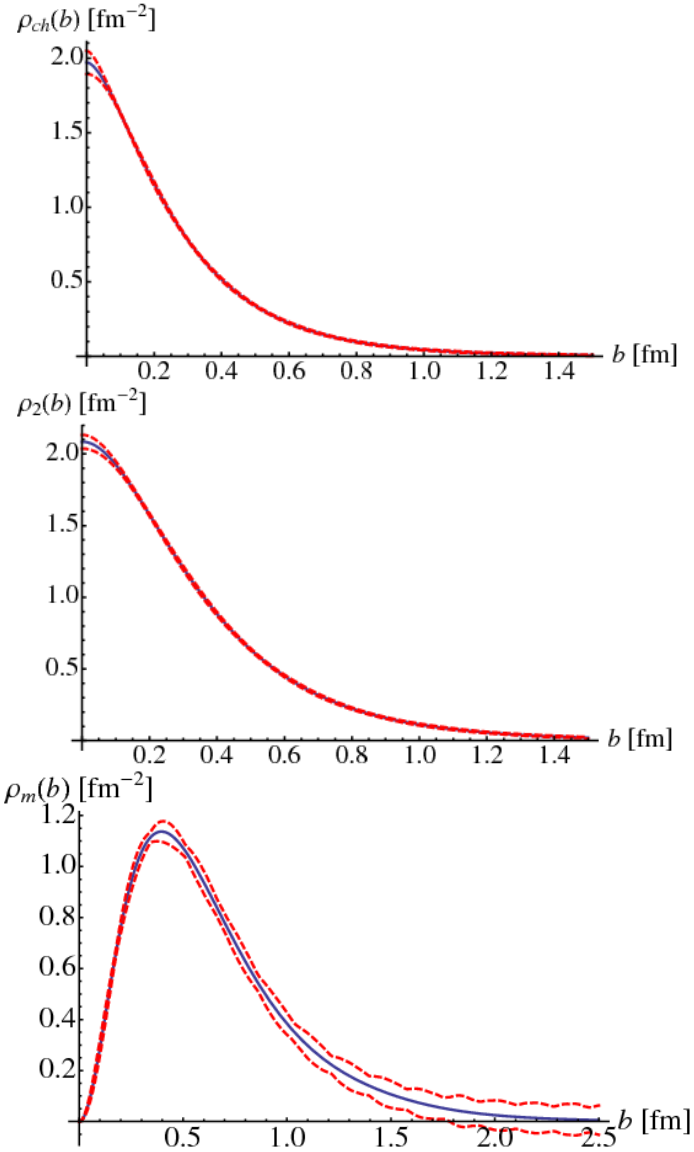

- Miller et al, **Phys. Rev. C, 83, 015203 (2011)**: ***model-independent,*** impact parameter-space charge and magnetization densities in the infinite momentum frame.
- Proton results shown for
  - Charge
  - 2D Fourier transform of F_2 (Pauli FF)
  - Anomalous magnetization density

$$\rho_{ch}(b) = \frac{1}{2\pi}\int QdQJ_0(Qb)F_1(Q^2)$$

$$\rho_2(b) = \frac{1}{2\pi}\int QdQJ_0(Qb)F_2(Q^2)$$

$$\rho_m(b) = -b\frac{d}{db}\rho_2(b) = \frac{b}{2\pi}\int Q^2dQJ_1(Qb)F_2(Q^2)$$

FFs and "imaging": transverse densities, II

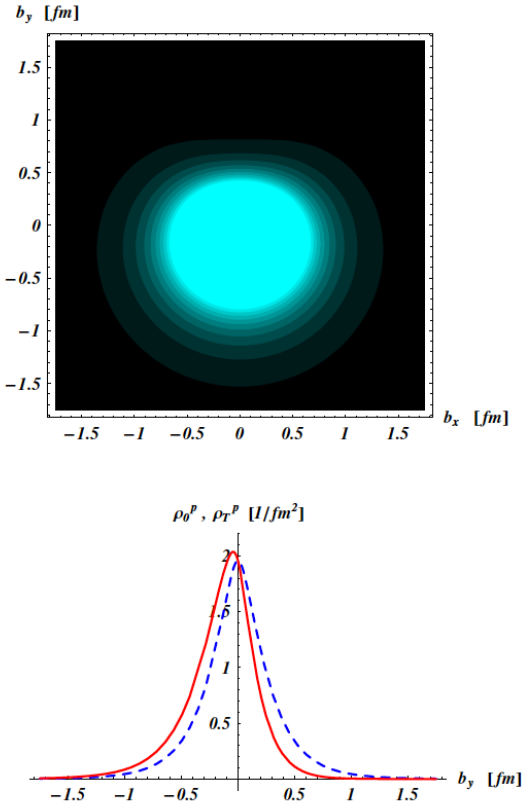

FIG. 1: Quark transverse charge densities in the *proton*. The upper panel shows the density in the transverse plane for a proton polarized along the x-axis. The light (dark) regions correspond with largest (smallest) values of the density. The lower panel compares the density along the y-axis for an unpolarized proton (dashed curve), and for a proton polarized along the x-axis (solid curve). For the proton e.m. FFs, we use the empirical parameterization of Arrington *et al.* [14].

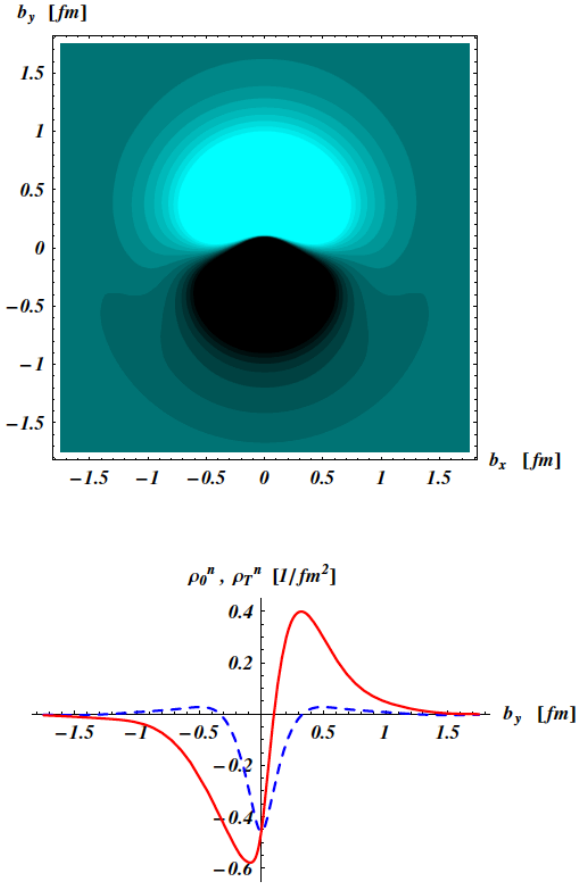

FIG. 2: Same as Fig. 1 for the quark transverse charge densities in the *neutron*. For the neutron e.m. FFs, we use the empirical parameterization of Bradford *et al.* [15].

Proton (left) and neutron (right) 2D polarized transverse charge densities from Carlson and Vanderhaeghen: Phys. Rev. Lett. 100, 032004 (2008)

High-Q^2 Nucleon Form Factors, GPDs and Spin

Flavor decomposition of nucleon EMFFs (neglecting strangeness):

$$F_{1,2}^{p} \approx e_u F_{1,2}^{u} + e_d F_{1,2}^{d}$$

$$F_{1,2}^{n} \approx e_u F_{1,2}^{d} + e_d F_{1,2}^{u}$$

Quark flavor FFs are integrals of valence quark GPDs H and E at zero skewness :

$$F_1^q(t) = \int_0^1 H_v^q(x,t)dx$$

$$F_2^q(t) = \int_0^1 E_v^q(x,t)dx$$

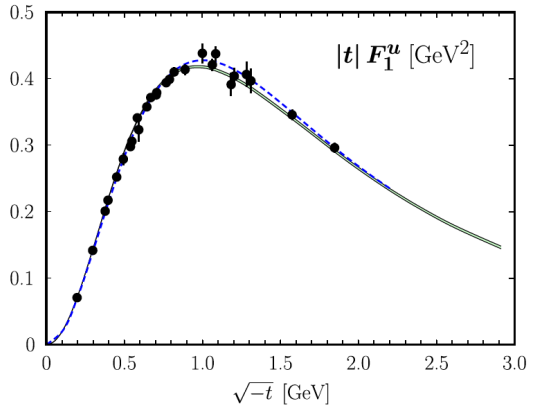

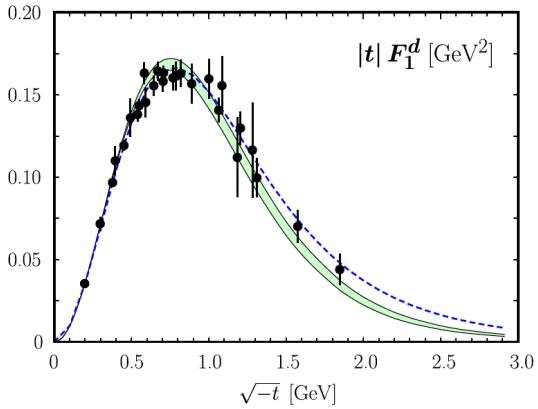

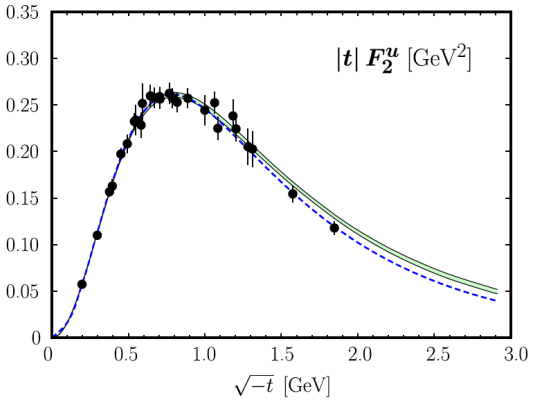

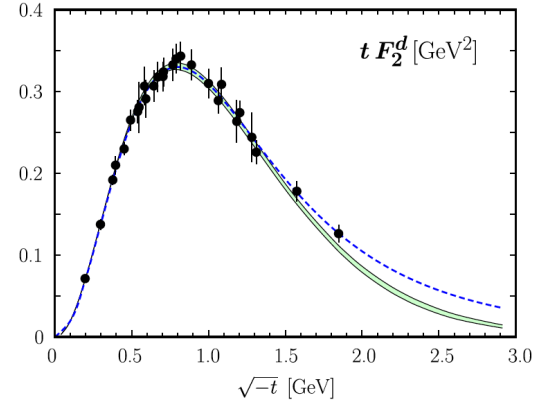

Phys.Rev.Lett. 78 (1997) 610-613: Ji sum rule for total angular momentum

$$J_q = \frac{1}{2}\int_{-1}^{+1} dx x[H^q(x,\xi,t=0) + E^q(x,\xi,t=0)].$$

Diehl, Kroll. Eur. Phys. J. C (2013) 73:2397

- FF data + forward PDFs from global DIS fits → model-dependent extraction of GPDs
- Compute valence-quark contributions to the Ji sum rule:

$$J_v^u = 0.230^{+0.009}_{-0.024}, \qquad J_v^d = -0.004^{+0.010}_{-0.016}$$

The under-appreciated importance of knowledge of the high-Q^2 FFs in the extraction of GPDs from experiment

From the recent paper by **M. Diehl and P. Kroll. Eur. Phys. J. C (2013) 73:2397**

- "This requires an ansatz for the functional form of the GPDs and in this sense is intrinsically model dependent, but on the other hand it can reach values of the invariant momentum transfer t much larger than what can conceivably be measured in hard exclusive scattering..."
- "We note that the electromagnetic form factors provide indirect constraints on GPDs at high values of t, which will conceivably never be accessible in hard exclusive scattering processes."

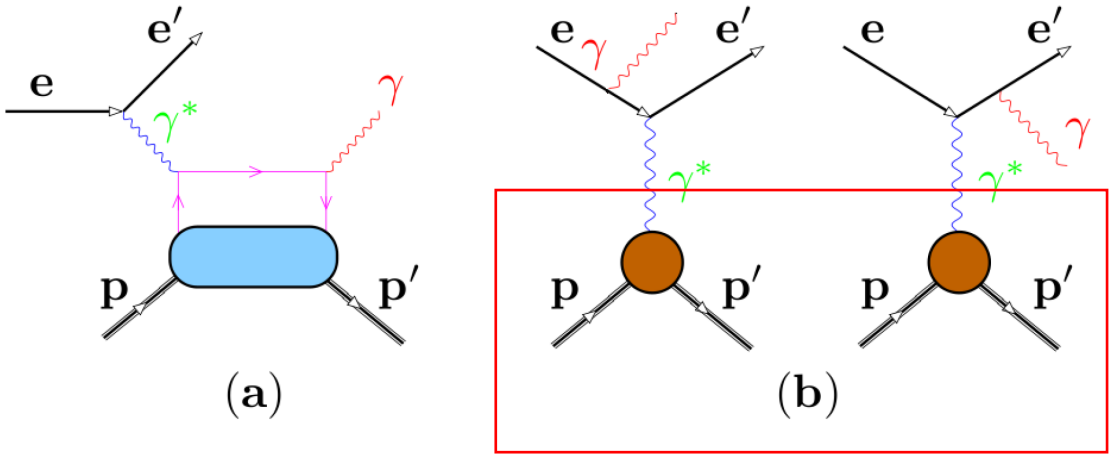

- DVCS experiments actually measure the interference of Bethe-Heitler and DVCS handbag mechanism at the same order of α→precise knowledge of elastic FFs over a wide range of Q^2 is needed to separate DVCS contribution!
- EMFFs thus provide both direct constraints to GPDs via the sum rules and crucial input to the extraction of Compton Form Factors from experimental observables

JLab detector landscape

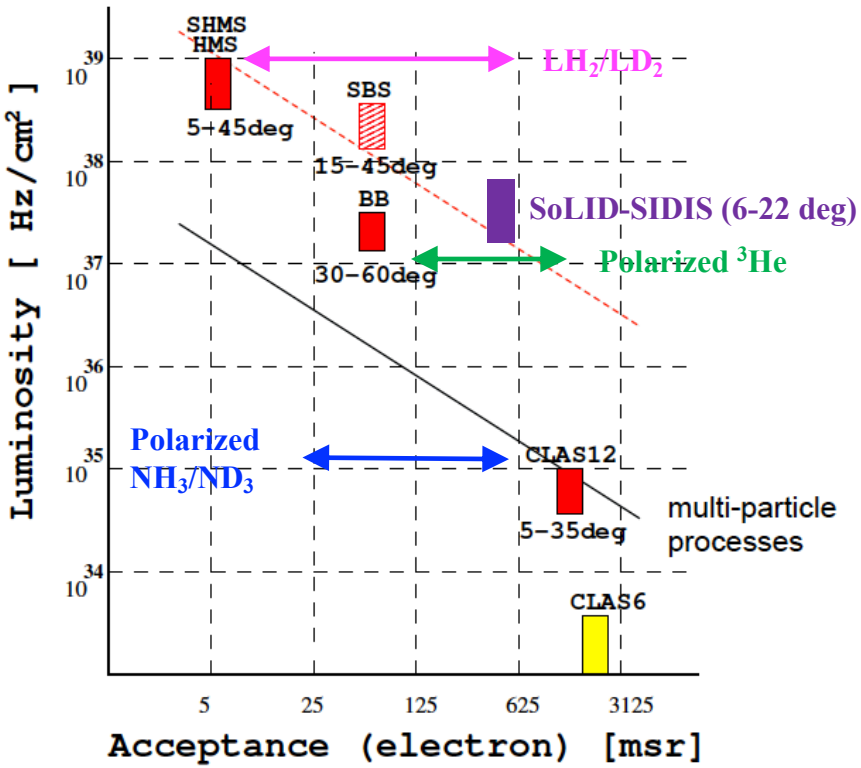

A range of 10^4 in luminosity.

A big range in solid angle:
from 5 msr (SHMS)
to about 1000 msr (CLAS12).

==========

The SBS is in the middle:
for solid angle (up to 70 msr)
and high luminosity capability.

In several A-rated experiments SBS was found to be the best match to the physics.

GEM allows a spectrometer with open geometry (->large acceptance) at high L.

11/16/15 Super Bigbite Spectrometer Review slide 9

- Complementary equipment/capabilities of Halls A, B, C allow optimal matching of (Luminosity x Acceptance) of the detectors to the luminosity capabilities of the targets, including state-of-the-art polarized target technology.

Historical Digression—Rutherford Scattering and the discovery of the nucleus

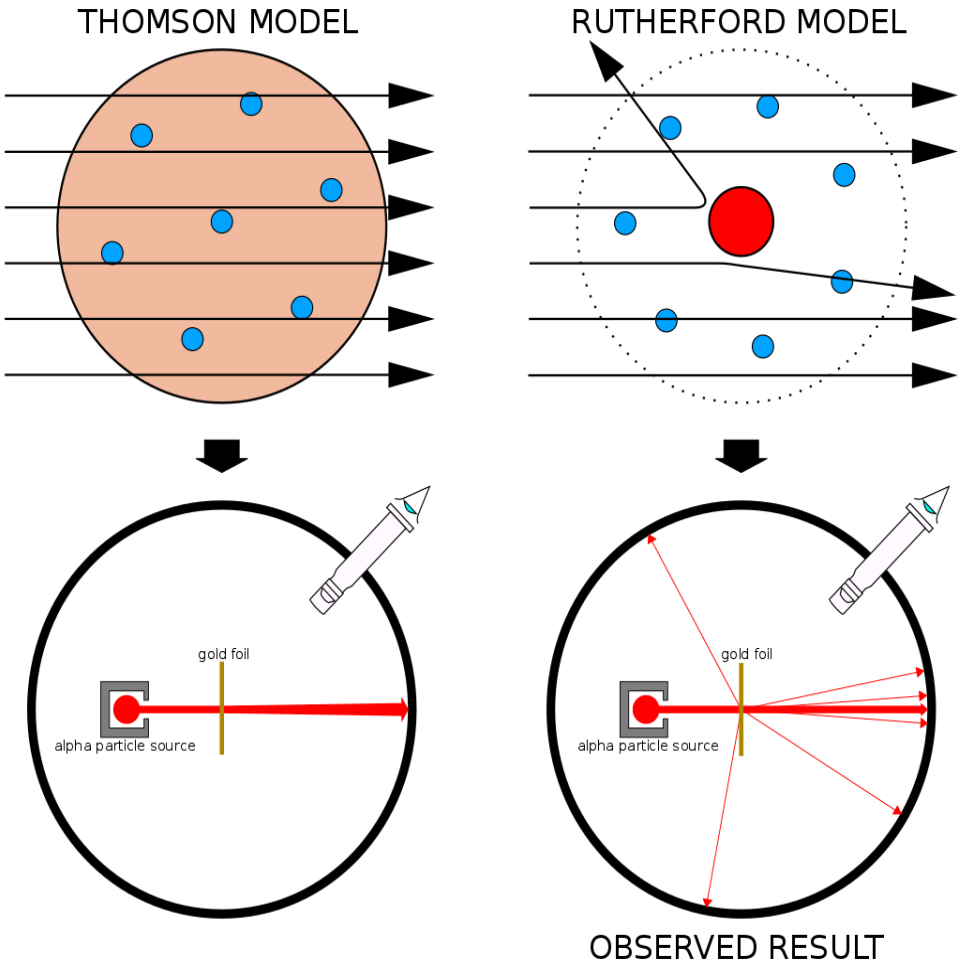

Classical Analysis of Rutherford Scattering

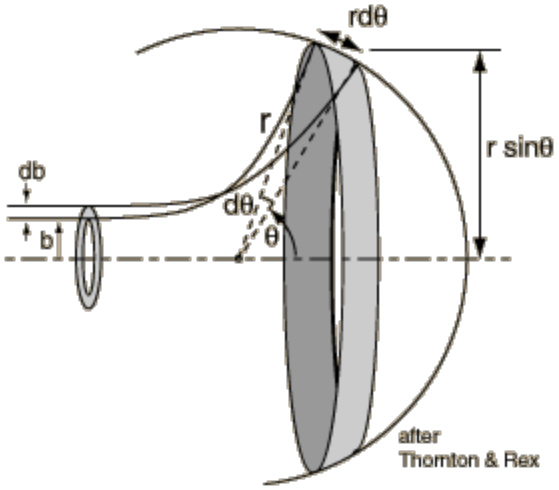

Figure credit: http://hyperphysics.phy-astr.gsu.edu/hbase/Nuclear/ruthcross.html

Assumptions:

- The incident α particle ($Z_\alpha = +2$) scatters from a *stationary, point-like* gold nucleus ($Z_{Au} = +79$).
- The interaction is repulsive and pure Coulomb: $U = \frac{Z_\alpha Z_{Au} e^2}{4\pi\epsilon_0 r}$
- Angular momentum conservation for a central force confines the motion to a plane
- The equation of the orbit $u(\theta) = \frac{1}{r(\theta)}$ is the solution to the *Binet* equation: $\frac{d^2u}{d\theta^2} + u = -\frac{Z_\alpha Z_{Au} e^2}{8\pi\epsilon_0 E b^2}$, where E is the α particle kinetic energy and b is the impact parameter.
- The impact parameter and the scattering angle are related by:
  - $b = \frac{Z_\alpha Z_{Au} e^2}{8\pi\epsilon_0 E}\cot\frac{\theta}{2} = \frac{Z_\alpha Z_{Au}\alpha_{em}\hbar c}{2E}\cot\frac{\theta}{2}$
- Closest-approach distance and scattering angle are related by:
  - $r_{min} = \frac{Z_\alpha Z_{Au} e^2}{8\pi\epsilon_0 E}\left(1 + \csc\frac{\theta}{2}\right) = \frac{Z_\alpha Z_{Au}\alpha_{em}\hbar c}{2E}\left(1 + \csc\frac{\theta}{2}\right)$

$$\alpha_{em} \equiv \frac{e^2}{4\pi\epsilon_0\hbar c} \approx \frac{1}{137.036}$$

- Rutherford differential cross section formula: $\frac{d\sigma}{d\Omega} = \left|\frac{bdb}{\sin\theta d\theta}\right| = \frac{(\alpha_{em}\hbar c)^2 Z_\alpha^2 Z_{Au}^2}{16E^2\sin^4\frac{\theta}{2}}$

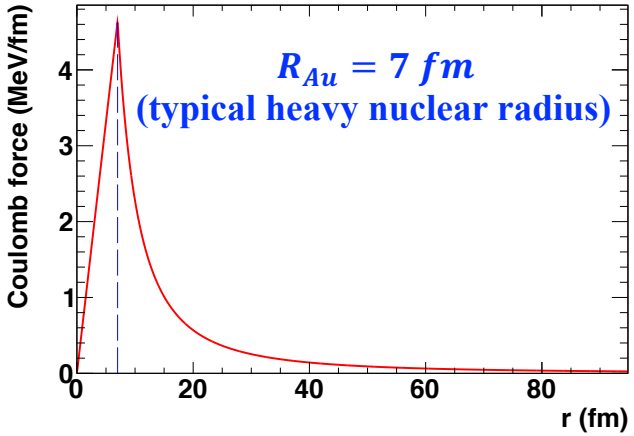

$$\text{Gauss' Law: } \mathbf{E} = \left\{ \begin{array}{l} \frac{Ze}{4\pi\epsilon_0 r^2}\hat{r}, r > R \\ \frac{Zer}{4\pi\epsilon_0 R^3}\hat{r}, r < R \end{array} \right\}$$

$$\text{Coulomb Force: } \mathbf{F} = \left\{ \begin{array}{l} \frac{zZe^2}{4\pi\epsilon_0 r^2}\hat{r}, r > R \\ \frac{zZe^2 r}{4\pi\epsilon_0 R^3}\hat{r}, r < R \end{array} \right\}$$

$$\text{Potential energy } U = \left\{ \begin{array}{l} \frac{zZe^2}{4\pi\epsilon_0 r}, r > R \\ \frac{zZe^2}{4\pi\epsilon_0 R}\left[\frac{3}{2} - \frac{r^2}{2R^2}\right], r < R \end{array} \right\}$$

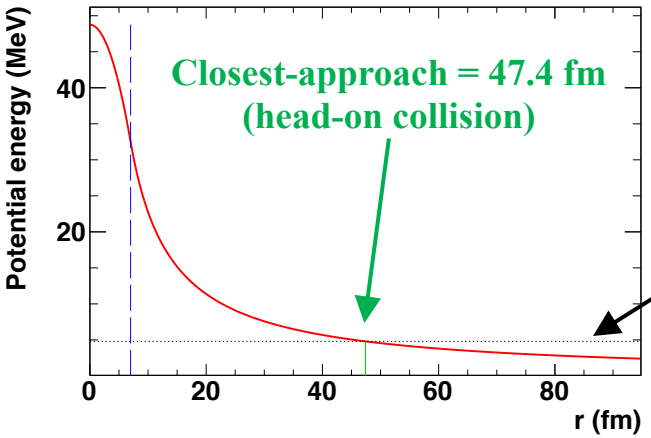

$E_\alpha = 4.8\ MeV$

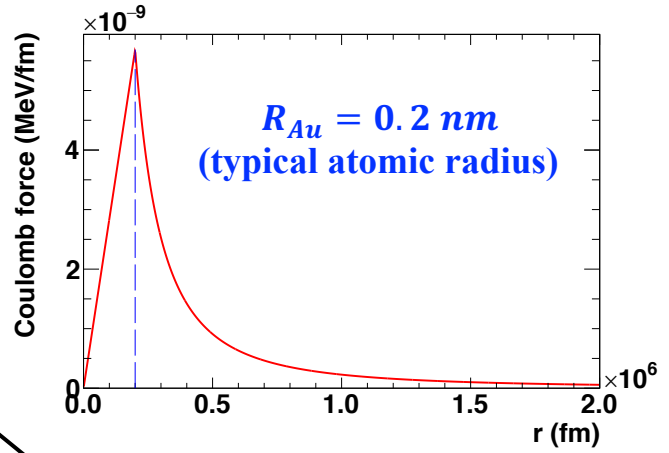

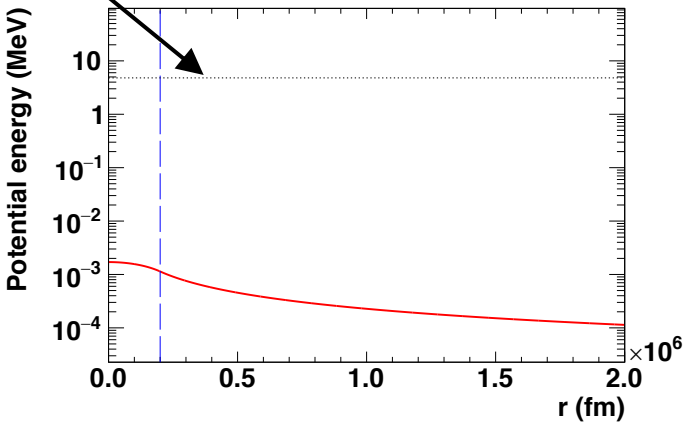

- Imagine the nucleus as a sphere of positive charge with uniform density throughout its volume (this approximation is not actually that far off)
- Even ignoring the atomic electrons, a Thomson-model nuclear charge density cannot produce large-angle deflections for MeV-scale kinetic energies

Deviations from the Rutherford formula and Nuclear size

Plots from: Eisberg and Porter, Rev. Mod. Phys, 33, 190 (1961)

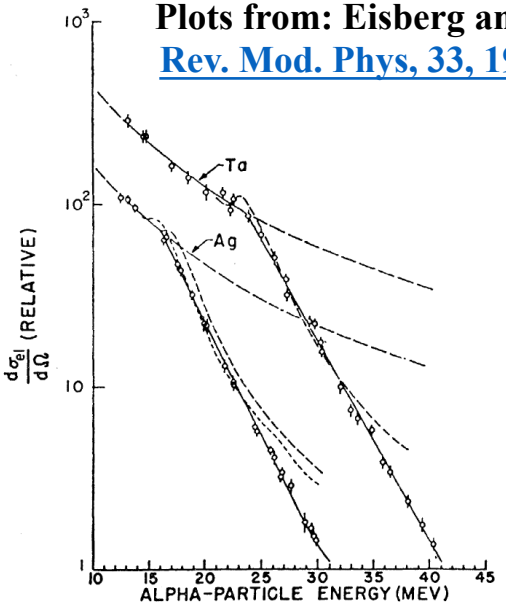

FIG. 14. Comparison of the differential cross section calculated from the APB model and experimental data for Ag and Ta. Experimental points were obtained from measurements at 60°. The broad dashed curve gives the Coulomb cross section and solid curves represent the experimental data of Farwell and Wegner. For Ag, two theoretical curves are shown; for the finer, $R=9.67\times10^{-13}$ cm; and for the coarser, $R=8.84\times10^{-13}$ cm. For Ta, the finer dashed curve gives the theoretical cross section for $R=10.54\times10^{-13}$ cm.

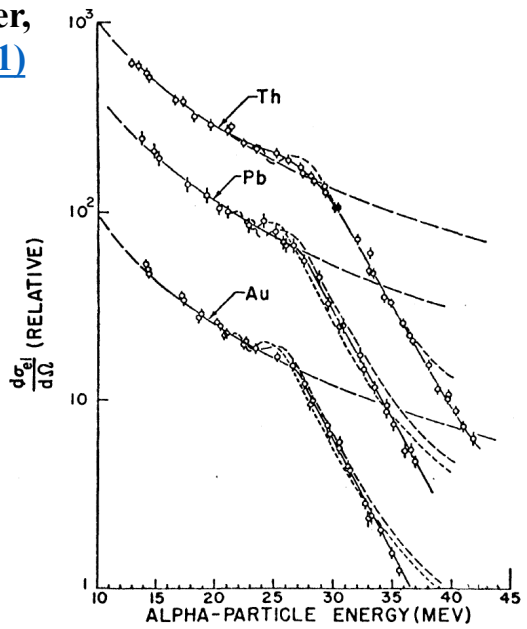

FIG. 15. Similar graphs for Au, Pb, and Th. For Au, the finer theoretical curve corresponds to $R=10.58\times10^{-13}$ cm and the coarser to $R=10.3\times10^{-13}$ cm. For Pb, the finer curve corresponds to $R=10.87\times10^{-13}$ cm and the coarser to $R=10.42\times10^{-13}$ cm. For Th, the dashed curve corresponds to $R=11.01\times10^{-13}$ cm.

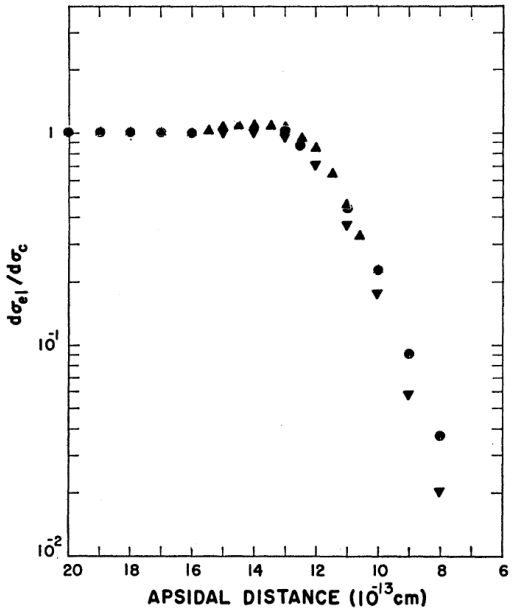

FIG. 19. Wegner plot of the experimental ratio of the differential cross section to the Coulomb cross section for the scattering of alpha particles by Au as a function of apsidal distance. Both angular data at fixed energy and energy data at fixed angle are shown. These data coincide for at least $(d\sigma_{el}/d\sigma_c) \geq 0.1$ suggesting that the major variation of the ratio for heavy nuclei enters primarily through the apsidal distance. ▲, α's on Au, 22 Mev, 20°–60°; ●, α's on Au, 13–44 Mev, 60°; ▼, α's on Au, 13–44 Mev, 95°.

- Recall: closest approach distance ("apsidal distance") in Coulomb scattering is given by:

$$r_{min} = \frac{Z_\alpha Z_{Au} e^2}{8\pi\epsilon_0 E}\left(1+\csc\frac{\theta}{2}\right) = \frac{Z_\alpha Z_{Au}\alpha_{em}\hbar c}{2E}\left(1+\csc\frac{\theta}{2}\right)$$

- With the advent of high-energy accelerators, the α's could be accelerated to sufficiently high energies to penetrate the charge distribution of the nucleus, leading to deviations from Rutherford's formula
- The distance of closest approach at which the drop-off occurs provides a measure of the size of the nuclear charge distribution.
- The energy/angle dependence of the deviation from point-like behavior is sensitive to the details of nuclear structure and the alpha-nucleus interaction

Electron-Nucleon Scattering in QED

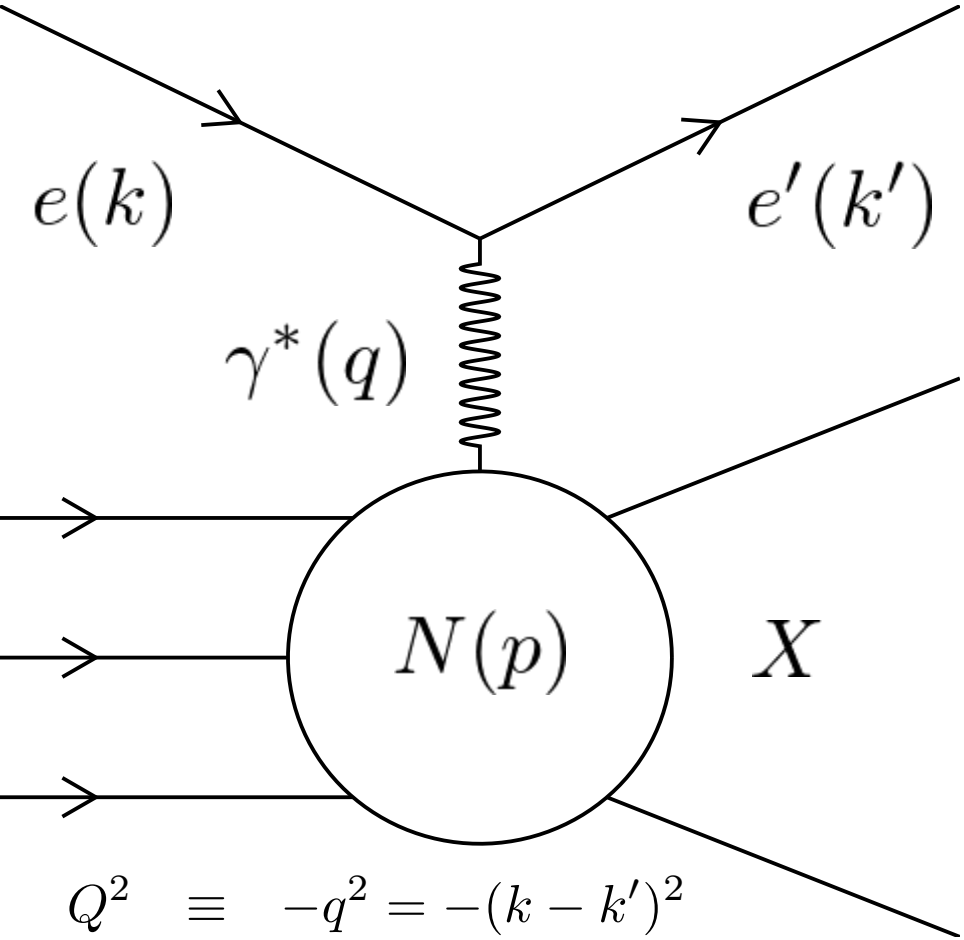

$$Q^2 \equiv -q^2 = -(k-k')^2$$

Feynman diagram for electron-nucleon scattering in the one-photon-exchange (Born) approximation

$$\alpha_{em} \equiv \frac{e^2}{4\pi\varepsilon_0\hbar c} = 1/137.035999074(44) \text{ (PDG 2012)}$$

- Charged leptons (e.g., electrons) interact with the charged constituents of nuclei predominantly via electromagnetic (EM) interaction (but also weak interaction).
- Electrons are point-like
- EM interaction is "weak"→low-order QED perturbation theory works well→"clean" theoretical interpretation
- EM interaction is well-described by the exchange of a single virtual photon of four-momentum q.
- Analogous to impulse approximation in classical mechanics
- Availability of high-quality electron beams w/ well-defined properties (energy, intensity, polarization, etc.) makes electron scattering a precision probe of nuclear structure